An Analysis of a Perplexing Group of Graves from Ancient Corinth, Greece

By

Grace Lenz

A thesis
presented to the University of Waterloo
in fulfillment of the
thesis requirement for the degree of
Master of Arts
in
Public Issues Anthropology

Waterloo, Ontario, Canada, 2023

Author's Declaration

I hereby declare that I am the sole author of this thesis. This is a true copy of the thesis, including any required final revisions, as accepted by my examiners.

I understand that my thesis may be made electronically available to the public.

Abstract

In 2019 a post-12th century C.E. cemetery was identified at Ancient Corinth, Greece, in the area northeast of the ancient theatre. The 2019 and 2022 excavation season uncovered a perplexing group of graves with limited cultural context and an unknown date of usage. Ten adults, and one juvenile were excavated from this cemetery. The age-at-death of the adults range from 18-45 years. The juvenile was between the ages of 12-15 years. Ten shallow pit graves, and one cist grave with evidence of reuse indicate this cemetery was used on multiple occasions. In addition, in 2022, two infants were unexpectedly discovered high up in the remains of a Roman building, ~50 metres to the south of the NET Cemetery where the excavation of a Roman road was taking place. This thesis is a pilot study, providing the first analysis of the 13 individuals buried here. The goal of this research is to interpret the funerary practices performed by the living through the discussion of grave styles and treatment of the body, and to analyze the paleopathological data. Results of this study indicate the burial practices reflect Christian traditions, with their heads facing east to anticipate the second coming of Christ. Reuse of the cist grave indicates the living were aware of the location of the cemetery, and may have been members of the same community or social group. Pathological analysis of the adults indicate lifestyles associated with strenuous activities. Linear enamel hypoplasia (LEH) speaks to some individuals having experienced non-specific periods of stress in their childhood. Evidence for tuberculosis and brucellosis was present in two different adult males, and evidence for scurvy was identified in the two juveniles. This research presents the first skeletal cases of tuberculosis and scurvy from Ancient Corinth.

Key Words: funerary archaeology, bioarchaeology, paleopathology, tuberculosis, scurvy

Acknowledgements

I have received a tremendous amount of support since entering this master's program in September 2021. To my graduate advisor, Dr. Maria Liston, thank you for all the hard work you put into finding me a thesis project, despite all the trials and tribulations thrown at us by the pandemic. Thank you for such a wonderful experience at the University of Waterloo, I am grateful to have had the opportunity to work with you over the past 16 months, in Waterloo and in Greece. Thank you to my committee members, Dr. Alexis Dolphin and Dr. Bonnie Glencross for your feedback and comments on my research. I appreciate you taking the time to read my work and lend me your advice.

Thank you to the Department of Anthropology, and to Dr. Jennifer Liu, Dr. Adrienne Lo, and Dr. Alexis Dolphin for your help during the coursework terms. A special thank you to my supportive cohort: Jessica Clarke, Nathan Homerski, Andrew Dasilva Furtado, Carey Matthews, Alice Xu, Yingjia Wang, Karen Rueb, Christina Saoud, and Menda Tesfaye-Visser.

To Johnathan Tomlinson, thank you for providing accommodations in Athens at the Canadian Institute in Greece (CIG). Thank you to Dr. Christopher Pfaff for inviting me to participate in the 2022 Corinth excavations with the American School of Classical Studies (ASCSA), and for allowing me to incorporate the NET skeletons into my thesis research. A special thanks to Mr. C. K. Williams II, Nancy Bookidis, Ioulia Tzonou, Manolis Papadakis, James Herbst, Colin Wallace, the Corinth maids, the Corinth excavators, and everyone involved in the 2022 excavation season. I am forever grateful for the wonderful experience, it was a pleasure to have been able to visit and work in Corinth.

I am also thankful for the financial support provided by the Iris Yuzdepski Memorial Award and the UW International Experience Award. Working for the University of Waterloo as a teaching assistant provided me with learning experiences that I am eternally grateful for. Thank you for this opportunity, and thank you to my students for helping me grow professionally and academically.

To my parents, you have always been my number one fans since day one. I could not have done this without your unwavering love and support throughout the years. Thank you for allowing me to follow my dreams and pursue what makes me happiest.

To my partner Matt, thank you for being by my side throughout this journey, and for having utmost confidence in my abilities. Thank you for taking care of my bunny, Delilah, while I was away in Greece for seven weeks, although I know this was not a difficult task. Thank you both for keeping me sane and happy these last 16 months, I could not have done this without you.

Finally, thank you to the NET skeletons, who were the focus of my research. It was a privilege and an honour to learn from you. Thank you for allowing me to be a part of your stories.

Table of Contents

List of Figures

List of Tables

List of Abbreviations

ASCSA	American School of Classical Studies at Athens
B.C.E.	Before Common Era
C.	Century
C.E.	Common Era
F	Female
IJPP	International Journal of Paleopathology
LEH	Linear Enamel Hypoplasia
M	Male
MNI	Minimum Number of Individuals
NET	North East of Theatre
TA2	Transition Analysis 2.0
TA3	Transition Analysis 3.0
TB	Tuberculosis
Y	Years

Chapter One: Introduction to the Northeast of Theatre Cemetery from Ancient Corinth, Greece, and Public Issues Anthropology

1.1 Introduction

In 2019 a post-12th century C.E. cemetery was identified at Ancient Corinth, Greece, in the area northeast of the ancient theatre. This cemetery was partially excavated in 2019 by the American School of Classical Studies at Athens (ASCSA) before the Covid-19 pandemic affected the ability to continue the excavation safely. In 2022, excavations resumed and the remaining graves were excavated. This cemetery will be referred to as 'the NET Cemetery'.

The 2019 and 2022 excavation seasons uncovered a perplexing group of graves with limited cultural context. Since 2018 the ASCSA's NET excavations have expanded multiple trenches to understand this area of the city, which has revealed the remains of an Early Roman building, a Byzantine-Ottoman road, and a 19th century C.E. house that was likely abandoned by the 1858 earthquake, among other finds (Pfaff, 2021). In 2019 ten graves were identified in close proximity to the 19th century C.E. house, and four were excavated (Pfaff, 2021). The graves partially penetrate the surface of the Byzantine-Ottoman road, and their discovery was not anticipated while expanding trenches. The relation of the graves to the Byzantine-Ottoman road, or to the 19th century C.E. house, if any, is not understood. There were no markers identifying the location of the graves, and no grave goods placed with the deceased. It has not been made clear who these people are, or why they were buried in this location.

Ten adults, and one juvenile were excavated from this Christian-style cemetery. In addition, in 2022, two infants were unexpectedly discovered high up in the remains of a Roman building, ~50 metres to the south of the NET Cemetery where the excavation of a Roman road was taking place. This thesis is a pilot study, providing the first analysis of the 13 individuals buried here. The goal of this research is to interpret the funerary practices

performed by the living through the discussion of grave styles and treatment of the body, and to analyze the paleopathological data. Due to the fact that I was directly involved with the excavation of seven graves, a discussion of the excavation process and funerary archaeology will be presented, along with an osteological analysis per skeleton. A discussion of estimated biological sex, age-at-death, and a survey of pathologies will follow.

1.2 Terminology Statement and Use of Photos

It is vital to acknowledge the use of terminology in this thesis. The term 'juvenile' will be used when referring to the skeletal remains of the three individuals under the age of 18 excavated at Ancient Corinth in 2022. With reference to Buikstra and Ubelaker (1994: 9), terminology will be further refined when discussing specific age categories: infant (birth-3 years), child (3-12 years), and adolescent (12-20 years). The term 'adult' will be used when referring to individuals who are over 18 years of age. Although socially perceived notions of adulthood vary spatially and temporally, from a biological perspective, the term 'adult' will refer to the NET individuals who have reached skeletal maturity.

When referring to sex, the term is used strictly through a biological lens. The terms 'male' and 'female' will be used with the intention to refer to biological physiology, as determined by the X- and Y- sex chromosomes. The term 'sex' will be used in reference to the sexually dimorphic osteological features that are expressed differently through hormone secretion between males and females at different stages of life. The term 'gender', and any social aspects of gender will not be a focus for this analysis.

Drawing from Martin and Harrod (2016: 161-162), the term 'pain' will be used with reference to the "normal and frequent experience of discomfort produced by biological insults". Understanding the relationship and connection between pathology and pain in the past can be difficult, and notions of pain differ cross-culturally. However, the term 'pain' is a

“universal aspect of disease and injury”, not to be confused with the subjective term ‘suffering’, which implies a longer-term emotional coping mechanism.

All photos included in this thesis are used with the permission of the Corinth Excavations and the Greek Archaeological Service of the Ministry of Culture and Sport.

1.3 Limitations

It is vital to note that estimating biological sex, age-at-death, and analyzing pathological conditions in human skeletal remains is not without limitations. Angel (1969) notes that no two bioarchaeologists will ever agree completely when analyzing a single skeleton, thus, it is important to recognize one's own biases in this sort of work. Especially since interpreting life in the past is told through perceptions of the bioarchaeologist, the researcher must approach this work with respect, cooperation, and rigorously explore all possible explanations (Buikstra & DeWitte, 2019; Grauer & Buikstra, 2019). Bioarchaeologists cannot speak for the dead, they can only interpret and hypothesize what the data mean. The interpretations presented here are from my own data collection supervised by Dr. Maria Liston in Ancient Corinth, Greece. Therefore, conclusions drawn in this thesis are not to be mistaken with absolute truth, rather, are my own interpretations of the data.

The state of preservation and size of the sample must be taken into consideration as well. Preservation of the skeletons is moderately good, however taphonomic processes and fragmented skeletal elements did have an impact on method selection for estimating biological sex, age-at-death, and surveying pathologies. This study incorporates data from 13 skeletons, which is a small sample size, but adequate for the interpretations that follow.

1.4 Issues of Dating

Situating the individuals buried in the NET cemetery temporally is difficult. Green glaze-ware pottery sherds from the Byzantine period were identified in the grave fills during excavation, and the graves partially penetrated the packed dirt surface of a

Byzantine-Ottoman road (Pfaff, 2021). This gives the cemetery a *terminus post quem* of 12th century C.E. for the time it was in use (Pfaff, 2021). The burial style and depth of the graves were the only other clues to indicate the potential time period of this cemetery. Since there is a *terminus post quem* of 12th century C.E., these individuals may have lived and died in the Frankish period (1210-1458 C.E.), First Ottoman period (1458-1687 C.E.), Venetian period (1687-1715 C.E.), Second Ottoman period (1715-1821 C.E.), or the Hellenic Republic (1821 C.E. - present day) (Sanders et al., 2018: 9). At this point, we do not know.

Moreover, the two infants excavated to the south of the cemetery are not known to be associated with the individuals buried in the NET Cemetery. Therefore, the time period in which these individuals lived and died may very well be different. We know they are post-Roman because they were excavated above the ruins of a large Roman building excavated during the 2022 field season.

1.5 Public Issues Anthropology

In order to discuss the public issue related to this research project, it is important to first define the public. While the Merriam-Webster Dictionary defines public as "of or relating to people in general", it is impossible to consider people, or the public, as analogous through time and space. There are many different publics, and topics of public concern within the context of bioarchaeological research. With this, there is no universal application of a public bioarchaeology — each project must be considered within its own specific context.

In Greece, handling human skeletal remains is less restrictive due to the common modern practice of secondary burial. The Greek Orthodox Church continues to support the practice of exhumation, where the primary burial is rented out until decomposition is complete. It is believed by some that the soul slowly ascends to paradise as the body decomposes, thus, the deceased is no longer tied to their physical skeletal remains (Danforth, 1982; Dubisch, 1989). After the lengthy mourning activities cease, which can last from five

to seven years, the final memorial service involves exhuming the deceased's body from their primary burial, and moving the skeletal remains to an ossuary (Danforth, 1982). The incorporation of the deceased's skeleton into the village ossuary marks the integration of the deceased with the world of the dead (Danforth, 1982). This is the final stage of burial rites in rural Greece, and the relationship between the living and the dead almost ceases after exhumation (Danforth, 1982). After the deceased's body has decomposed and has been moved to their final resting place, the ossuary, the grave structure is available to be reused again (Dubisch, 1989). As a result, handling human skeletal remains in Greece is not seen as disrespectful to this particular public.

Within the context of my research and bioarchaeological studies in Ancient Corinth, the specific public is anyone involved in the ongoing excavations (ASCSA), and/or anyone who has an interest in the work that comes from this region of the Mediterranean. Results of the ongoing excavations at Ancient Corinth are routinely published in *Hesperia* and *American Journal of Archaeology*, and in final excavation volumes published in the Corinth series by the ASCSA, which include osteological analyses of other excavated cemeteries (see Williams et al., 1998; Zervos et al., 2009). The public would also include the people who live in the Old Corinth village. The ongoing excavations by the ASCSA and students who come to Corinth for their MA and PhD research are very much a part of everyday life, and tourism in the village.

The Corinth Excavations also have a well-developed and active program of presenting the results of the ongoing excavations to school groups and the general Greek public through site tours and internet resources. The Corinth Excavations work hard to bridge the gap between academia and public knowledge, with publicly accessible digital resources and outreach programs to educate the public on the site and what life was like in ancient Greece. With their educational resources ranging from kindergarten through grade 12, students can

learn about archaeological methodology and the vast history of Ancient Corinth (https://www.ascsa.edu.gr/excavations/ancient-corinth/outreach-and-education).

This level of public engagement and drive to disseminate archaeological knowledge to the public, in hopes to encourage more interest and research in Ancient Corinth, made this research a particularly rewarding and enriching experience. During our time excavating the graves, school groups would frequently visit the site and spend time learning about the 2022 NET excavations. During our post-excavation analysis period, we were visited by other school groups and the ASCSA students involved in the excavations to the south of the NET Cemetery. Short presentations of our preliminary research were given by myself and my colleague Jessica Clarke, in hopes to educate the public on bioarchaeological work being conducted in Corinth, and to further work to bridge the gap between academia and public knowledge. The first step in making this thesis research available to the public will be to have a digit copy available through UW Space (https://uwspace.uwaterloo.ca/). Hopefully this accessibility will encourage future discussions and further bioarchaeological interest in Ancient Corinth.

It should be noted that there is a need to prioritize a better storage system for housing the skeletons excavated at Ancient Corinth. To ensure the preservation of these skeletons in storage, the bones should be moved from their wooden containers and into something more stable, such as conservation quality plastic bags or containers. For future bioarchaeological research to continue with the skeletons excavated at Ancient Corinth, it would be beneficial to have proper storage to ensure long-term survivability of the skeletons with climate control to ensure the preservation of these organic materials.

1.6 Proposed Venue for Publication

It would be appropriate to publish chapter two of my thesis research in the *International Journal of Paleopathology* (IJPP). This journal publishes original research

articles and case studies that focus on human disease through the analysis of skeletal remains using a variety of methods, such as direct observation. A main interest of the IJPP is to present discussions of methodological applications to reconstruct health, disease, and life histories of people in the past (https://www.elsevier.com/journals/international -journal-of-paleopathology/1879-9817/guide-for-authors). “The journal also encourages papers covering interpretive and theoretical issues and those that place the study of disease at the centre of a bioarchaeological or biocultural approach” (https://www.elsevier.com/journals/ international-journal-of-paleopathology/1879-9 817/guide-for-authors).

Chapter Two: An Analysis of a Perplexing Group of Graves from Ancient Corinth, Greece

2.1 Introduction to Ancient Corinth

Corinth is an ancient Greek city and archaeological site rich with thousands of years of history and material culture. Corinth has been occupied from the Early Neolithic period (6500-5750 B.C.E.) to the present day (Zervos et al., 2009; Sanders et al., 2018). The city is located near a stretch of land 6 km across, called an isthmus that separates the Gulf of Corinth, which extends east from the Adriatic Sea, from the Saronic Gulf, which extends south into the Aegean Sea (*Figure 1* and *2)*. The isthmus is what connects the Peloponnese to mainland Greece, and is crucial to understanding Corinth's long, rich history. Dominating and controlling the isthmus, the wealthy city prospered as an *entrepôt* and an emporium, and is described as being the centre of all road communications in southern Greece (Sanders et al., 2018: 11).

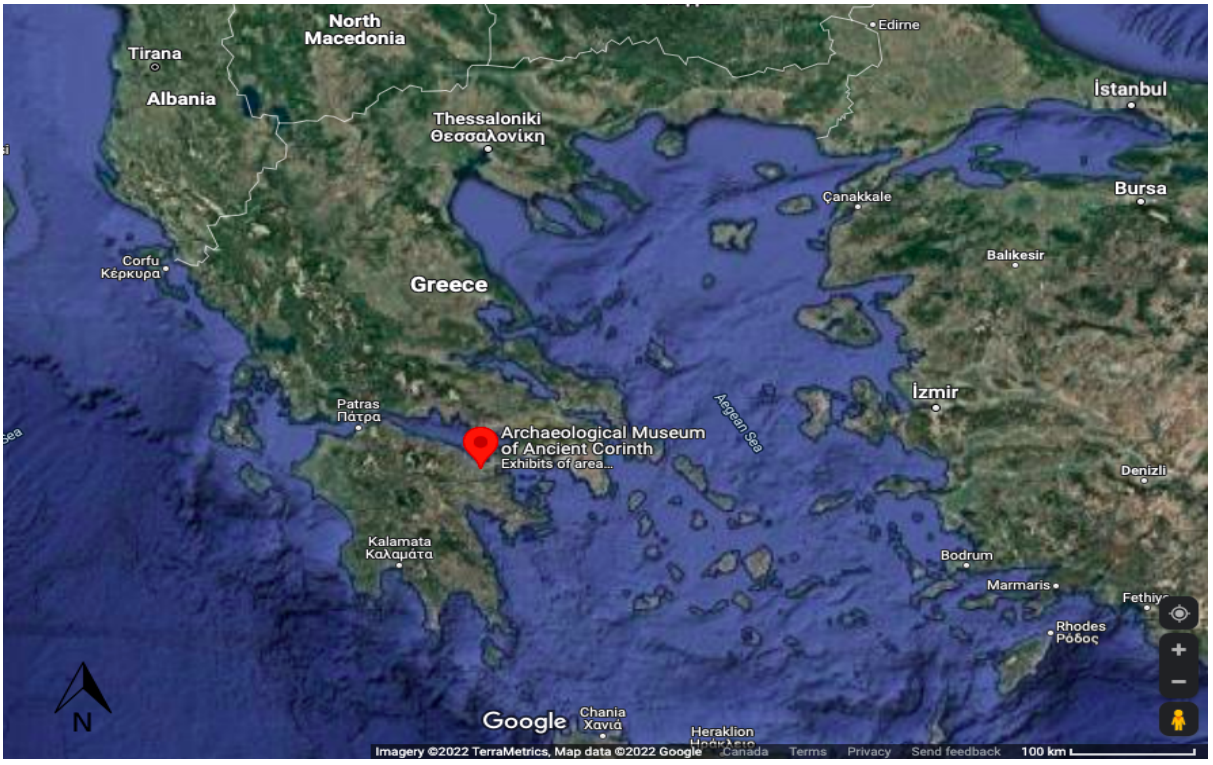

Figure 1: *Map of Greece with Archaeological Museum of Ancient Corinth located in red (photo: Google Earth)*

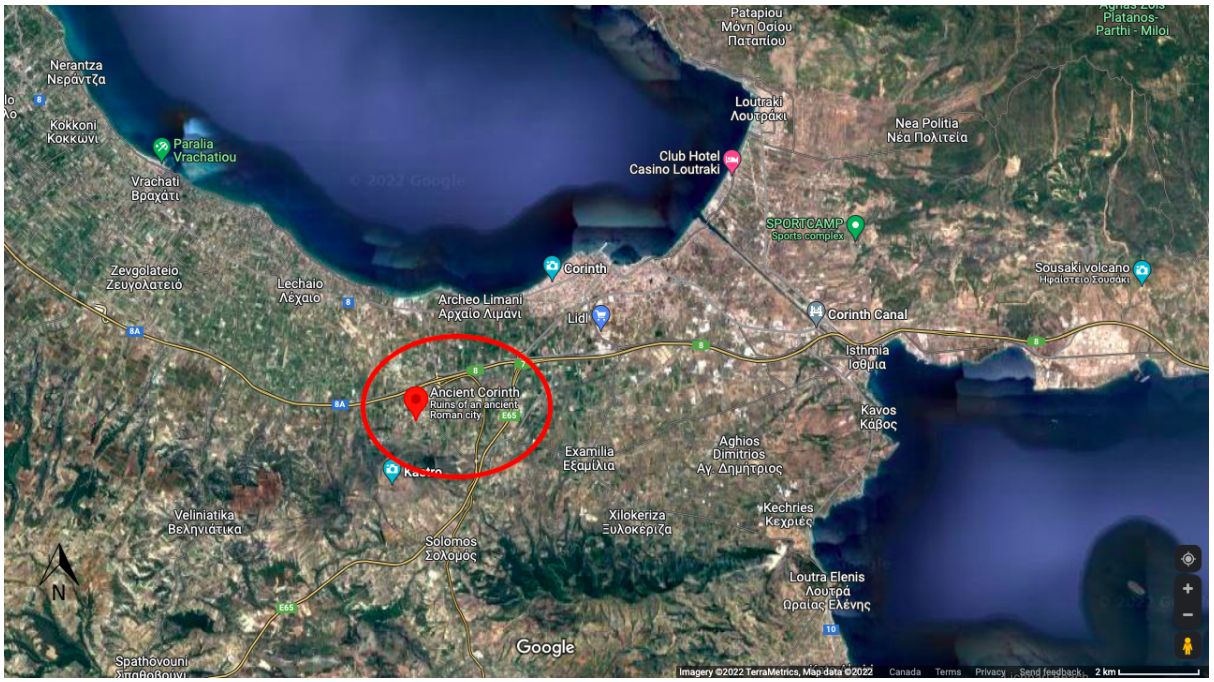

Figure 2: *Close up map with Ancient Corinth located in red (photo: Google Earth)*

Excavations at Ancient Corinth began in 1896, and it is the longest-running excavation of the American School of Classical Studies at Athens (ASCSA) (https://www.ascsa.edu.gr/excavations/ancient-corinth). The ASCSA has focused excavations on the area surrounding the Temple of Apollo (*Figure 3*). Excavations over the years have revealed thousands of years of material culture including coins, ceramics, and other objects, which are housed and studied at the Corinth Museum and the new excavations *apothiki* (Greek for 'warehouse/storage'). (https://www.ascsa.edu.gr/excavations/ancient-corinth/about-the-excavations-1).

While there is a remarkable amount of published literature regarding archaeological material from antiquity (*Hesperia* and *American Journal of Archaeology*), information concerning post-medieval Corinth is comparatively scarce (Zervos et al., 2009). Even more so, bioarchaeological investigations in Ancient Corinth have received little attention, although J. Lawrence Angel studied them for several decades, beginning with his dissertation work (Angel, 1944; 1945; 1964; 1966; 1969; 1972), and in the last several decades, Ethne

Barnes of Arizona State University has periodically published studies (Barnes & Ortner, 1997; Williams et al., 1998; Barnes, 2003; Zervos et al., 2009). The skeletons are also occasionally the subject of graduate and PhD research (Fox Leonard, 1997; Garvie-Lok, 2001; Siek, 2014).

In 1998, Williams et al. published an article on the 1990's excavations at Ancient Corinth, which were conducted to the south and southeast of the Corinth Museum (*Figure 3)*. These excavations explored the remains of the city during the Frankish period (1210-1458 C.E.), and a cemetery from the late 13th century C.E. was identified. This cemetery was in the process of being excavated since 1991, contained more than 200 individuals, and was likely related to a hospice (Williams et al., 1998). Osteological analyses of these graves were conducted by Ethne Barnes, who identified skeletal evidence of anemia, brucellosis, rheumatoid and septic arthritis, and trephination, to name a few.

In 2009, Zervos et al. published an excavation report and osteological analysis of 81 graves excavated from an early Ottoman period (17th century C.E.) cemetery in Panayia Field (*Figure 3).* This cemetery was excavated from 1995-1997, and contained both Christian and Muslim grave styles, containing a total of 133 individuals. Osteological analyses by Ethne Barnes revealed that these people were subject to functional stress reflecting habitual behaviours, and skeletal evidence of anemia, brucellosis, trauma, metastatic cancer, and periodontal disease were identified, among others.

2.2 The Northeast of Theatre (NET) Cemetery

The 2022 excavation season at Ancient Corinth was conducted in the area northeast of the ancient theatre where work commenced in the spring of 2018 (*Figure 3*). The aim of the 2022 ASCSA excavation was to understand this part of the city in both its Greek and Roman phases (for more information see Pfaff, 2020; Pfaff, 2021). While the northeast of the ancient theatre (NET) excavations were underway in a complex of Roman buildings to the south, Dr.

Maria Liston, Jessica Clarke, and I conducted our own excavations ~50 metres to the north, where a section of a 12th century C.E. or later date cemetery had been identified and partially excavated in 2019. Early in the 2022 season the soil overlying the graves had been removed, and the outline of the grave cuts had been defined before we arrived.

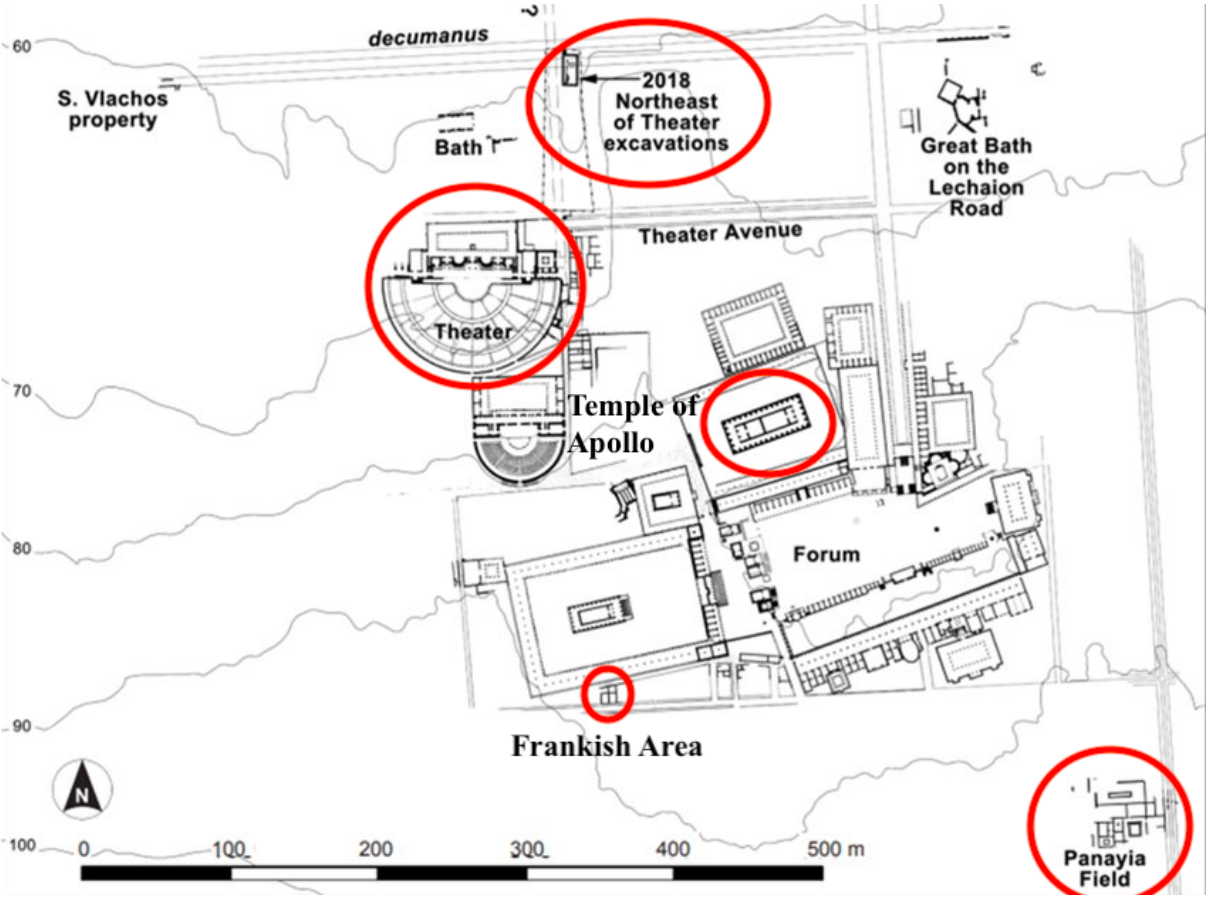

Figure 3: *Map of Corinth Excavations (from Pfaff, 2020: 127. Modified by G. Lenz)*

Four graves were excavated from the NET Cemetery in 2019 by the ASCSA from trench 2C — 2019-1, 2019-2, 2019-5, and 2019-7. The skeletons were sent to the *apothiki*, where all of the skeletons excavated at Corinth are housed and studied. The aim of the 2022 excavation season was to excavate the remaining graves identified in trenches 2B and 3B, and create a preliminary report of each skeleton. Combining the four skeletons excavated in 2019, and the seven graves excavated in 2022, a total of 11 skeletons have been identified and excavated. Burial ID numbers, skeleton numbers, deposit numbers and bone lot numbers

were assigned for each skeleton. For the purpose of this thesis, burial ID numbers (or grave numbers) will be used for identification of each individual (*Table 1*).

Prior to our arrival at Ancient Corinth in May 2022, a roof tile grave of a young child was unexpectedly discovered in dumped fill to the south of the NET Cemetery in trench 15B. This grave and individual's remains were excavated and given the grave number 2022-1. The skull of another child was excavated in trench 14B in June 2022, also in the excavation to the south. Due to the fact that this individual did not have a clear, identifiable grave, nor any other skeletal elements besides a partially complete skull, no grave number was assigned but rather, a skeleton number. This individual will be referred to as 'Skeleton 17'.

Table 1: List of the NET Skeletons

Grave Number	Skeleton Number	Deposit Number
2022-2	13	NET 2B-10
2019-1	13	NET 2C-18
2019-2	22	NET 2C-21
2019-3	12	NET 2B-8
2019-4	11	NET 2B-7
2019-5	50	NET 2C-49
2019-6	14	NET 2B-9
2019-7	64	NET 2C-63
2019-8	15	NET 3B-7
2019-9	16	NET 3B-8
2019-10	17	NET 3B-9
2022-1	19	NET 15B
(No grave)	17	NET 14B

The full extent of the NET Cemetery and time of use is not known. An olive tree grove to the west of the excavated trenches limits the ability to extend the cemetery at this

time, although the excavations have recently purchased the land. Future extension of the excavations to the west and south may unearth more graves that are associated with this cemetery, and the individuals buried there. Due to the fact that the two juveniles excavated in trenches 14B (Skeleton 17) and 15B (2022-1) are not known to be associated spatially or temporally with the individuals buried in the NET Cemetery, these two individuals will be discussed separately.

2.3 The Graves

It is noteworthy that it is relatively rare for newly excavated, unpublished material to be the focus of a Master's thesis. The mortuary context of the graves and interpretation of funerary practices performed by the living will be discussed in the following section. A discussion of estimated biological sex, age-at-death, and a survey of pathologies per skeleton will follow.

Before proceeding, it is important to distinguish between the terms 'burial' and 'grave' used in the following sections. Drawing from Parker Pearson (1999), a 'burial' represents one single funeral, where the living place a deceased person's corpse into a prepared 'grave'. It is possible that more than one individual can be placed into a grave, and it was common in ancient Greece for graves of nearly all periods to be reused (Kurtz & Boardman, 1971). The reopening of an older grave to place a newly deceased individual within indicates that the individuals who buried the deceased were aware of the location of the cemetery and graves (Kurtz & Boardman, 1971). This was observed in one grave in the NET Cemetery, and will be discussed in further detail.

From mid-May to mid-June 2022, the remaining previously identified seven graves from the NET Cemetery were excavated and sent to the *apothiki* for further analysis — 2019-3, 2019-4, 2019-6, 2019-8, 2019-9, 2019-10, and 2022-2. The four skeletons excavated by the ASCSA in 2019 had excavation notes available from the previous excavators.

The position of the head, arms, hands, and legs can contribute to interpreting funerary behaviour and differentiating between different grave styles (Parker Pearson, 1999). Christian graves are oriented east-west, with the person lying on their back, head at the west end, legs extended, and arms folded over the chest or pelvic area (Parker Pearson, 1999). In the Early Byzantine period in Greece (4th - 7th century C.E.), Christian graves often took the form of simple single-burial pit graves, single-burial tile graves, and cist graves — sometimes containing multiple burials (Poulou-Papadimitriou et al., 2012). Christian graves often include sparse, if any, funerary objects. By the 6th century C.E., nearly all burials in Greece were oriented this way (Poulou-Papadimitriou et al., 2012: 379). Christian graves were commonly seen in Ancient Corinth during the Late Roman period (~ 284-476 C.E.), and continue to be seen in the present day (Zervos et al., 2009).

All 11 individuals are supine, with their legs extended and their arms placed across their chest or abdomen (with the exception of 2019-7 — their right arm was placed at their side). The heads are at the west end of the grave and in some cases, were propped up intentionally with a rock or mound of dirt to face the east. This practice would allow the deceased to face Christ at his second coming (Parker Pearson, 1999). While no *identical* position of the hands and arms were observed, each individual had their arms extended across their body in a similar fashion. This would suggest that the importance of exactly replicating the position of the arms and hands of each deceased individual would not necessarily have been a major concern to those who buried them. This also might suggest that the individuals buried here were not all placed in the graves at the same time. Since there is no identical arm and hand position, and some heads were propped up or surrounded with stones, it is possible that each person was laid to rest on separate occasions. There is nothing to suggest that this cemetery represents a mass-casualty event such as a battle or epidemic.

The graves lie parallel to one another, and with the exception of the cist grave of 2022-2, the other ten graves in the cemetery were simple, shallow pit graves. Simple pit graves have been observed in numerous Greek cemeteries as early as the Mycenaean period of the Bronze Age (~ 1750-1050 B.C.E.), and this grave style continues to be used today (Kurtz & Boardman, 1971). In post-medieval Corinth, both Christians and Muslims buried their dead in pit graves, which would have been simple enough to dig in as little as an hour before placing the deceased into the grave (Zervos et al., 2009). The cist grave of 2022-2 was located to the northwest, and clearly differed from the other graves in the cemetery (*Figure 4*). Cist graves are lined and often covered in stones, which were the "standard grave type" throughout the Middle Bronze Age, or 1200 B.C.E. (Kurtz & Boardman, 1971: 24).

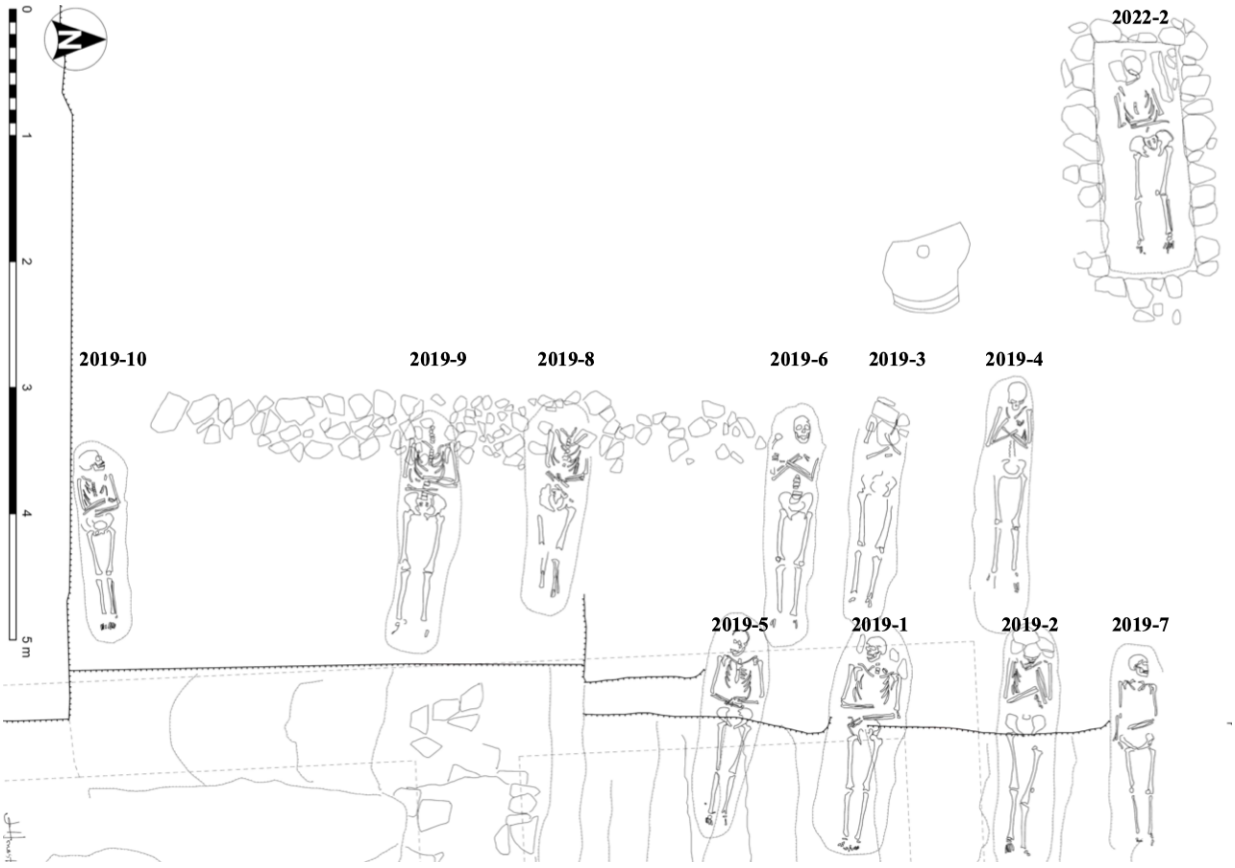

Figure 4: *The NET Cemetery Site Plan (photo: J. A. Herbst. Modified by G. Lenz)*

The pit graves are extremely shallow. From the exposed ground surface that we started with, the skeletons were buried ~ 30 cm deep. From the unexposed road surface, the

graves were no deeper than ~ 90 cm. There were no grave goods, and no headstones or identifying markers for the location of the graves. No nails were recovered during excavation, which leads to the interpretation that no coffins were used during burial. The shallow, tight size of the graves also suggests that there would not have been room surrounding the body to allow for a coffin. During excavation, some skeletons were noted to have 'verticalization' of their clavicles. This suggests that when the deceased was placed into the grave, their shoulders were pushed upward into a narrow space (Duday, 2009). This speaks to how little room there was in the graves for the bodies — there was just enough room in the pits graves to fit the body of the deceased.

Unlike the other individuals buried in the NET Cemetery, who had their heads facing east, the head of 2019-10 had fallen to the side and was facing north (*Figure 5)*. It is important to note that 2019-10 was the only juvenile excavated from the NET Cemetery. After removing the skull during excavation, it became obvious that the orientation of the skull was not intentional, and is likely the result of taphonomic processes acting on the corpse after death. The first cervical vertebrae (C1) was not articulated with the foramen magnum of the occipital (*Figure 6*), therefore the head shifted to the left during decay. If the rotation of the head had been intentional while placing the body into the grave, the first two cervical vertebrae would be rotated and the atlas (C1) and occipital would be better articulated (Duday, 2009). Based on the position of C1 and C2, it is likely that the head of this juvenile was propped up to face east, not north, when this individual was placed in the grave.

Figure 5: *2019-10 in situ with head rotated to the north (photo: G. Lenz)*

Figure 6: *2019-10 in situ, close up of foramen magnum, C1 and C2 (photo: M. Liston)*

Duday (2009) notes that this is possibly the result of the decomposition of a perishable element supporting the head, and happens when a void forms around the decomposing corpse. The force of gravity and the position of the body contributes to the displacements of other skeletal elements, such as the collapse and disarticulation of the pelvis (Duday, 2009). This is often seen in Christian burials where the individual is laid out on their back, and when there is a wide enough space in the grave for displacement to take place

(Duday, 2009). Although the verticalization of clavicles observed in multiple graves suggests that the area surrounding the shoulders and head was narrow, the disarticulation of skeletal elements in various graves indicates that these individuals may have been buried in a shroud, and there was adequate room for displacement during decomposition. It is speculated based on the Christian grave style, lack of coffins, and taphonomic evidence from grave 2019-10 that these individuals may have been tightly wrapped in a cloth shroud before burial. However, no direct evidence of this was discovered during excavation, as material evidence for the practice of shrouding seldom survives in the archaeological record (Poulou-Papadimitriou et al., 2012). Moreover, the position of 2019-10's skull indicates that this was the only individual in the cemetery who was buried with a perishable element supporting their head.

Preservation of the skeletons is moderately good. The area under which the cemetery was found was used for numerous years by the ASCSA as a road to and from the excavation site, before the cemetery and graves had been identified. Considerable post-mortem damage was done to the skeletons, and most have evidence of post-mortem pressure fractures, likely the result of vehicles driving over the shallow graves. In Greece and the Mediterranean, skeletal preservation is often poor based on the taphonomic conditions (Roberts & Buikstra, 2003: 171). Several roots from nearby orange trees penetrated through bone, severely impacting the condition of the skeletons. The state of preservation of skeletons directly impacted the data collection that followed, and the ability to accurately and precisely estimate sex, age-at-death, and make observations for pathologies.

Three out of the seven graves excavated in the summer of 2022 were affected by the subsequent construction of a rock wall, which probably formed the base of a taller mud brick wall — Wall 26 (*Figure 4* and *Figure 7*). While the timing of the construction is unknown, it is clear that whoever built Wall 26 discovered that the graves were located below — in three

skeletons, the skulls had been removed; 2019-3, 2019-8, and 2019-9 (*Figure 8*). While excavating these graves, it was noted that whoever constructed this rock wall had removed their skulls, and filled the space where the heads had been with wall construction. One skeleton, 2019-6, was located in between 2019-3 and 2019-8, however their skull remained undisturbed by the construction of Wall 26 due to the fact that their head had not been propped up to face east — it was lying flat on the ground, deeper in the grave than the others (*Figure 9*). For this reason, whoever constructed Wall 26 only removed the skulls from those who had their heads propped up higher, impacting the construction. The rest of the bodies were not disturbed by the construction. Due to the fact that the skulls of three individuals were never recovered, dental and cranial data from 2019-3, 2019-8, and 2019-9 was limited. The mandible of 2019-8 remained in-situ, and some isolated teeth were recovered, indicating that the skulls had originally been buried with the bodies. There is no evidence for decapitation or perimortem severing of the necks of these bodies.

Figure 7: *2019-3 in-situ with the base of Wall 26 covering the head (photo: G. Lenz)*

Figure 8: *2019-3 in-situ with base of Wall 26 removed. No skull recovered (photo: G. Lenz)*

Figure 9: *2019-6 in-situ with skull undisturbed by Wall 26 (photo: G. Lenz)*

As mentioned at the beginning of the section, the reuse of an older grave was observed once in the NET Cemetery — the cist grave of 2022-2. The Minimum Number of Individuals (MNI) for this grave was 2. While completing inventory recording forms in the *apothiki* after the skeleton had been removed, we noted that there were duplicate bones, with two fragments that could not have come from this individual: a fragment of the right posterior parietal and a fragment of the left pubis. The fragments of bone not belonging to 2022-2 were

heavily mineralized and pigmented, and the colour did not match that of the other skeletal elements of 2022-2. Based on this, this cist grave was used on at least two separate occasions to inter a newly deceased person. As noted in section *1.5, Public Issues Anthropology*, exhumation is a common practice in Greece, in the past and today. The body of the deceased is temporarily deposited in a grave, where it can stay for several months, to many years before being exhumed and taken to its final resting place — a village ossuary (Danforth, 1982; Dubisch, 1989; Weiss-Krejci, 2011). Moreover, the reuse of graves was not an uncommon practice in ancient Greece. Cist graves of nearly all periods are commonly reused (Kurtz & Boardman, 1971).

While not associated spatially with the NET Cemetery, it is likely that the roof tile grave of the juvenile 2022-1 from trench 15B also reflects Christian traditions. The head of this infant is also at the west end, facing east however, there is a slight deviation in orientation. While the 11 graves in the NET Cemetery are clearly laid out to face east, the location of the head of 2022-1 is slightly oriented south-west (*Figure 10* and *Figure 11*).

Tile graves in Greece were first identified in the Late Archaic period (~ 800-480 B.C.E.) and expanded from the mainland throughout the country, where they became increasingly common in the Classical period (~ 510-323 B.C.E.) (Kurtz & Boardman, 1971; Kyle et al., 2018). By the Hellenistic period (~ 323-33 B.C.E.) in Greece, the practice of lining the grave and individual buried inside with ceramic roof tiles or tile fragments was the most frequently used grave style (Kurtz & Boardman, 1971). In the early post-Frankish period (late 13th century C.E.) in Ancient Corinth, the practice gradually died out (Zervos et al., 2009). Due to the fact that there is no evidence to suggest that 2022-1 is in any way associated with the individuals in the NET Cemetery, it is possible this grave was used at a different period. Moreover, it is not uncommon to find infants and/or juveniles buried differently than adults and/or outside of formal cemeteries, in locations “set aside”

specifically for them (Kurtz & Boardman, 1971: 55; Renshaw & Powers, 2016). The location of the only juvenile from the NET Cemetery, 2019-10, in relation to the adults (*Figure 4*), and the rather perplexing location of 2022-1 and Skeleton 17, supports this. With reference to Skeleton 17, even less mortuary context exists. Only half of this individual's skull was identified in between two poros blocks, and no evidence of a grave was found. With this, estimating a date for this individual is impossible based solely on the excavation information.

Figure 10: *Roof Tile Grave of 2022-1 (photo: C. Pfaff)*

Figure 11: *2022-1 in situ (photo: J. A. Herbst)*

To summarize this section, the burial style observed in the NET Cemetery reflects Christian traditions. Based on the orientation of the burials and the reuse of the cist grave, it appears that the individuals buried here were probably members of the same community, or social group. However, based on the small sample size, lack of DNA testing, inadequate preservation, and unobserved cranial and dental metric and non-metric traits, it is not possible to interpret that these individuals were members of the same family. Due to the fact that the cist grave was used more than once, this may indicate that the local population remained aware of the location of the cemetery, and would have used this area on multiple occasions to inter newly deceased. In addition, starting ~ 7th century C.E. and into the Late Byzantine period (13th-15th century C.E.), organized Christian cemeteries are typically found near

monastery churches or in ruined ancient sites (Poulou-Papadimitriou et al., 2012: 413). Since this is a post-Byzantine cemetery, this adds to the perplexing nature of the NET graves and the individuals buried here, as it remains unclear why this location was chosen as a cemetery. Perhaps the location of the graves has something to do with the close proximity to the ancient theatre.

2.4 Dating the Cemetery

Estimating a precise chronology is always an issue, especially since single-burial pit graves, and single-burial or reused cist graves have been frequently identified across different time periods in Greece, starting in the Bronze Age (~ 1750-1050 B.C.E.) and persisting into modernity (Kurtz & Boardman, 1971). Tile graves, too, have been a common grave style in Greece as early as the Late Archaic period (~ 800-480 B.C.E.) (Kurtz & Boardman, 1971). Moreover, Christian burials have been observed in various Greek cemeteries, including at Corinth, from the Late Roman period (~ 284-476 C.E.), and continue to persist today (Zervos et al., 2009).

As noted above, no grave goods or artifacts were recovered from any of the graves during excavation. While not purposely situated with the graves themselves, green glaze-ware pottery sherds from the Byzantine period were found and identified in the grave fill, and the graves partially penetrated the packed dirt surface of a Byzantine-Ottoman road, giving a *terminus post-quem* of 12th century C.E. for the time it was in use (Pfaff, 2021). It can be said with certainty that this is at least a "post-Byzantine" cemetery, however, this provides us with a large temporal range — the 12th century C.E. was roughly 8-900 years ago, and these individuals could have been buried in this cemetery during any point later than the years 1101-1200 C.E..

In order to situate the NET skeletons within their temporal context, directly radiocarbon dating the bones is the best method. This thesis will be completed before this can

take place, therefore this is a limitation that must be acknowledged before proceeding. While speculative, it may be interpreted based on how close to the modern ground surface the graves were that they could be as late as the 19th century C.E.. Excavations in 2019 revealed the walls of a 19th century C.E. house within the layers of the Byzantine-Ottoman road (Pfaff, 2021), however, its relationship (if any) to the graves is unknown.

2.5 Methodology

All 13 skeletons excavated from the 2019 and 2022 NET excavations at Ancient Corinth are included in the sample. After excavation, all data collection took place in the bone *apothiki* in Ancient Corinth, Greece. Non-destructive methods were chosen for analysis. Data tables can be found in Appendix A. At the *apothiki* the skeletons were cleaned with water and inventoried. Depending on the preservation, biological sex and age-at-death were estimated using various methods from *Standards for Data Collection from Human Skeletal Remains* (Buikstra & Ubelaker, 1994) and *Juvenile Osteology* (Schaefer et al., 2009). Femoral head diameters were also recorded when possible to supplement the identification of sex (Bass, 1987).

Biological sex was estimated in the ten adult skeletons, but not for the three juveniles, due to the fact that methods for estimating biological sex in skeletal remains rely on sexually dimorphic osteological features in the pelvis and skull that result from differences in hormone secretion during puberty (Luna et al., 2017). Age-at-death was estimated for the 13 skeletons. For the ten adults, the following methods were selected and applied accordingly: pubic symphysis (Todd, 1921a, 1921b; Brooks & Suchey, 1990; Suchey & Katz, 1986), auricular surface (Lovejoy et al., 1985; Meindl & Lovejoy, 1989), cranial suture closure (Meindl & Lovejoy, 1985), and Standards of Occlusal Wear of Molar Teeth for Age Classification (Brothwell, 1981). The three juvenile's age-at-death were estimated from dental and skeletal development (Ubelaker, 1989; Schaefer et al., 2009; AlQahtani et al., 2010).

We also chose to estimate age-at-death in the adult skeletons using a newer method developed by Boldsen et al. (2002), called Transition Analysis 2.0 (TA2), in part because this method is being used by other projects in Greece and would allow the data to be compared more easily in future studies. TA2 can be applied to individual skeletons, and when there are incomplete or poorly preserved scoring features. Similar to the methods from *Standards for Data Collection from Human Skeletal Remains* (Buikstra & Ubelaker, 1994), this method involves scoring skeletal features from the cranial sutures, pubic symphysis, and auricular surface. However, with TA2, 19 features are scored independently, rather than as a group. This method is available as a computer program that can be downloaded on compatible devices, in which users make reference to the attached scoring manual. TA2 produces a maximum likelihood of age-at-death, along with a 95% confidence range. Eight out of the ten adult skeletons were preserved well enough to apply this new method. TA2 Scores for these individuals can be found in Appendix B.

Although a newer version was released in 2019, TA3, (Milner et al., 2019), this updated method did not work well for this sample. With TA3, features from the entire skeleton are scored in conjunction with the cranial sutures, pubic symphysis, and auricular surface, increasing the number of scorable features from 19 to 121 (Milner et al., 2019). TA3 was attempted, but it was soon discovered that TA2 was more suitable for this sample based on the state of preservation — too few features preserved well enough to score using TA3.

For the two infants, 2022-1 and Skeleton 17, age-at-death was estimated by measuring the length of loose deciduous teeth, and inserting the measurements into regression equations (Schaefer et al., 2009: 79) (Appendix A, *Table 7*). Age-at-death for 2022-1 was also estimated using postcranial measurements (Shaefer et al., 2009) (Appendix A, *Table 8*). Age-at-death was estimated for the one juvenile from the NET Cemetery, 2019-10, using

Ubelaker's (1989) Dental Development chart, and AlQahtani et al. (2010) Atlas of Human Tooth Development and Eruption. These were accessed via the internet.

It is vital to consider the fact that identifying biological parameters such as age-at-death and biological sex is "a probability statement" (White & Folkens, 2005: 360). We can never know with 100% certainty the exact age-at-death, biological sex, ancestry or stature of an individual solely through the analysis of their skeletal remains. However, we can get estimates that are accurate and precise to varying degrees, using different reliable and replicable methodologies from standardized sources.

With reference to *Standards for Data Collection from Human Skeletal Remains* (Buikstra & Ubelaker, 1994: 9) this skeletal sample is composed of two infants, one child/adolescent, six young adults, and four middle adults (*Table 2*). *Figure 12* displays the cemetery site plan with the corresponding biological sex and age-at-death estimations.

Table 2: Age Categories of the NET Skeletons

Age Category	Age range	Total Number	NET Skeleton(s)
Infant	birth-3 years	2	2022-1, Skeleton 17
Child	3-12 years	1	2019-10
Adolescent	12-20 years	1	2019-10
Young Adult	20-35 years	6	2019-1, 2019-2, 2019-3, 2019-4, 2019-6, 2019-8
Middle Adult	35-50 years	4	2022-2, 2019-5, 2019-7, 2019-9
Old Adults	50+	0	

The 30-39 year old female (2022-2) does not fit neatly into these categories, but falls closer within the range of 'middle adult'. The 12-15 year old juvenile (2019-10) also does not fit neatly into these categories, but based on the lack of sexual dimorphism in the skeleton, it can be inferred that they were likely prepubescent. The maximum estimated age-at-death is

45 years. By today's standards, this is relatively young, however life expectancy in past communities is not the same as it is now (Angel, 1947). From 3000 B.C.E to 1300 C.E. in Greece, there is a gradual rise in average age-at-death in adult skeletons (Angel, 1947). There is roughly a 4-5 year increase in life expectancy from any given time period — likely the result of hygiene and living conditions improving with time (Angel, 1947). He notes that even though life expectancy increased in Greece over time, the average age-at-death from the third millennium B.C.E to the medieval period is still well below modern-day life expectancy. Due to the fact that the skeletal sample from the NET excavations is small, the biological profile of these individuals is only representative of what has been excavated so far and may not be a representative sample.

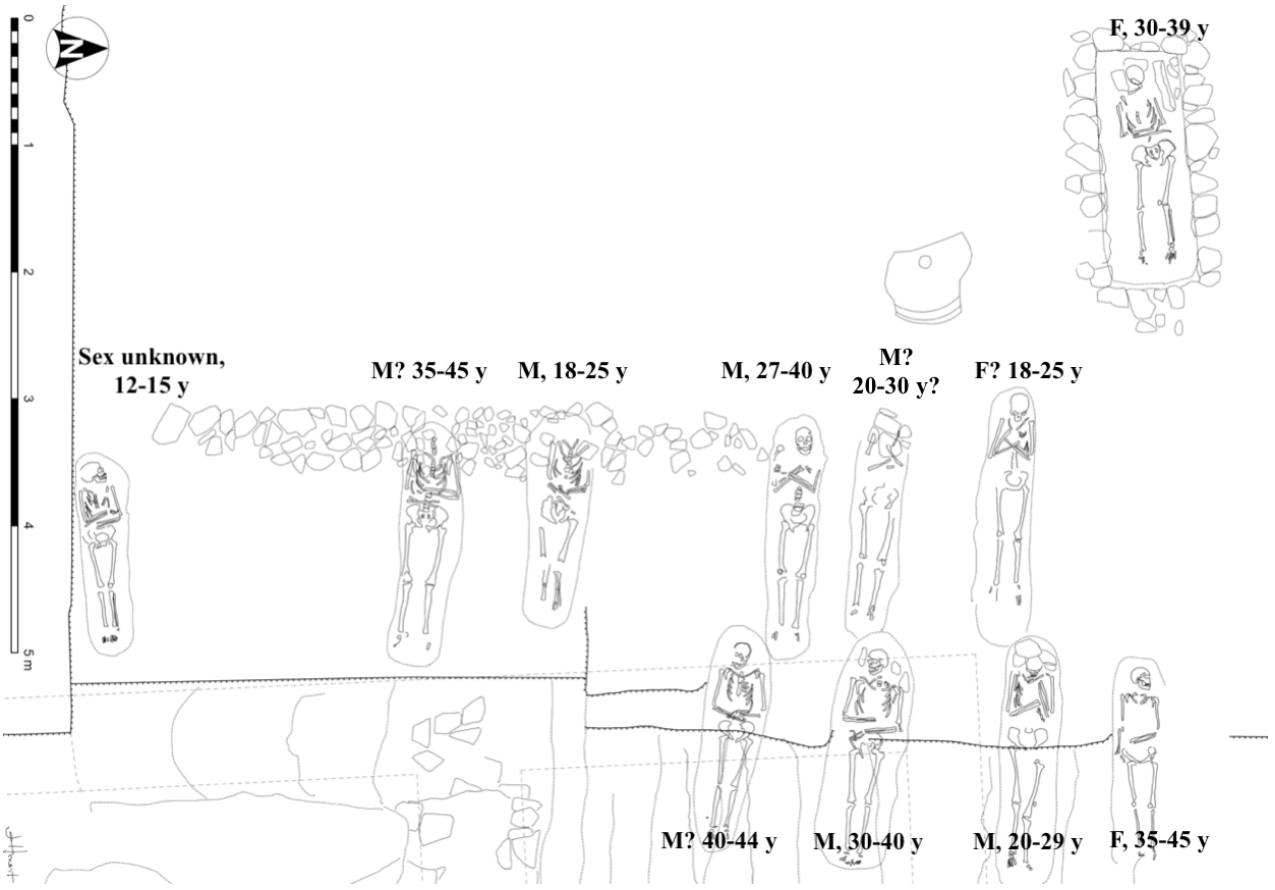

Figure 12: *The NET Cemetery Site Plan with Biological Sex and Age-at-death (photo: J. A. Herbst, Modified by G. Lenz)*

While the full extent of the NET Cemetery has not been identified at this time, it is worth noting that the females are at the north end of the rows, and the juvenile is at the south end of one row, slightly separated from the other graves. It is not clear if this pattern has any significance.

Following the estimation of biological sex and age-at-death for the NET skeletons, observations for pathological conditions were recorded as written description. Each skeleton was carefully examined macroscopically for any abnormalities or visible signs of pathology. *The Human Bone Manual* (White & Folkens, 2005) *The Archaeology of Disease* (Roberts & Manchester, 2007) and *Ortner's Identification of Pathological Conditions in Human Skeletal Remains* (Buikstra, 2019) were the main texts used for identifying abnormalities.

2.6 Osteological Analysis of the NET Cemetery Skeletons

This section will serve as a discussion of the pathologies observed in each of the NET Cemetery skeletons, and will provide an in-depth analysis for each individual. The order in which each individual is presented is simply numerical order, starting with 2022-2 so as to keep the three juveniles together: 2019-10, 2022-1 and Skeleton 17. The two infants will be discussed together in section *2.7, Osteological Analysis of the Infant Skeletons*.

Grave Number: 2022-2
Sex: Female
Age-at-death: 30-39 years

Description: Osteophytes were observed in the first two cervical vertebrae of this female's neck, at the atlas (C1) and axis (C2), where the dens articulates with the atlas (*Figure 13*). There is moderate dental wear exposing dentine, and significant buildup of calculus — especially in the right first and second maxillary molars (*Figure 14*). Linear enamel hypoplasia (LEH) was identified on some maxillary teeth, on the left canine, and the right and left first premolars. Antemortem tooth loss was noted in the mandible, as well as an

abscess (*Figure 15*). The right and left second premolar, and the right first, second, and third molars were lost during life. No dental caries observed.

Analysis: Osteophytes are bone spurs that grow from joint surfaces, and can form when the body compensates for the stress applied to the joint over a period of time (Roberts & Manchester, 2007: 135). The osteophyte growth seen in this female's neck is likely the result of repeated mechanical stress over time, and due to the location, may have been the result of carrying heavy loads on their head (Roberts & Manchester, 2007). The formation of osteophytes is also noted as being a result of aging, which likely was a factor, but not the only one. It is suggested that the formation of osteophytes in this individual's neck is a skeletal marker of occupation and age.

The presence of calculus (calcified bacterial plaque that forms on tooth surfaces throughout an individual's life), but no dental caries (cavities), suggests that this may indicate that this female had a diet high in protein and carbohydrates (Roberts & Manchester, 2007; Kinaston et al., 2019). Losing permanent teeth occurs either through trauma, chronic pathology, or through intentional means (Kinaston et al., 2019: 770). The loss of permanent molars during life would have impacted this female's ability to chew on that side of their mouth. The dental wear in the left mandibular molars indicate that this female likely chewed exclusively on the left side, as a result of the tooth loss.

LEH is defined as "horizontal bands of depression that run along the tooth's surface" (Kinaston et al., 2019: 753), which are "non-specific indicators of stress" (Roberts & Manchester, 2007: 75). The presence of LEH suggests that this individual went through periods of stress in their childhood, when their teeth were still forming (Hillson, 1996; Roberts & Manchester, 2007). Since these defects are the result of systemic growth disruptions that permanently alter the tooth's surface, the presence of LEH in this 30-39 year old female indicates that they went through periods of stress in their childhood, resulting

from either metabolic stress, nutritional deficiency, or childhood illness (Hillson, 1996; Roberts & Manchester, 2007). However, they survived and overcame the non-specific stress endured in childhood, and lived into adulthood.

Figure 13: *2022-2 — Osteophyte growth of C1 and C2 (photo: M. Liston)*

Figure 14: *2022-2 — Calculus deposits on right maxillary molars (photo: M. Liston)*

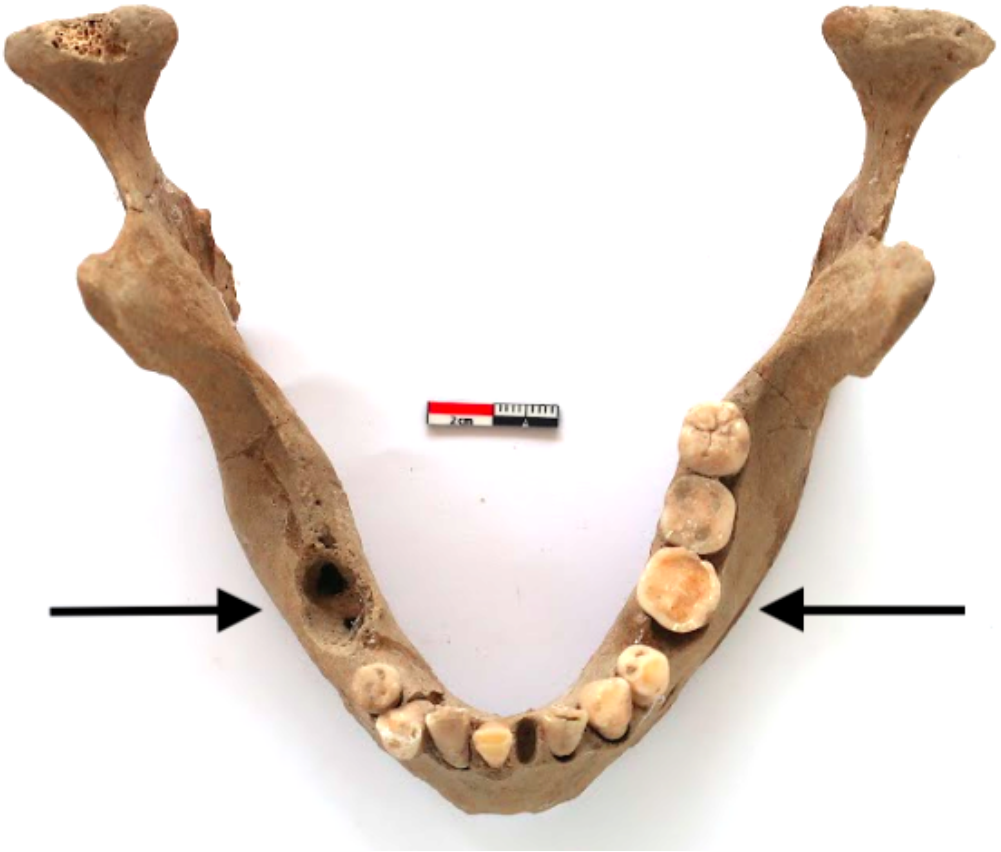

Figure 15: *2022-2 — Antemortem tooth loss and tooth wear in the mandible (photo: M. Liston)*

Grave Number: 2019-1
Sex: Male
Age-at-death: 30-40 years

Description: This 30-40 year old male has possible osteochondritis dissecans in their left foot, in the first proximal phalanx, and first metatarsal — both at the proximal articulation (*Figure 16*). Possible osteochondritis dissecans was also identified in their right hand at the proximal articulation of the third metacarpal (*Figure 16*). With reference to Roberts and Manchester (2007: 121), this diagnosis should be cautioned, as the lesion observed in these anatomical locations may be the result of defects in the joint that are sometimes confused with osteochondritis dissecans.

LEH was observed on the mandibular teeth, on the left and right canines, the left and right first premolars, and the left second molar. In the maxilla, LEH was identified on the right first and second premolar, and the first molar. On the left side of the maxilla, LEH was identified on the second premolar. There is agenesis or impaction of the left third molar in the mandible. Dentine is exposed in both first molars on the left and right side of the mandible, and small deposits of calculus was observed, most noticeably in the mandibular incisors and canines. No dental caries or antemortem tooth loss was observed.

This male also has bilateral septal apertures of the olecranon fossa in their distal left and right humerus (*Figure 17*), which is a genetic variant that Klaus and Lynnerup (2019: 59) describe as falling within the “range of normal”.

Analysis: Osteochondritis dissecans is a disease associated with trauma and vascular deficiencies (Grauer, 2019: 500). Resnick et al. (1995: 2611) describe osteochondritis dissecans as a process involving fragmentation of cartilage and in some cases, subchondral bone. When osteochondritis dissecans is present, there is an observable depression on the articular surface of a skeletal element (Grauer, 2019: 501). Zúñiga Thayer et al. (2020) noted in their study that the first proximal phalanx of the foot is a non-typical joint for

osteochondritis dissecans. Wells (1974) describes the use of shoes that "reduce flexion during walking and microtrauma related to physical activities" as a potential causation of osteochondritis dissecans at this particular joint (Zúñiga Thayer et al., 2020: 83). Zervos et al., (2009: 545) noted wear facets on the first metatarsal in four adult males in their study from Panayia Field in Ancient Corinth, interpreting that this abnormality may reflect habitual kneeling positions. Perhaps the skeletal lesions seen in this male's feet and hand bones are a reflection of these types of physical activities.

Similar to 2022-2, the presence of LEH on this individual's mandibular and maxillary teeth indicates that they went through non-specific periods of stress in their childhood, resulting from either metabolic stress, nutritional deficiency, or childhood illness (Hillson, 1996; Roberts & Manchester, 2007). Again, this male survived into adulthood, but evidence for growth disruptions in childhood as a result of non-specific stress is still visible in their dentition. As with 2022-2, the presence of calculus may suggest a diet high in protein and carbohydrates (Roberts & Manchester, 2007; Kinaston et al., 2019).

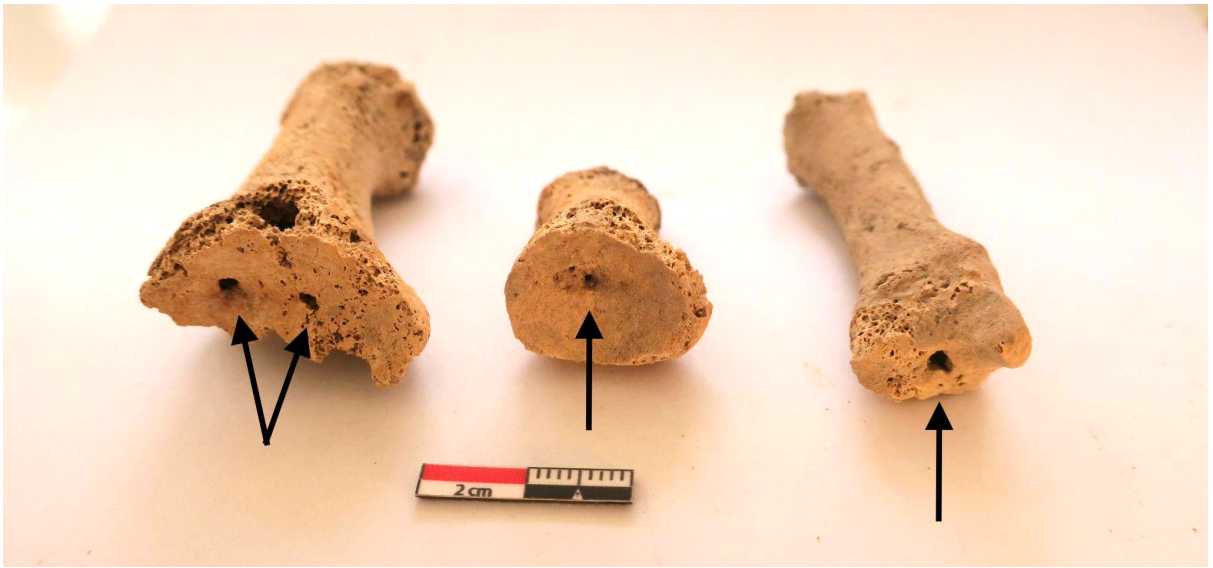

Figure 16: *2019-1 — Possible osteochondritis dissecans of the left first metatarsal (left), left first proximal foot phalanx (middle), and right third metacarpal (right) (photo: M. Liston)*

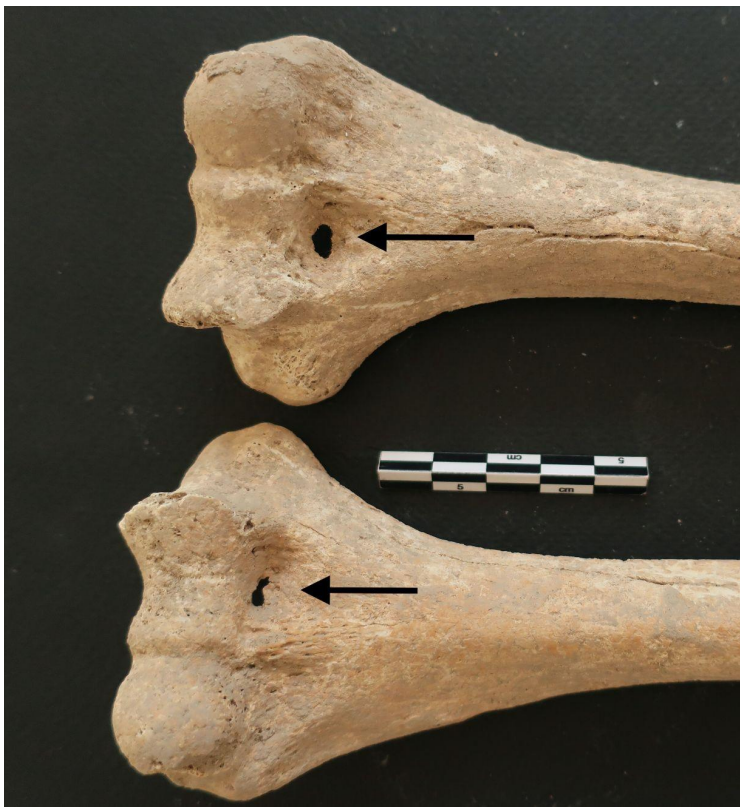

Figure 17: *2019-1 — Bilateral septal apertures (photo: M. Liston)*

Grave Number: 2019-2
Sex: Male
Age-at-death: 20-29 years

Description: This young adult male has an entheseal change in their left medial clavicle (rhomboid fossa), at the attachment site of the costoclavicular ligament (*Figure 18*). They also have an entheseal change located at the right proximal fibula (*Figure 19*). There is a bilateral entheseal change of the left and right distal ulna — well developed flexor (*Figure 20*). In the right distal ulna, there is a well developed extensor carpi ulnaris groove (*Figure 21*). In the initial recording forms, it was noted that the metatarsals and phalanges have atrophied. Small deposits of calculus and minor wear with some dentine exposure was noted in the dentition. No dental caries or antemortem tooth loss were observed.

Analysis: Entheseal changes, or enthesopathies, are identified as either new bone formation (exostosis) or bone erosion at muscle attachment sites (Mariotti et al., 2004). Entheseal changes are often referred to as musculo-skeletal stress markers, and can be analyzed to

interpret activity patterns and lifestyles in the past (Roberts & Manchester, 2007: 146). However, entheseal changes have multifactorial etiologies (Mariotti et al., 2004). The development of these skeletal changes may be "an expression of idiopathic factors in the bone's response to various stimuli or even be part of normal age-related changes" (Mariotti et al., 2004: 148). The entheseal change noted in the medial clavicle (rhomboid fossa) may represent an erosive bone response to mechanical stress over a period of time, and could indicate that this person was involved in strenuous activities with their left arm (Milella et al., 2012). The skeletal changes at numerous muscle attachment sites in this individual's skeleton may be associated with activity, and/or age-related changes.

Figure 18: *2019-2 — Entheseal change of the left medial clavicle (rhomboid fossa) (photo: M. Liston)*

Figure 19: *2019-2 — Entheseal change of the right proximal fibula (photo: M. Liston)*

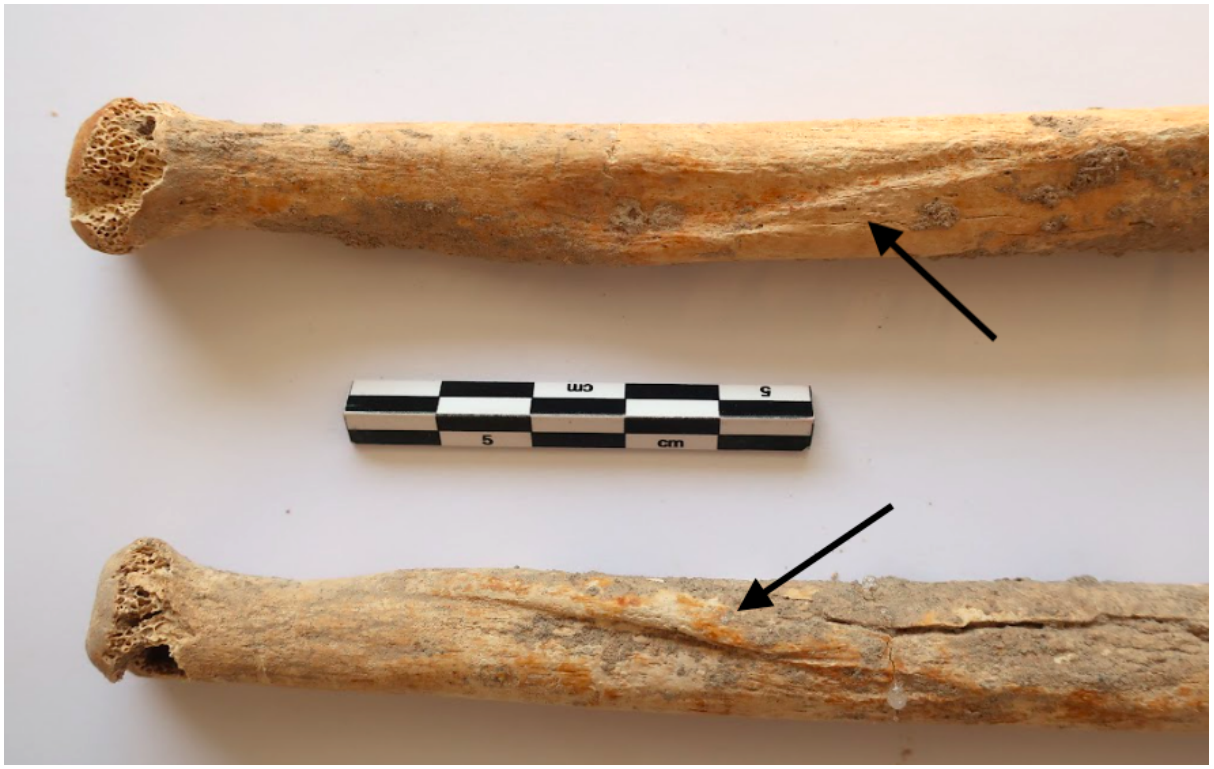

Figure 20: *2019-2 — Entheseal changes of the left and right distal ulnae (photo: M. Liston)*

Figure 21: *2019-2 — Well developed extensor carpi ulnaris groove of the right distal ulna (photo: M. Liston)*

Grave Number: 2019-3
Sex: Male?
Age-at-death: Late 20's-Early 30's?

Description: 2019-3 has robust muscle attachments in their right hand: on the second, third, and fifth metacarpals (*Figure 22*). There is also a minor osteophyte growth on their left scaphoid (*Figure 23*). Bilateral entheseal changes were noted on the proximal left and right fibulae (*Figure 24*), and on the proximal right humerus at the insertion of the pectoralis major (*Figure 25*).

Analysis: This individual is the poorest preserved. Estimates for biological sex and age-at-death were based solely on in-situ appearances while excavating this individual's grave, as no scorable features were preserved. Based on the narrow subpubic angle and robusticity of skeletal elements, this individual is a probable male. The epiphyses of the long bones were all fused, and there was a lack of degenerative changes such as osteoarthritis,

suggesting this individual was a younger adult. If we had not been involved in the excavation, this individual's biological sex and age-at-death could not be estimated using standardized methods (Buikstra & Ubelaker, 1994). The entheseal changes noted in this individual may reflect what could be normal skeletal variation (Mariotti et al., 2004). The enlarged muscle attachments seen in the metacarpals could also represent an entheseal change as a result of manual labour over a period of time (Roberts & Manchester, 2007).

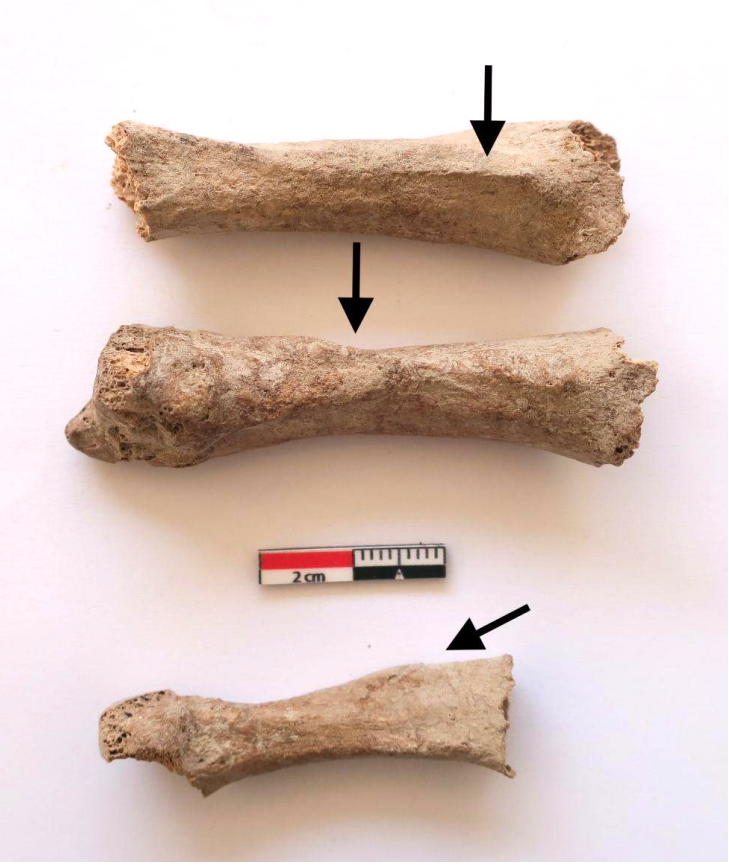

Figure 22: *2019-3 — Robust muscle attachments of the right hand; second (top), third (middle), and fifth (bottom) metacarpals (photo: M. Liston)*

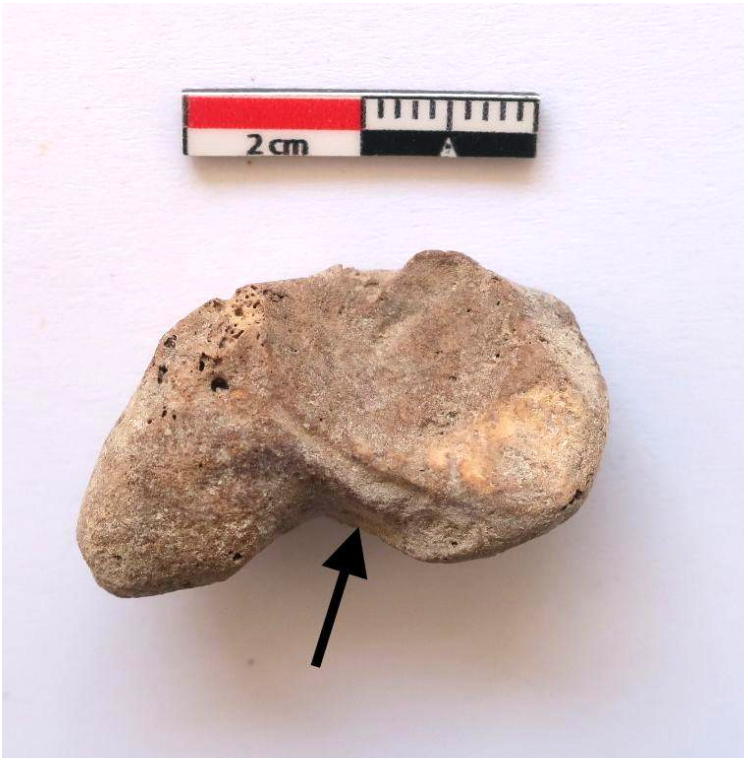

Figure 23: *2019-3 — Osteophyte growth of the left scaphoid (photo: M. Liston)*

Figure 24: *2019-3 — Entheseal changes of the proximal left and right fibulae (photo: M. Liston)*

Figure 25: *2019-3 — Entheseal change of the proximal right humerus (photo: M. Liston)*

Grave Number: 2019-4
Sex: Female?
Age-at-death: 18-25 years

Description: This probable female has bilateral entheseal changes located on the proximal left and right humerus (*Figure 26*). Similar to 2019-2, 2019-4 has an entheseal change in their left medial clavicle (rhomboid fossa), at the attachment site of the costoclavicular ligament (*Figure 27*). Unlike 2019-2, this probable female has *bilateral* entheseal changes — erosion was also noted in their right medial clavicle. The erosion noted in their right clavicle is smaller than the depression seen in their left clavicle. There is also an enlarged mental and mandibular foramen in the left side of their mandible, and an enlarged mandibular foramen in the right side (*Figure 28*). This may be the result of an unknown infection (Hillson, 1996; Roberts & Manchester, 2007). This individual also has moderate tooth wear, and small deposits of calculus.

Analysis: In clinical cases, entheseal changes at the attachment site of the costoclavicular ligament in medial clavicles can be unilateral, as seen in 2019-2, or bilateral, as seen in this individual (Koudela et al., 2015). These changes are typically seen in younger males, with more significant erosive changes frequently seen in 20-30 year olds (Koudela et al., 2015).

The entheseal change noted in the left and right medial clavicles may represent a bone response to mechanical stress over a period of time, and could indicate that this person was involved in strenuous activities with both of their arms (Milella et al., 2012). However, it is important to reiterate that entheseal changes have a multifactorial etiology, with many potential factors related to the changes seen in the medial clavicle (Mariotti et al., 2004). Moreover, when an entheseal change in the medial clavicle is bilateral, it is more likely that this is associated with skeletal variation, and is non-pathological (Rogers et al., 2000).

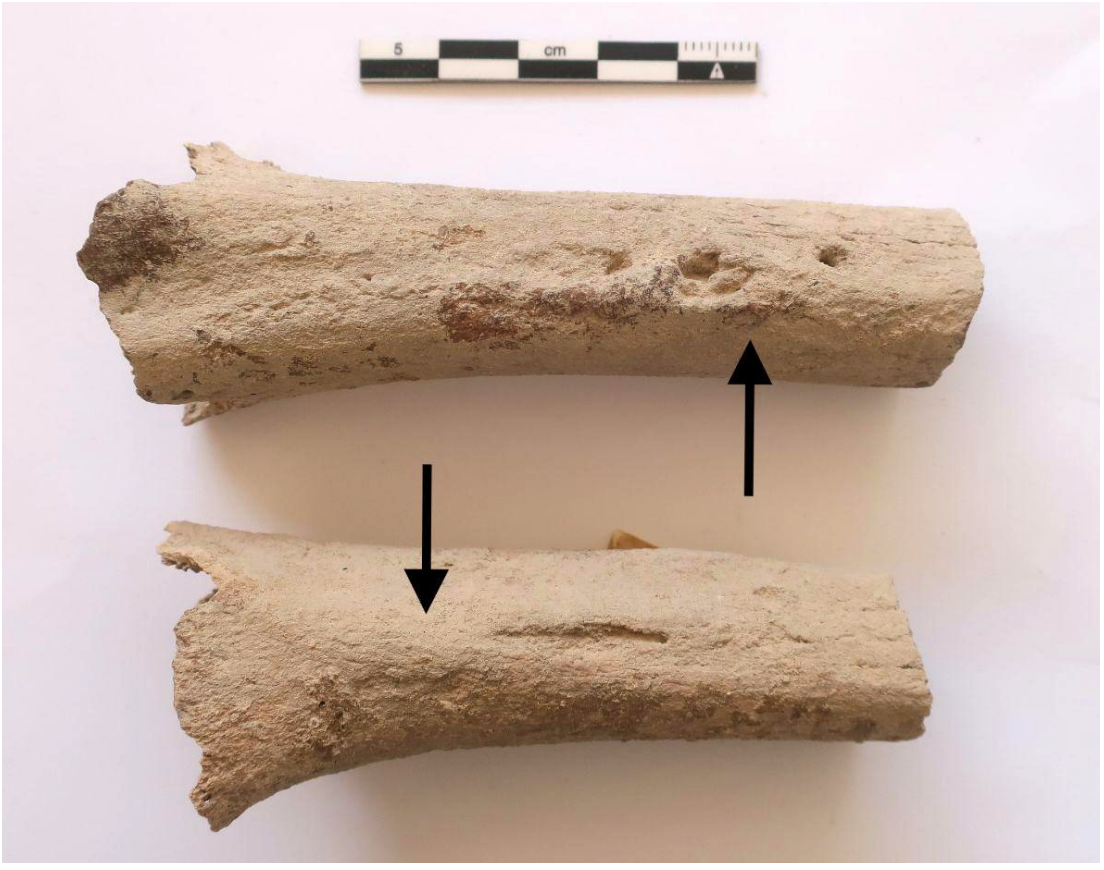

Figure 26: *2019-4 — Entheseal changes of the proximal left and right humerus (photo: M. Liston)*

Figure 27: *2019-4 — Entheseal changes of the left and right medial clavicle (rhomboid fossa) (photo: M. Liston)*

Figure 28: *2019-4 — Enlarged mandibular foramen (photo: M. Liston)*

Grave Number: 2019-5
Sex: Male?
Age-at-death: 40-44 years

Description: In this individual's cervical vertebrae, bifurcate spinous processes were identified in C3-C6 (*Figure 29*). This likely represents morphological skeletal variation, and is non-pathological (Ludwisiak et al., 2019). The right superior articular facets of C3 and C5 also have evidence of abnormalities, which resemble osteophyte growth (*Figure 30*). The right superior articular facet of C3 possibly resembles a healed fracture. A rib fragment of unknown side or number has an osteophyte protruding from the articular facet (*Figure 31*).

This probable male has LEH on numerous teeth. LEH was identified on the right maxillary canine, and second and third molars. From the left side of the maxilla, LEH was identified on the first premolar, and second and third molars. In the mandible, LEH was identified on the right and left canines. Reduction of the alveolar bone in the mandible was also identified (*Figure 32*). This individual has minor tooth wear facets and minor deposits of calculus. No dental caries or antemortem tooth loss.

Analysis: It is possible that the abnormalities noted on the right superior articular facets of C3 and C5 is a case of facet joint osteoarthritis, which is more common in the mid-cervical region and commonly affects older adults (Gellhorn et al., 2013). Similar to 2022-2, the osteophyte growth in the cervical vertebrae and isolated rib fragment may be the body's way to compensate for stress being applied to the joint over a period of time (Roberts & Manchester, 2007: 135). It is also possible that this could be a normal result of aging, as this individual likely died while they were in their 40's.

As with the other two adults with LEH (2022-2 and 2019-1), this 40-44 year old went through non-specific periods of stress in their childhood (Hillson, 1996; Roberts & Manchester, 2007). This individual also survived these periods of stress, and reached

middle-adulthood. The reduction of the alveolar bone may be associated with periodontal disease (Roberts & Manchester, 2007).

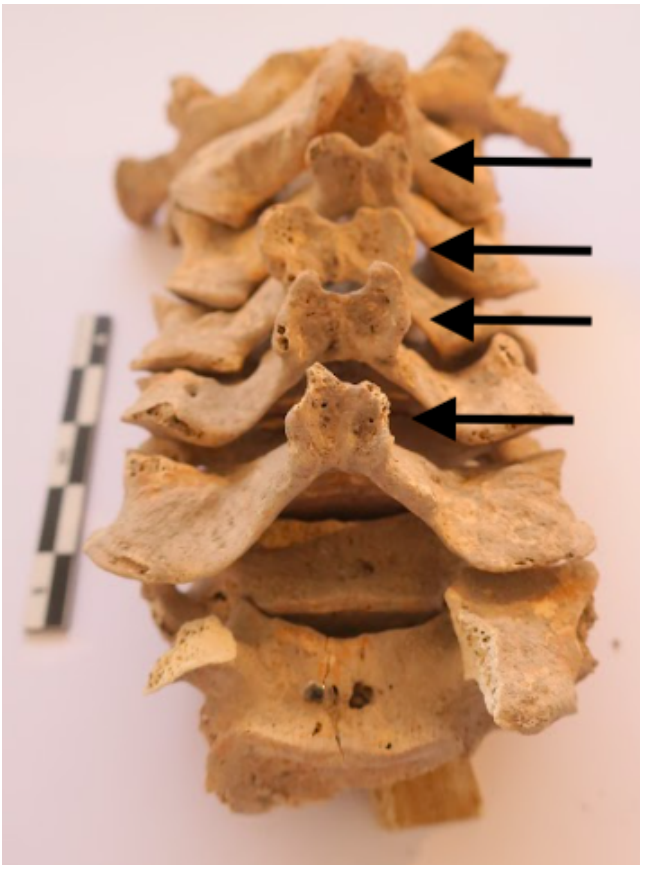

Figure 29: *2019-5 — Bifurcated spinous processes of C3-6 (photo: M. Liston)*

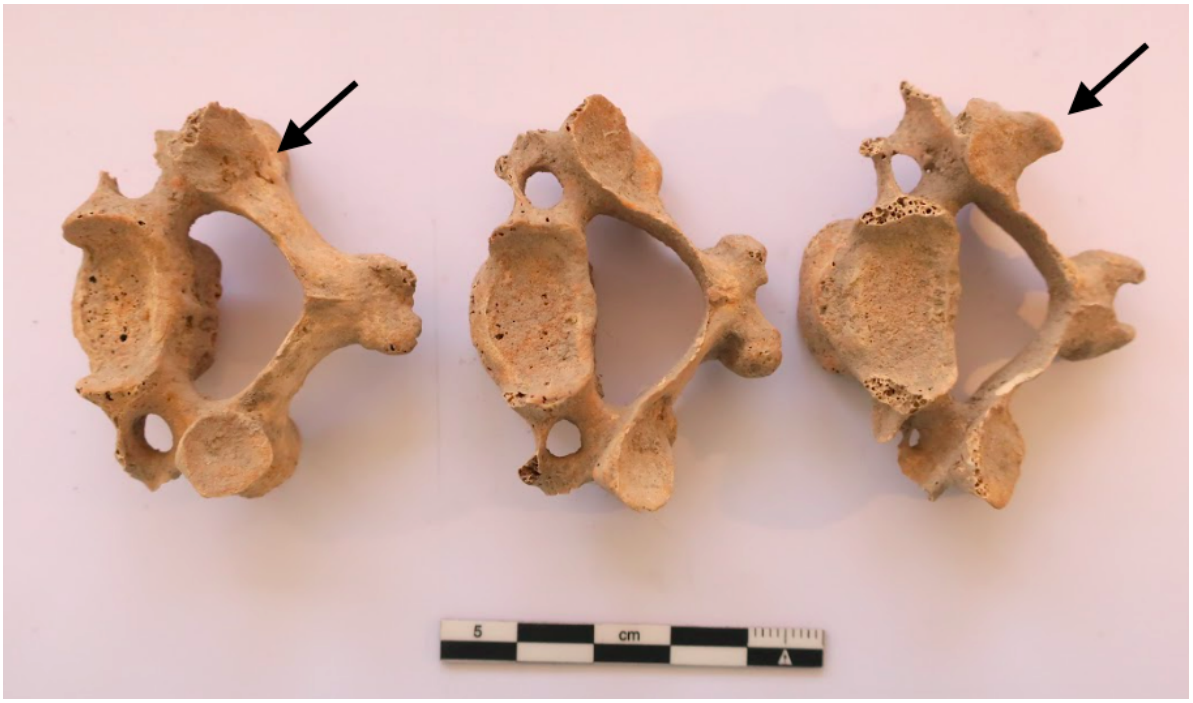

Figure 30: *2019-5 — Right superior articular facets of C3 and C5 (photo: M. Liston)*

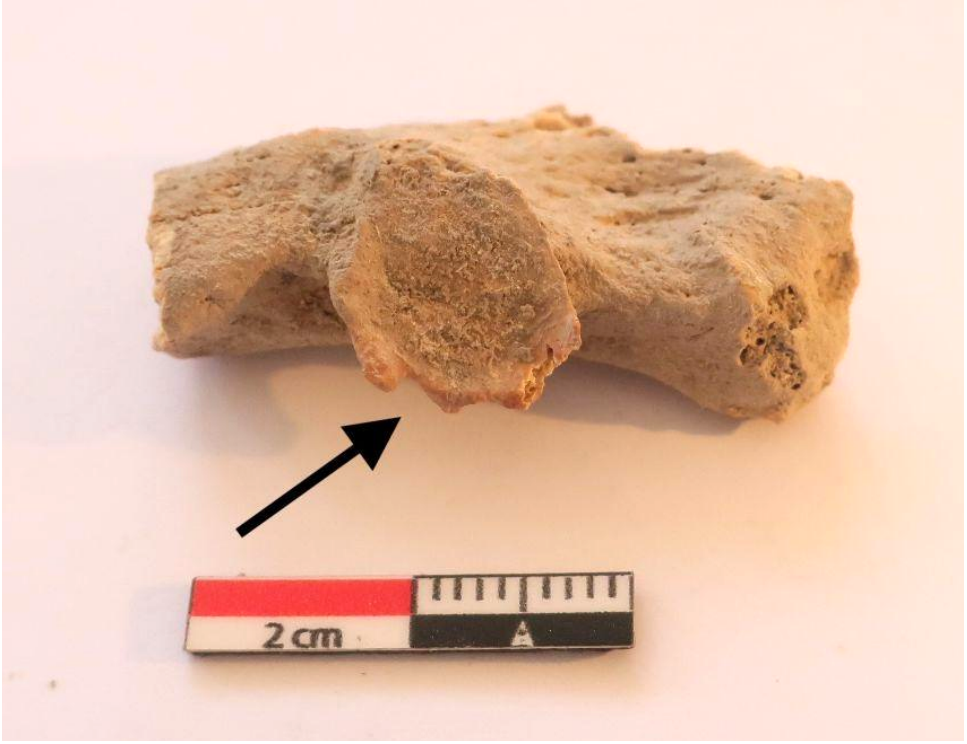

Figure 31: *2019-5 — Osteophyte growth of articular facet of rib fragment (photo: M. Liston)*

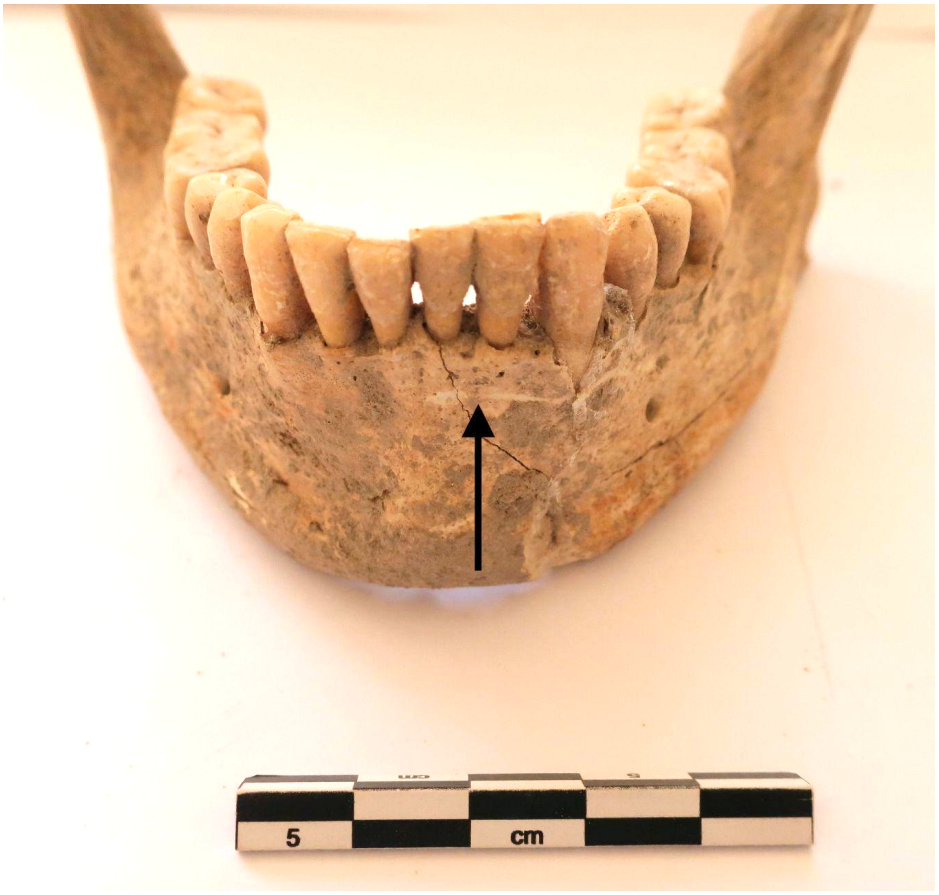

Figure 32: *2019-5 — Reduction of alveolar bone in the mandible (photo: M. Liston)*

Grave Number: 2019-6
Sex: Male
Age-at-death: 27-40 years

Description: Significant spinal abnormalities were noted while cleaning the skeleton after excavation. The neural arches of T3 and T4 are fused. There is a cavitating lesion with smooth edges on the anterior inferior body of T3, ~ 1.0 cm width/depth. This cavitating lesion penetrates more than 50% of the approximate length of the body of T3. The body of T4 collapsed from the superior surface. The vertebral body of T5 has collapsed, but appeared intact. T3-T6 are block vertebrae, with fused neural arches. T6 has a smaller cavitating lesion on the lateral inferior surface of the body, ~ 1.0 cm wide. The lesion penetrates into the central body with uneven depth — lateral side and in the centre of the centrum. T7 has evidence of porous reactive bone on the lateral left superior and side of the body. At the location of the left transverse, the pedicle has been completely destroyed, leaving a rounded surface on the body and a pointed projection extending from the lamina below the superior articular facet — pseudoarthrosis (*Figure 33*). Kyphosis was noted in T3-T7 (*Figures 34-37*), and four rib fragments have evidence for this vertebral collapse. These spinal anomalies are consistent with a diagnosis of tuberculosis (TB), and is the most characteristic skeletal change associated with the disease (Klaus & Lynnerup, 2019: 82-83; Roberts & Buikstra, 2019: 321-363). Refer to *Table 3* for a differential diagnosis. Individual 2019-9 is included in *Table 3* due to similar spinal abnormalities.

Additional spinal abnormalities include an osteophyte growth on the anterior bodies of T11 and T12, which had fused the two together (*Figure 38*). This osteophyte growth broke apart while excavating the skeleton. There is also a slight depression in the anterior body of T12. Arthritic lipping was noted on the anterior body of L1, and the neural arch of S1 is unfused (*Figure 39*).

This male also has osteochondritis dissecans in their distal left humerus (*Figure 40*). Several skeletal elements of the left and right foot also showed evidence of abnormalities. Osteochondritis dissecans was identified in the left navicular (*Figure 41*), however as with 2019-1, this diagnosis should be cautioned, as the lesion observed in these anatomical locations may be the result of defects in the joint that are confused with osteochondritis dissecans (Roberts & Manchester, 2007: 121). The right navicular has evidence for inflammation at the proximal articulation (*Figure 41*). Trabecular bone is visible. The left third metatarsal showed evidence of an entheseal change on the plantar surface. The left third and fifth metatarsal showed evidence for inflammation on the plantar surface (*Figure 42*). It is possible that the left fourth metatarsal also showed evidence for inflammation, however this may be post-mortem damage. A proximal phalanx from the foot (side unknown) has an enlarged nutrient foramen on the plantar surface. The abnormalities in the tarsals and metatarsals may be related to an unknown infection, or could possibly be other skeletal changes associated with TB (Roberts & Buikstra, 2003: 98; Roberts & Buikstra, 2019: 323). Minor calculus and tooth wear was observed, and two small cavities on the buccal side of the left and right mandibular third molars.

Analysis: TB is one of the most frequently encountered bacterial diseases in the world today, and causes thousands of deaths per year (Roberts & Buikstra, 2003). A reemerging disease, TB is responsible for infecting 10.4 million people, and causing the deaths of 1.7 million in 2016 (Roberts & Buikstra, 2019: 321). When left untreated, TB "weakens and debilitates and can disable victims; eventually it can kill" (Roberts & Buikstra, 2003: 11).

The extent of vertebral destruction and resulting kyphotic deformity in this adult male likely means that they had TB for a number of years before they died. Although, it is not possible to determine when this individual contracted the disease and when bone damage started (Roberts & Buikstra, 2003: 49). Only 3-5% of people with untreated TB will develop

evidence in the skeleton (Roberts & Buikstra, 2019: 323), and since it is a highly contagious bacterial infection, it is entirely possible that other individuals in the NET Cemetery had TB at the time of death, but left no skeletal evidence for it (Wood et al., 1992).

Kyphosis and pedicle destruction is not uncommon in modern cases of spinal TB, and is described as being part of the disease process (Yusof et al., 2009). Kyphosis is more severe when pedicle destruction is involved (Yusof et al., 2009), which indicates that this male indeed had TB for a number of years, and may have had a more severe case of kyphosis in their spine. It cannot be said with any level of certainty how TB and resulting kyphotic deformity impacted this individual during life. Inferring the possible symptoms this individual experienced, or the potential disability or handicap that may have resulted is not always easy — people are exceptionally good at adapting (Roberts & Buikstra, 2003).

However, due to the extent of vertebral destruction, it is likely that the kyphotic deformity had some impact on this male's quality of life. If they experienced symptoms associated with TB such as: coughing, difficulty breathing, fever, weakness, lethargy, loss of appetite, chills, night sweats, and irritability (Roberts & Buikstra, 2003), these may have factored into their well-being and day to day life. While it is evident that this male had TB for a number of years, it cannot be concluded that TB caused this individual's death.

The osteophyte growth seen on the anterior vertebral bodies of T11 and T12 is possibly representative of the body's compensation for stress being applied to the joint over a period of time (Roberts & Manchester, 2007: 135). It is not certain if this skeletal change is associated with TB, and may have developed independent of the disease. Since this osteophyte growth had fused the two vertebrae together, it is possible that mobility may have been slightly impacted. The abnormality seen in S1 is likely to be a case of a cleft neural arch (Barnes, 2012). This happens when the two sides of the neural arch fail to fuse, and is caused

by an underlying developmental delay (Barnes, 2012: 71). Cases of cleft neural arch are not uncommon, and mild to moderate cases are non-pathological (Barnes, 2012).

Osteochondritis dissecans of the elbow involves a piece of dead bone (sequestrum) detaching from the main bone, which produces a rounded impression in the articular surface (Grauer, 2019). This is often seen in young males, and is the result of repetitive stresses and tenuous blood supply to the capitellum of the distal humerus (Churchill et al., 2016). The presence of osteochondritis dissecans in this individual's elbow suggests that they were likely subject to repetitive stress, or microtrauma (Grauer, 2019). In modern cases, osteochondritis dissecans of the elbow is often associated with young individuals engaging in repetitive, overhead activities such as baseball and weight lifting (Churchill et al., 2016).

Table 3: Differential Diagnosis for 2019-6 and 2019-9 Spinal Anomalies

Disease Characteristics	Tuberculosis	Brucellosis	2019-6	2019-9
Osteoclastic vertebral destruction (lytic lesions)	**x**	**x**	**x**	**x**
Anterior portion of vertebral body most affected	**x**	**x**	**x**	**x**
Superior anterior portion most affected		**x**		**x**
Cavitation (collapse) and kyphosis	**x**		**x**	
Does NOT lead to cavitation (collapse) and kyphosis		**x**		**x**
Lower spine most affected (lower thoracic, upper lumbar)	**x**	**x**	**x**	**x**
Multiple vertebrae affected	**x**	**x**	**x**	**x**
Osteoblastic activity (new bone formation) around and within margins of lytic foci	**x**		**x**	

Sometimes accompanied by sclerotic repair of the lytic focus resulting in osteoblastic activity (new bone formation) around the margins of lytic foci		**x**		
Observed at all ages	**x**		**x**	**x**
Adult males more affected than adult females		**x**	**x**	**x**

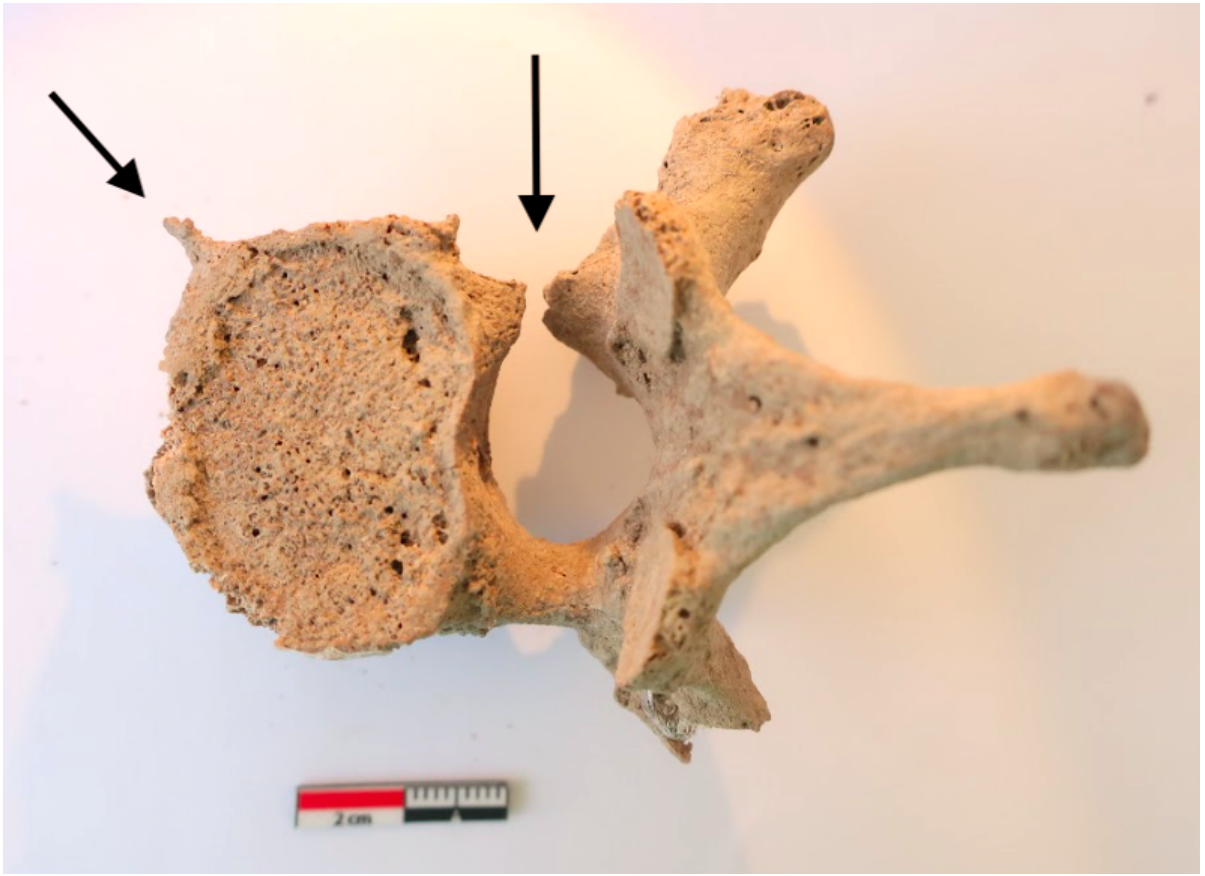

Figure 33: *2019-6 — Pedicle involvement of T7 (inferior view) (photo: M. Liston)*

Figure 34: *2019-6 — Posterior view of vertebrae T3-7 (photo: M. Liston)*

Figure 35: *2019-6 — Anterior view of vertebral destruction T3-7 (photo: M. Liston)*

Figure 36: *2019-6 — Lateral right view of vertebral destruction T3-7 (photo: M. Liston)*

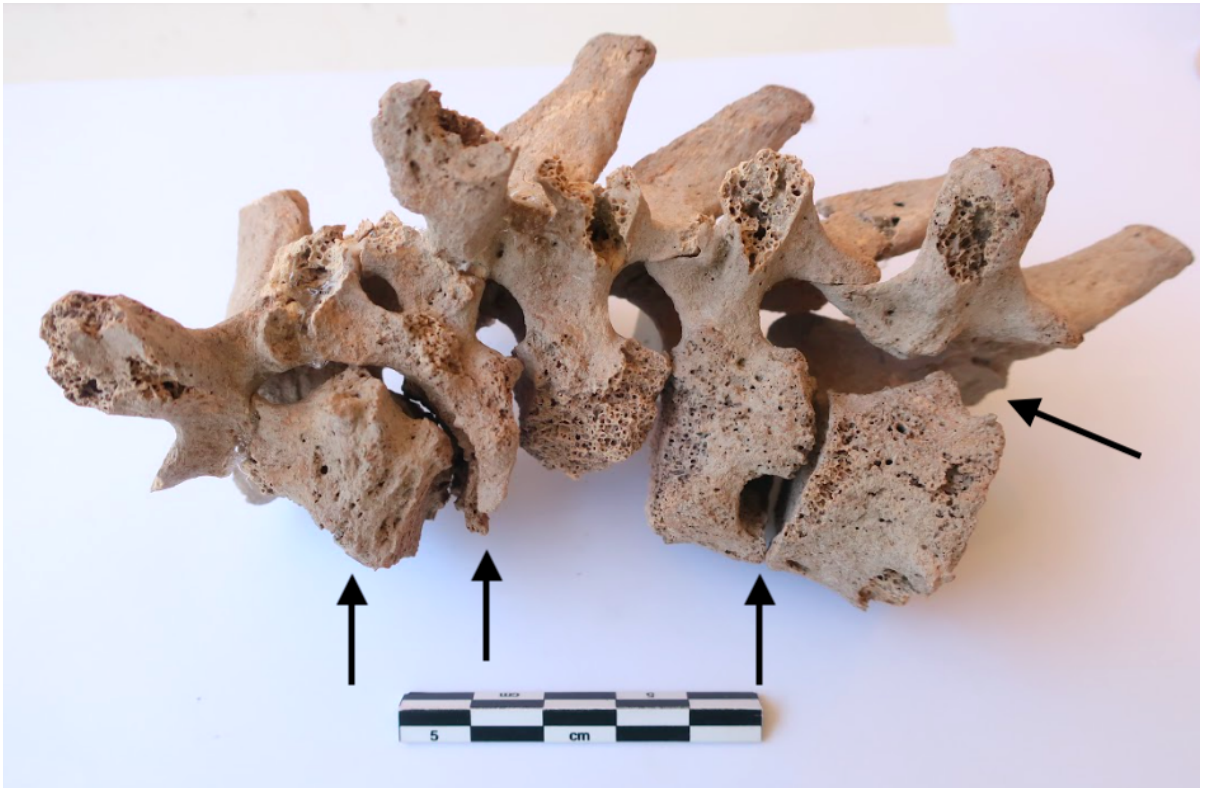

Figure 37: *2019-6 — Lateral left view of vertebral destruction T3-7 (photo: M. Liston)*

Figure 38: *2019-6 — Osteophyte growth of T11 and T12 (photo: M. Liston)*

Figure 39: *2019-6 — Unfused neural arch of S1 (photo: M. Liston)*

Figure 40: *2019-6 — Osteochondritis dissecans of the elbow (photo: M. Liston)*

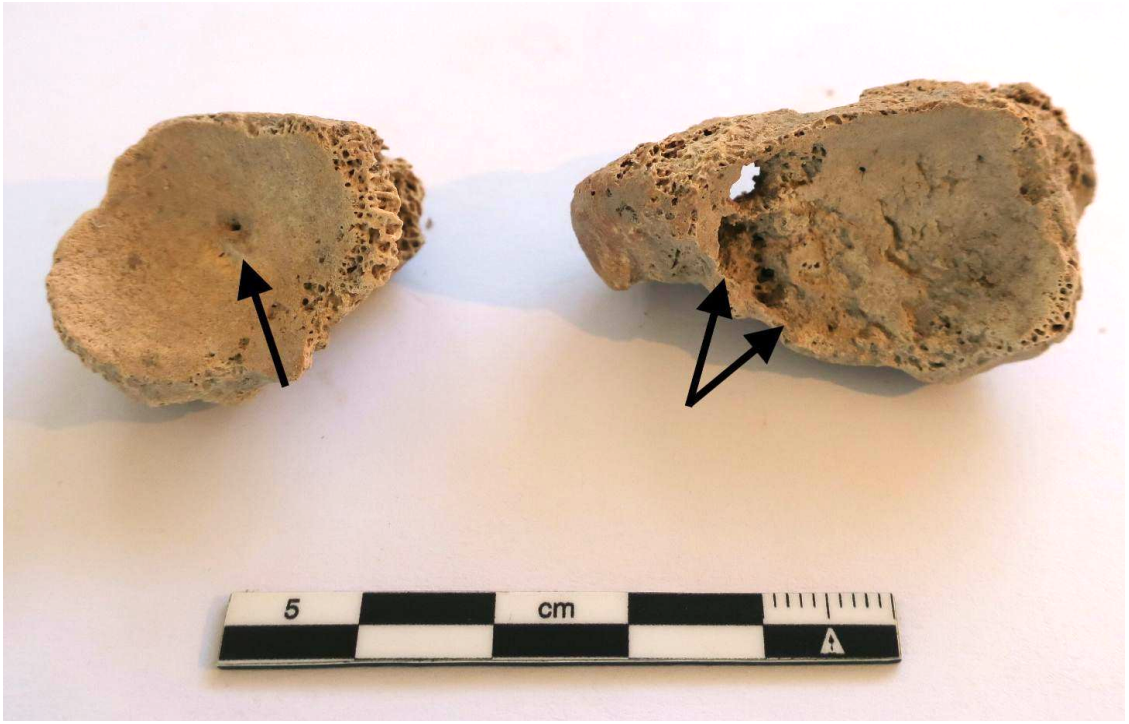

Figure 41: *2019-6 — Possible osteochondritis dissecans of the left navicular (left), possible infection of right navicular (right) (photo: M. Liston)*

Figure 42: *2019-6 — Abnormalities of the left foot, plantar surface of: fifth metatarsal (left), fourth metatarsal (left middle) and third metatarsal (right middle) (photo: M. Liston)*

Grave Number: 2019-7
Sex: Female
Age-at-death: 35-45 years

Description: This adult female has a healed Colles' fracture in their distal right radius (*Figure 43*). There is also evidence for osteophyte growth of the vertebrae: two cervical vertebrae and one thoracic have osteophytes on the anterior vertebral bodies, two thoracic have ossification of the lamina, and two lumbar have ossification of the spinous ligament (*Figure 44*). Due to the state of preservation, it was not possible to identify the specific number of each vertebra.

This female has significant dental pathologies. There is considerable tooth wear with dentine exposed, and small deposits of calculus (*Figure 45)*. The maxillary right and left second premolars have significant dental caries that completely consumed the tooth crown. The maxillary right second molar has moderate dental caries on the distal interproximal side.

The third right maxillary molar has moderate dental caries on the mesial interproximal side. The first left mandibular molar has large dental caries that have consumed most of the mesial side of the crown (*Figure 46)*. Decay extends to the roots.

Analysis: The Colles' fracture observed in this female's right wrist may have been the cause of a fall, where this individual put their hand out to break the impact, and ended up breaking their wrist (Redfern & Roberts, 2019: 216). This fracture is well healed, so it must not have happened close to the time this female died. However, it is likely that this fracture impacted this female's wrist mobility for a period of time, and would have been painful (Brickley, 2002). Colles' fractures are fairly common, and in modern clinical literature, they are the most frequently sustained fractures in Caucasian females under 70 years old (Brickley, 2002). Although a Colles' fractures can occur anytime in an individual's life, this specific fracture has been linked with osteoporosis, particularly in elderly females (Brickley, 2002; Mays, 2006). This is due to changes in hormones as a result of menopause, which can accelerate bone loss (Brickley, 2002). Based on modern populations, menopause generally starts when a female has reached their late 40's (Mays, 2006). In this particular case, it is possible that the Colles' fracture was osteoporosis related, however, we cannot know for sure simply by macroscopic observation of the bone.

This is the only individual from the NET Cemetery with considerable dental caries. 2019-6 is the only other person with evidence of minor caries, which are the most common form of dental disease found in archaeological populations (Roberts & Manchester, 2007; Kinaston et al., 2019). The presence of caries in this individual's dentition may suggest their diet differed slightly from the others, who only had deposits of calculus. While their cause is multifactorial, caries are the result of bacteria on the teeth, and can result from a diet with high sugar and carbohydrates (Roberts & Manchester, 2007). The extent of dental caries in the maxilla and mandible of this female suggest they may have been painful (DeWitte &

Bekvalac, 2010). If these caries did cause this individual pain, it is possible that they may have disrupted their sleep, and the ability to chew food and eat (DeWitte & Bekvalac, 2010).

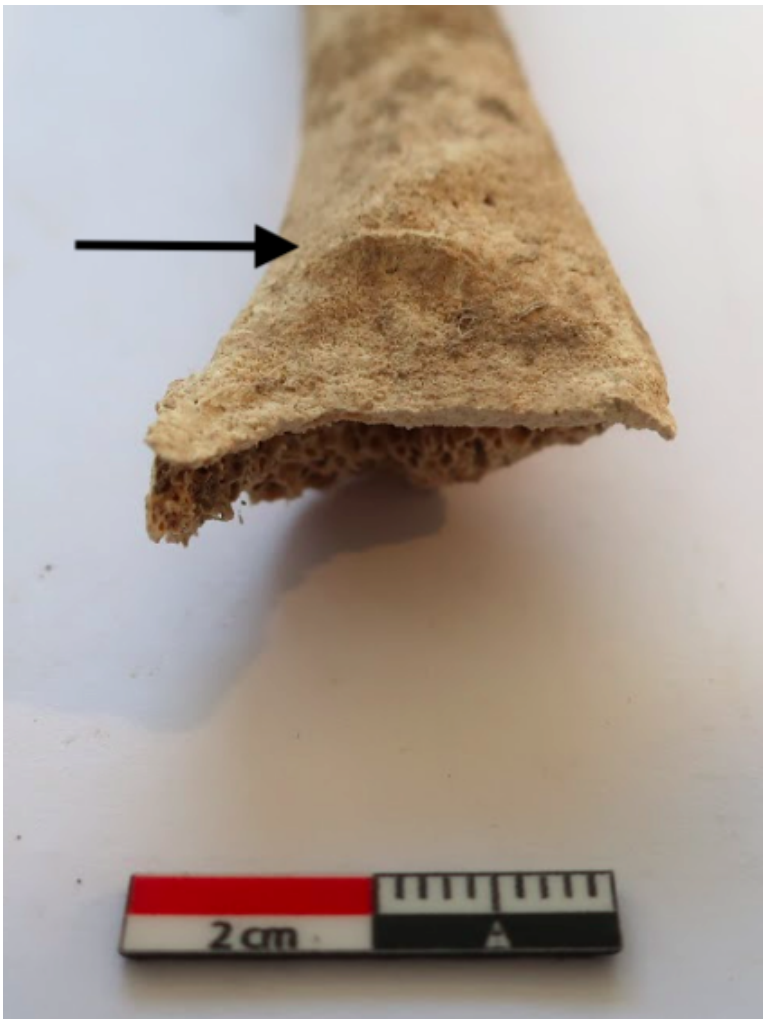

Figure 43: *2019-7 — Colles' fracture of the distal right radius (photo: M. Liston)*

Figure 44: *2019-7 — Osteophyte growth of the vertebrae (photo: M. Liston)*

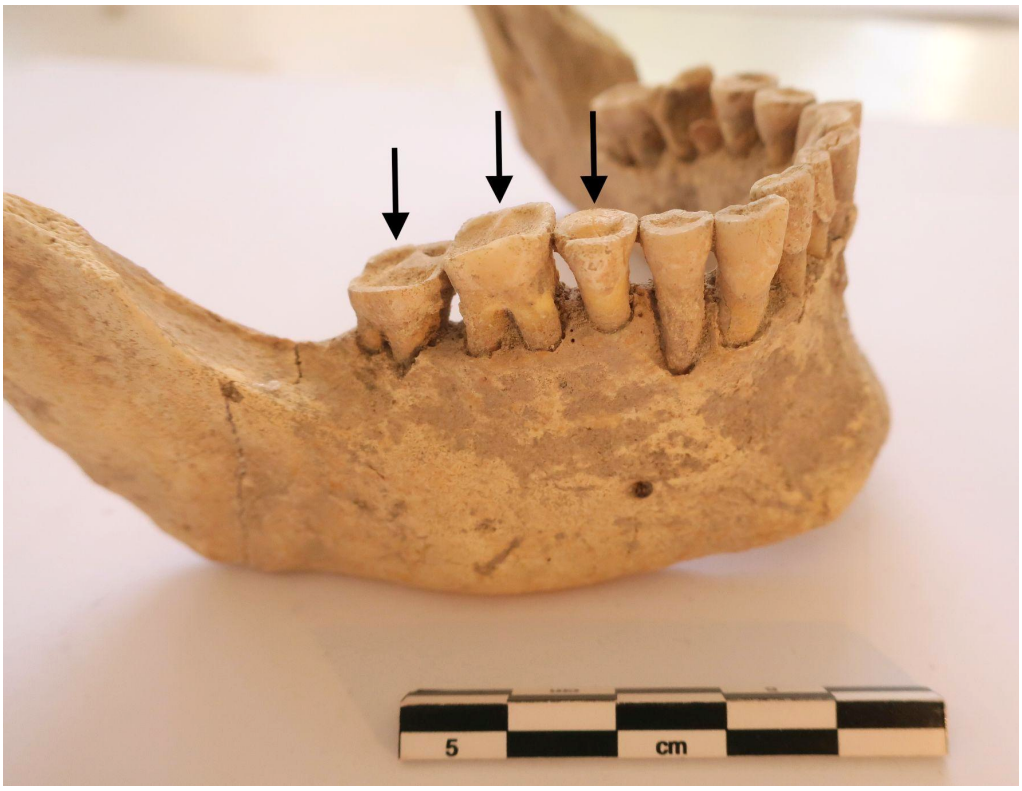

Figure 45: *2019-7 — Tooth wear of the right mandibular molars (photo: M. Liston)*

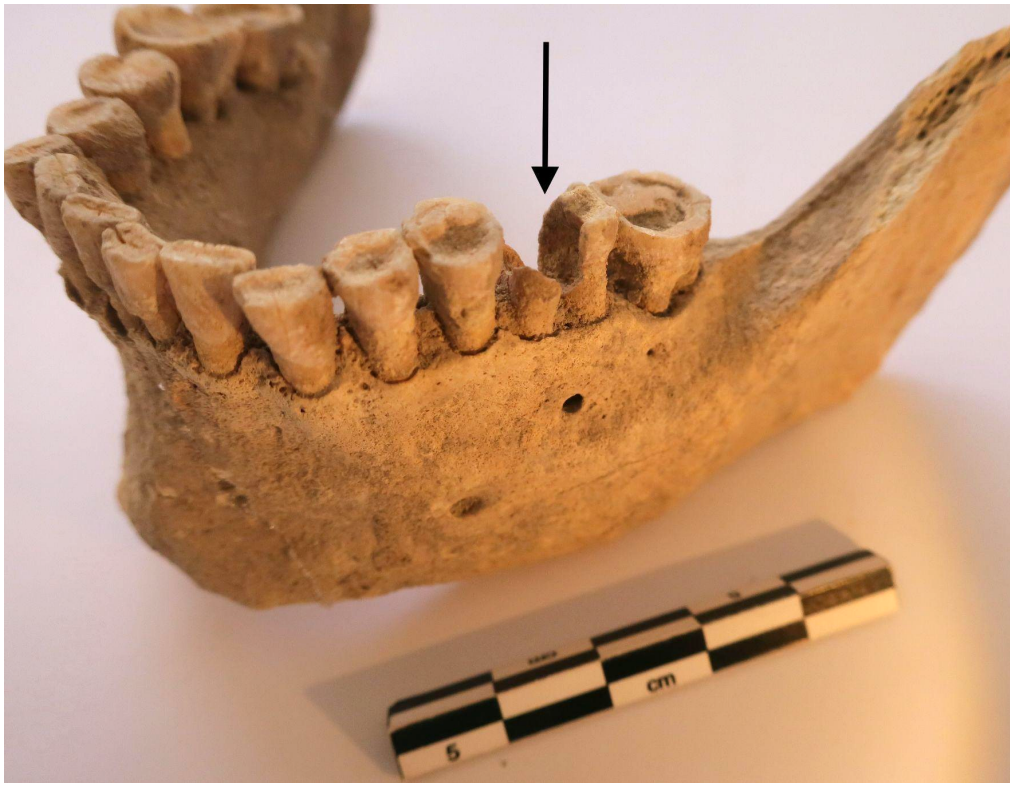

Figure 46: *2019-7 — Significant dental caries in left first mandibular molar (photo: M. Liston)*

Grave Number: 2019-8
Sex: Male
Age-at-death: 18-25 years

Description: This young adult male has osteochondritis dissecans in their distal left humerus (*Figure 47*). On the inferior surface of the capitulum there is a distinct circular lesion with subchondral bone destruction with a 9.10 x 8.73 mm diameter with depressed subchondral bone on the medial half and pits with bone destruction on the lateral half. There is no evidence of inflammation. Similar to 2019-2 and 2019-4, this male has an entheseal change in their left medial clavicle (rhomboid fossa), at the attachment site of the costoclavicular ligament (*Figure 48*). Schmorl's nodes were noted on the inferior vertebral bodies of T7-T11, and the superior vertebral bodies of T8 and T11 (*Figure 49*). Although the skull of this individual was removed during the construction of Wall 26, some maxillary and mandibular teeth were recovered during excavation. Moderate wear and dentine exposure was noted, and small deposits of calculus.

Analysis: This young male has evidence for heavy manual labour, but not acute trauma. Similar to 2019-6, osteochondritis dissecans in the elbow is caused by a combination of factors, most likely the result of injury from repetitive microtrauma and tenuous blood supply to the humerus (Churchill et al., 2016: 567).

The entheseal change seen in the medial clavicle (rhomboid fossa) is similar to the entheseal change seen in the clavicles of 2019-2 and 2019-4. Again, These changes are typically seen in young adult males, with significant entheseal changes seen in 20-30 year old males (Koudela et al., 2015). The entheseal change noted in the medial clavicle may represent a bone response to mechanical stress over a period of time, and could indicate that this person was involved in strenuous activities with their left arm (Milella et al., 2012).

Faccia and Williams (2008: 29-30) describe the process of Schmorl's nodes formation as "an inferiorly or superiorly directed extrusion of nucleus pulposus material. Subsequently, the fluid travels through a break or fissure in the cartilaginous endplate and erodes into the vertebral body. Here, degeneration of local trabeculae ensues, resulting in a small 'cavitation' in the surface of the vertebral body". Traumatic events such as a fall from a height has been suggested as a possible cause, as well as congenital defects and senescent processes (Faccia & Williams, 2008). Since this individual is a young adult male with osteochondritis dissecans of the elbow and erosion in the medial clavicle, it is more likely that the Schmorl's nodes are the result of a traumatic event. While Schmorl's nodes are relatively frequent in archaeological populations, the specific impact they have on an individual's quality of life — such as mobility and level of pain — is not well understood (Faccia & Williams, 2008). In clinical cases, Faccia and Williams (2008) found that patients frequently report pain when the Schmorl's node is located in the central portion of the vertebral body. These results support the idea that these Schmorl's nodes may have been painful for this young male. However, the impact they had on quality of life (if any) is not certain.

Figure 47: *2019-8 — Osteochondritis dissecans of the elbow (photo: M. Liston)*

Figure 48: *2019-8 — Entheseal change of the left medial clavicle (rhomboid fossa) (photo: M. Liston)*

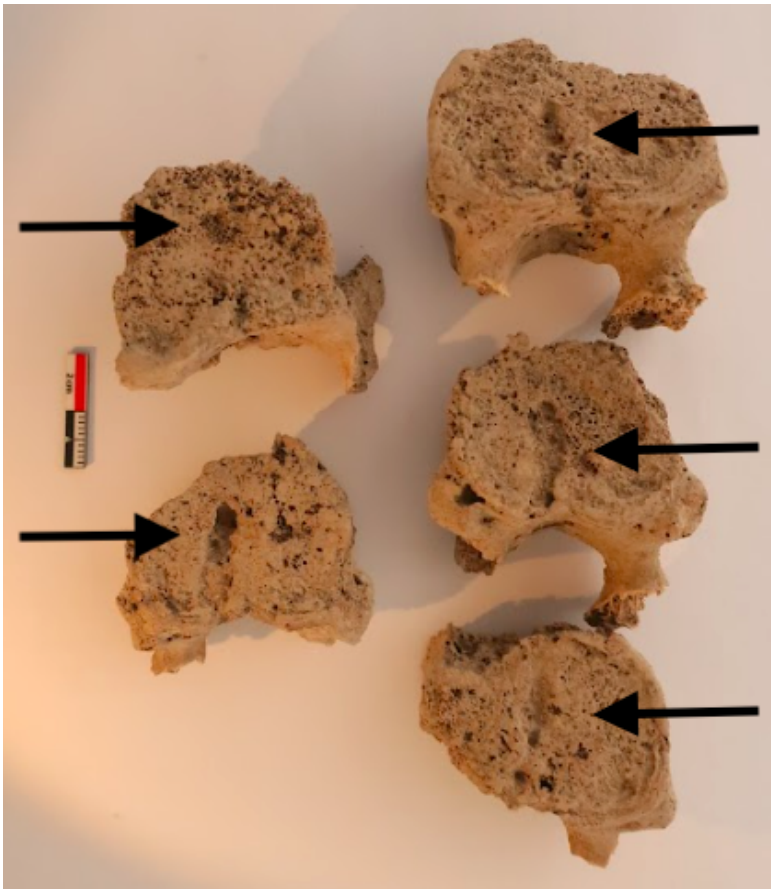

Figure 49: *2019-8 — Schmorl's nodes on the inferior vertebral bodies of T7-11 (photo: M. Liston)*

Grave Number: 2019-9
Sex: Male?
Age-at-death: 35-45 years

Description: This 35-45 year old possible male has Schmorl's nodes on the superior and inferior vertebral body of T12, and on the superior vertebral bodies of L1-L4 (*Figure 50*). There is an osteophyte on the superior anterior vertebral body of L4. The spinous processes of three thoracic vertebrae have an abnormal shape, and are bent in different directions (*Figure 51*). It is estimated that these are T8, T9, and T11. On the anterior vertebral body of L3 and L4, lytic lesions were noted (*Figure 52*). This individual also has unilateral septal aperture of the olecranon fossa in their distal left humerus (*Figure 53*), which is a genetic variant that Klaus and Lynnerup (2019: 59) describe as falling within the "range of normal". No skull was recovered during excavation.

Analysis: Similar to 2019-8, this individual has evidence for Schmorl's nodes, which may be the result of trauma, congenital defects or senescent processes (Faccia & Williams, 2008). Due to their location on the central portion of the vertebral body, it is possible that the Schmorl's nodes caused this individual some pain (Faccia & Williams, 2008). However it is important to reiterate that the impact they had on quality of life (if any) is not certain. The bent spinous processes of three thoracic vertebrae are rather perplexing, and their etiology remains unclear. The lytic lesions noted on the anterior vertebral bodies of L3 and L4 could be a skeletal change associated with brucellosis infection or possibly early stage TB (Roberts & Buikstra, 2019: 420-426). Refer to *Table 3* for a differential diagnosis.

Brucellosis and TB are both bacterial infections which can produce lytic lesions and destroy the anterior vertebral bodies, mostly affecting the lower spine (Roberts & Buikstra, 2019). Skeletal changes resulting from brucellosis are relatively common, affecting anywhere from ~2-70 % of those infected with the disease (Roberts & Buikstra, 2019: 421). Unlike TB, skeletal changes of the spine seen in cases of brucellosis do not result in vertebral collapse or kyphosis (Roberts & Buikstra, 2019). Typically, lytic lesions are observed on the superior anterior portion of the vertebral bodies in cases of brucellosis (Roberts & Buikstra, 2019).

Evidence for brucellosis was identified in other skeletons in Frankish Corinth (1210-1458 C.E.) (see Williams et al., 1998), as well as skeletons from an early Ottoman period (17th century C.E.) cemetery in Panayia Field (see Zervos et al., 2009). After the domestication of sheeps and goats ~10,000 years ago, brucellosis spread throughout the Mediterranean region, where it was transmitted to humans through infected milk for centuries (Williams et al., 1998; Zervos et al., 2009; Roberts & Buikstra, 2019). A differential diagnosis of TB is possible for this individual, based on similar skeletal changes, and the diagnosis of TB in 2019-6.

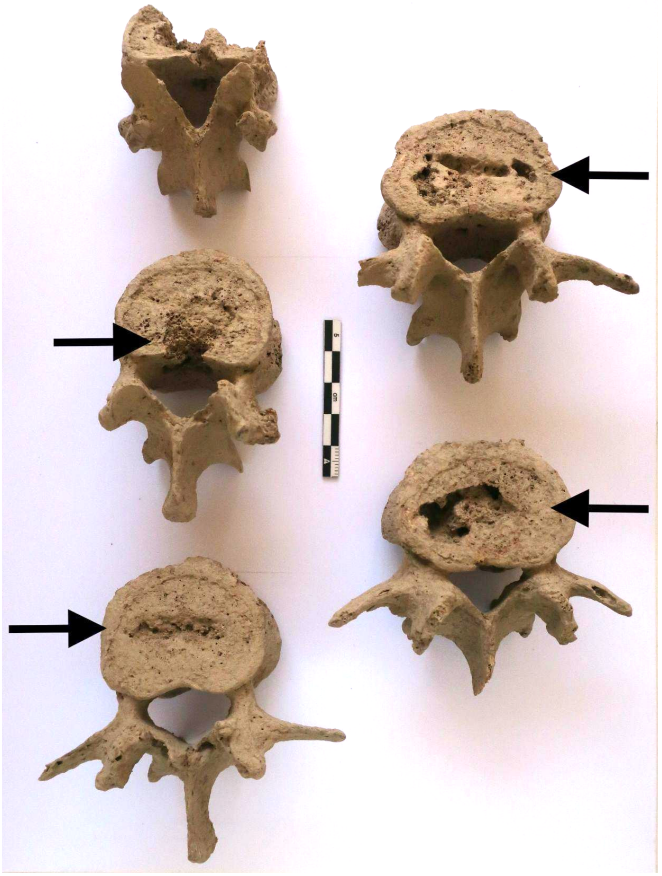

Figure 50: *2019-9 — Schmorl's nodes on the superior vertebral bodies of L1-4 (photo: M. Liston)*

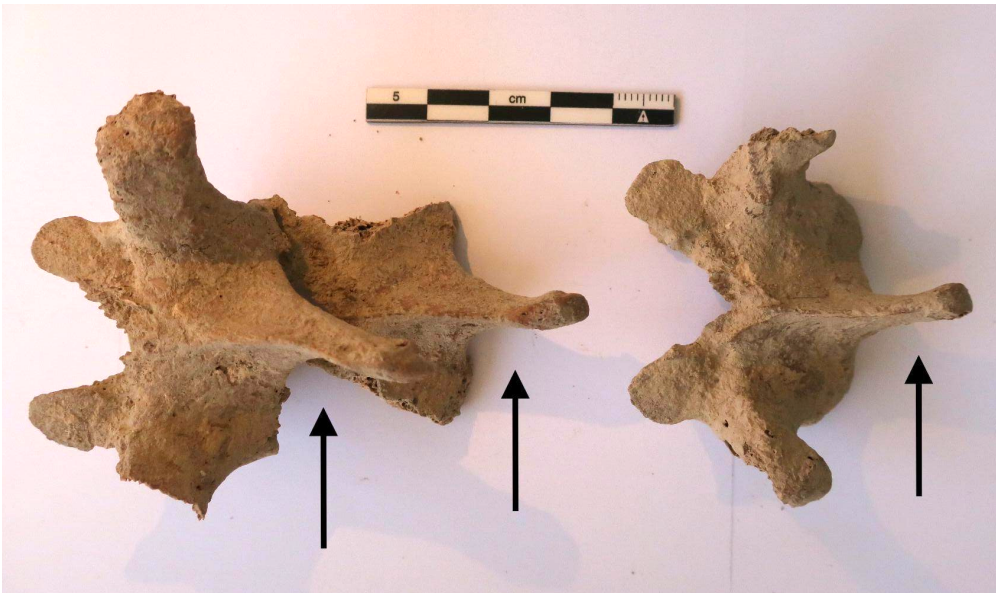

Figure 51: *2019-9 — Bent spinous processes of T8, T9 and T11 (photo: M. Liston)*

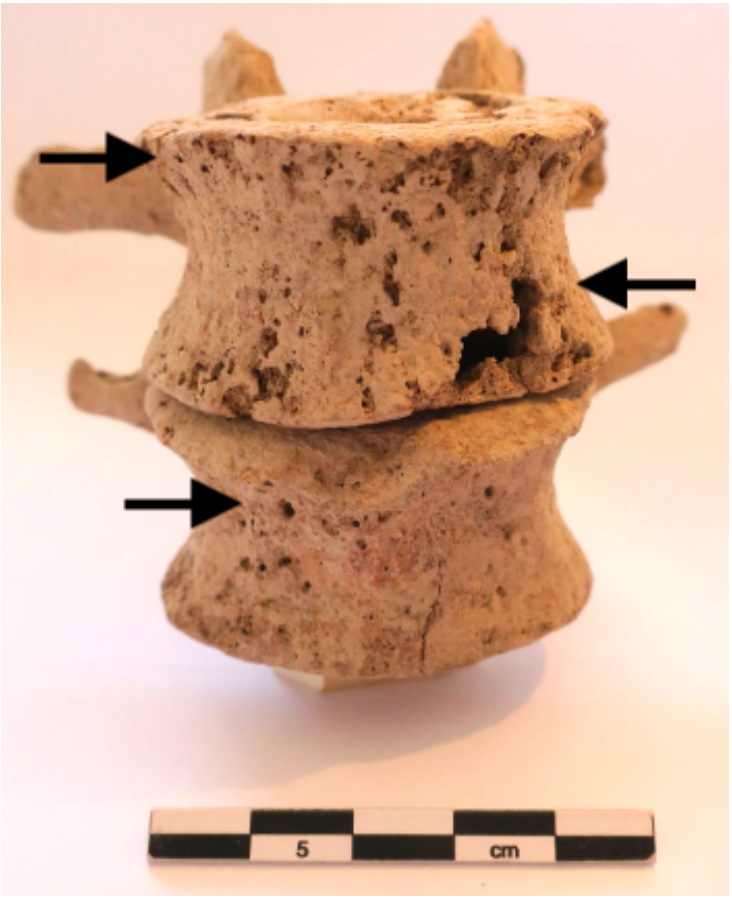

Figure 52: *2019-9 — Lytic lesions on anterior vertebral bodies of L3 and L4 (photo: M. Liston)*

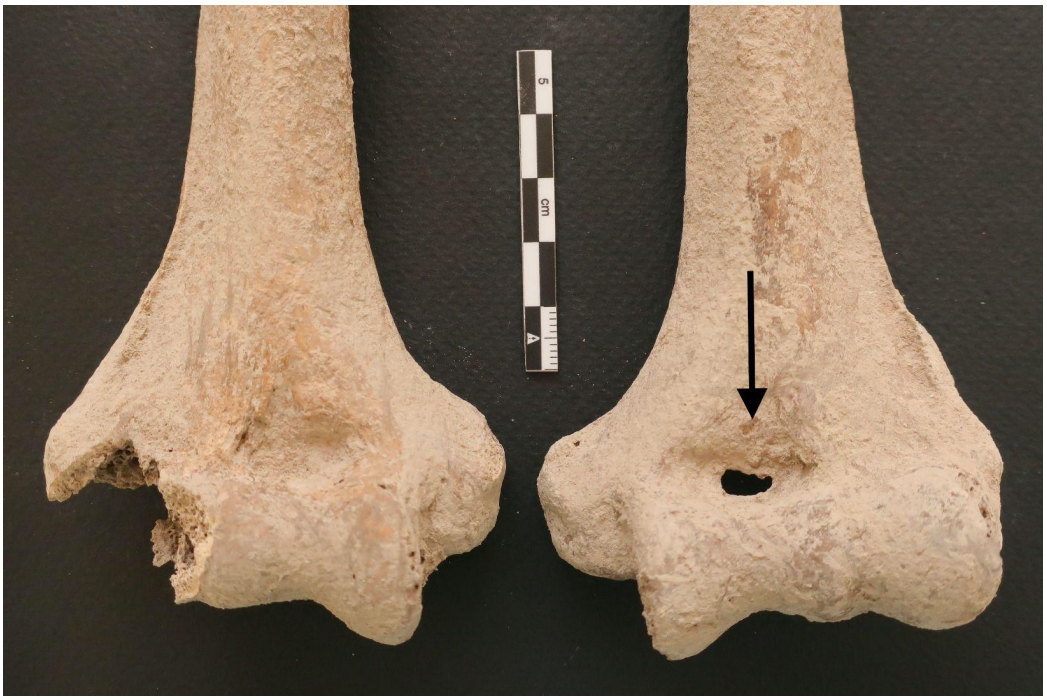

Figure 53: *2019-9 — Unilateral septal aperture (photo: M. Liston)*

Grave Number: 2019-10
Sex: Unknown
Age-at-death: 12-15 years

Description: Cribra orbitalia was noted in the left eye orbit (*Figure 54*). LEH was also identified on the maxillary and mandibular teeth (*Figure 55*). LEH was identified on all maxillary incisors, canines, and the left first premolar (n = 7) and the all mandibular incisors, canines, premolars, and the left first molar, right first and second molars (n = 13). Carabelli's cusps were noted on both maxillary first molars, and slight shovel shaped central incisors of the maxilla. No evidence of calculus, and minor tooth wear. This juvenile also has abnormally bent radii (*Figure 56*). Refer to *Table 4* for a differential diagnosis.

Analysis: While the descriptive term for abnormal porosity in the eye orbits is cribra orbitalia, this is not an independent disease itself, rather, a symptom (Schultz, 2001). The possibility that this cranial porosity is the result of multiple conditions such as anemia, scurvy, rickets, and/or trauma must be considered, as these pathological processes can also result in orbital roof porosity (Walker et al., 2009). However, since the 1950's, anemia has routinely been attributed to the presence of cribra orbitalia in past populations (Walker et al., 2009), including two cemetery populations from Ancient Corinth. In Frankish Corinth (1210-1458 C.E.) and an early Ottoman period (17th century C.E.) cemetery in Panayia Field, cribra orbitalia was identified in several juveniles. Anemia was discussed as being the cause in these cases, possibly associated with malaria, which has been a problem in Corinth for centuries until its eradication in the 1930's (Williams et al., 1998; Zervos et al., 2009).

In archaeological cases of anemia, the cranial porosity is the result of red marrow expansion to facilitate red blood cell production (Brickley, 2018). In this particular case, it would appear as if the orbital porosity is slightly remodelled. This may support the differential diagnosis of anemia, as abnormal porosity may remain once red blood cell production returns to normal (Brickley, 2018). In adults who have recovered from childhood

anemia, porosity in the eye orbits may look remodelled (Brickley, 2018). Even though 2019-10 is not an adult, this may suggest that they were anemic in their younger years and were in the process of healing at the time of death. Without radiographic evidence of red marrow expansion, we cannot know for certain if the abnormal porosity in the eye orbit is the result of anemia. The orbital porosity seen in this individual may be the result of anemia, scurvy, rickets, trauma, or a combination of any, as these conditions frequently co-occur (Brickley & Ives, 2008) .

The presence of LEH in numerous maxillary and mandibular teeth indicates that this juvenile was exposed to developmental disruptions caused by non-specific stress, such as disease or dietary insufficiencies (Hillson, 1996; Roberts & Manchester, 2007). Unlike the three adults with evidence of LEH (2022-2, 2019-1, 2019-5), this juvenile likely did not recover from the periods of stress, as they did not survive into adulthood. Since there are multiple horizontal lines of depression along various tooth surfaces, as well as cribra orbitalia, it can be inferred that this juvenile was repeatedly exposed to periods of stress throughout their life, and eventually succumbed. Estimating the precise chronology of LEH formation was not presented in this research.

With respect to the abnormally bent radii, bowing of long bones is a symptom often associated with rickets (vitamin D deficiency) (Brickley & Ives, 2008). The primary cause of rickets is prolonged lack of exposure to sunlight, and/or dietary deficiency whereby inadequate amounts of vitamin D are ingested (Brickley & Ives, 2008). Rickets prevents calcium from entering the developing cartilage in children, hindering bone mineralization, resulting in bending deformities in long bones (Brickley & Ives, 2008). Cribra orbitalia is sometimes a symptom of rickets as well (Brickley & Ives, 2008). However, rickets may not be a preferred diagnosis in this case, as the weight-bearing limbs — femur, tibia, fibula — are typically affected (Brickley & Ives, 2008). No deformities in the leg bones were noted.

Whenever there is a case of abnormal bowing in long bones, acute plastic bowing deformities (APBD) resulting from trauma should be considered (Stuart-Macadam et al., 1998). In juveniles, subtle bowing deformities typically affect the radii and ulnae, and can be the result of a fall with an outstretched hand (Stuart-Macadam et al., 1998). Moreover, Madelung's deformity should be considered a differential diagnosis as well. Knutsen and Goldfarb (2014: 289) describe this deformity as "an abnormal growth arrest of the palmar-ulnar distal radius physis". This involves "a shortened radius that is bowed dorsally and laterally" (Lewis, 2019: 623). When there is bilateral bowing of the radii, as seen in this individual, it is likely that this deformity is congenital (Lewis, 2019). If this is the case, it is possible that this individual had a limited range of motion with their wrists (Lewis, 2019). Clearly, the abnormally bent radii is rather perplexing. A differential diagnosis of rickets, childhood trauma (APBD), Madelung's deformity and perhaps normal skeletal variation must be considered here.

Table 4: Differential Diagnosis for 2019-10 Abnormally Bent Radii

Disease Characteristics	**Rickets**	**Acute plastic bowing deformity**	**Madelung's deformity**	**2019-10**
Bilateral bending deformities of arm bones	**x**	**x**	**x**	**x**
Bilateral bending deformities of leg bones	**x**	**x**		
Metaphyseal swelling/cortical thickening	**x**	**x**		
Porosity of long bone growth plates	**x**			
Fraying of long bone growth plates	**x**			
Shortened radius that is bowed dorsally and laterally			**x**	**x**
Widened interosseous space			**x**	**x**
Appears in juveniles	**x**	**x**	**x**	**x**

Figure 54: *2019-10 — Cribra orbitalia of the left eye orbit (photo: M. Liston)*

Figure 55: *2019-10 — LEH on mandibular canine (photo: M. Liston)*

Figure 56: *2019-10 — Abnormally bent radii (left) with ulnae (right) (photo: M. Liston)*

2.7 Osteological Analysis of the Infant Skeletons

The osteological analysis of the two infants excavated to the south of the NET Cemetery will be discussed in this section. The interpretation portion for both individuals will be discussed together, due to similarities in pathological lesion type and location.

Grave Number: 2022-1
Sex: Unknown
Age-at-death: 1.1-1.6 years (+/- 0.17-0.25)

Description: Evidence for abnormal porosity was noted on multiple cranial bones: the external surface of the greater wings of the sphenoid (*Figure 57*), the body of the sphenoid (*Figure 58*), pars basilaris (*Figure 59*), medial surface of the zygomatics (*Figure 60*), inferior maxilla (*Figure 61*), sinuses (*Figure 62*), and medial surface of the mandible (*Figure 63*). Porosity was also noted on the alveolar bone of the maxilla and mandible. Cribra orbitalia was identified (*Figure 64*), as well as porotic hyperostosis on the right posterior parietal (*Figure 65*). The abnormal porosity on the side of this individual's skull is ~1x1 cm.

This infant also has an unfused mendosal suture on the occipital bone, which supports the young estimate of age. Normally the mendosal suture fuses during the first year of life (Scheuer & Black, 2004). With reference to *Table 7* and *Table 8* in Appendix A, the estimated age-at-death for this infant using dental measurements and postcranial measurements differed. The estimated age-at-death using dental measurements was ~1.1-1.6 years (+/- 0.17-0.25) (Schaefer et al., 2009: 79). The estimated age-at-death using postcranial measurements was ~6-12 months (Schaefer et al., 2009). Due to the fact that teeth are "under tighter genetic control" (White & Folkens, 2005: 364) thus, not as influenced by environmental factors as other elements of the skeleton, these inconsistencies in age-at-death estimations suggests this infant was small for their age. Moreover, dental development is more closely linked with chronological age, and is more precise at estimating age-at-death than estimates based on long bone length and epiphyseal fusion (Ubelaker, 1989; Buikstra & Ubelaker, 1994; Schaefer et al., 2009).

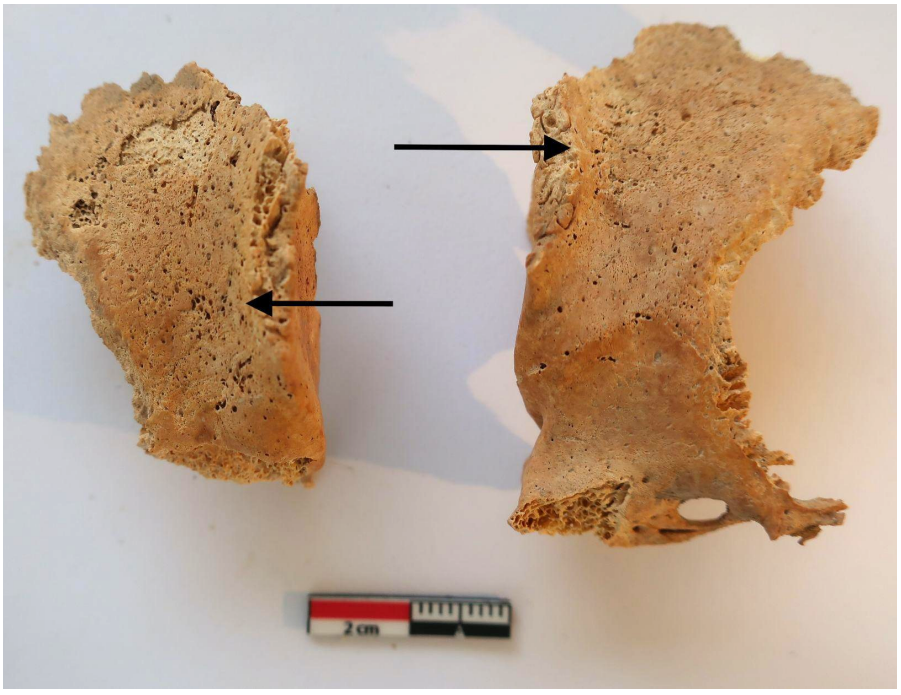

Figure 57: *2022-1 — Bilateral abnormal porosity of the external surface of the greater wings of the sphenoid (photo: M. Liston)*

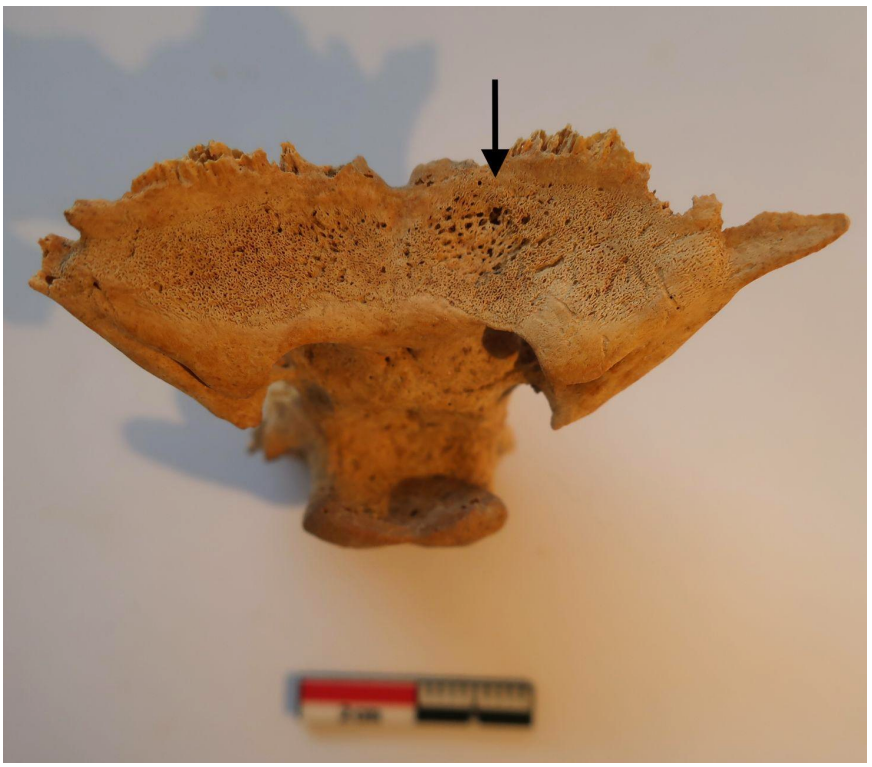

Figure 58: *2022-1 — Abnormal porosity of the body of the sphenoid (photo: M. Liston)*

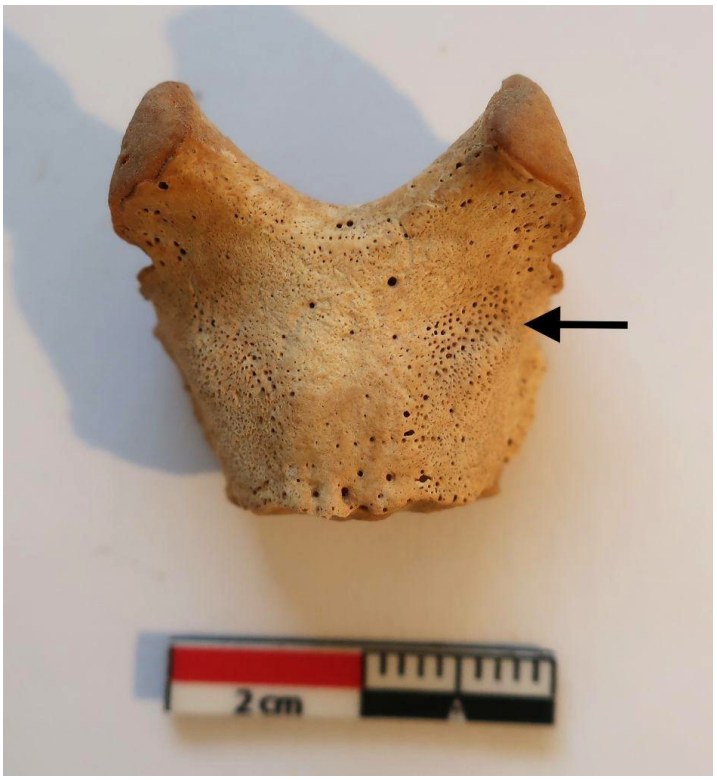

Figure 59: *2022-1 — Abnormal porosity of the pars basilaris (photo: M. Liston)*

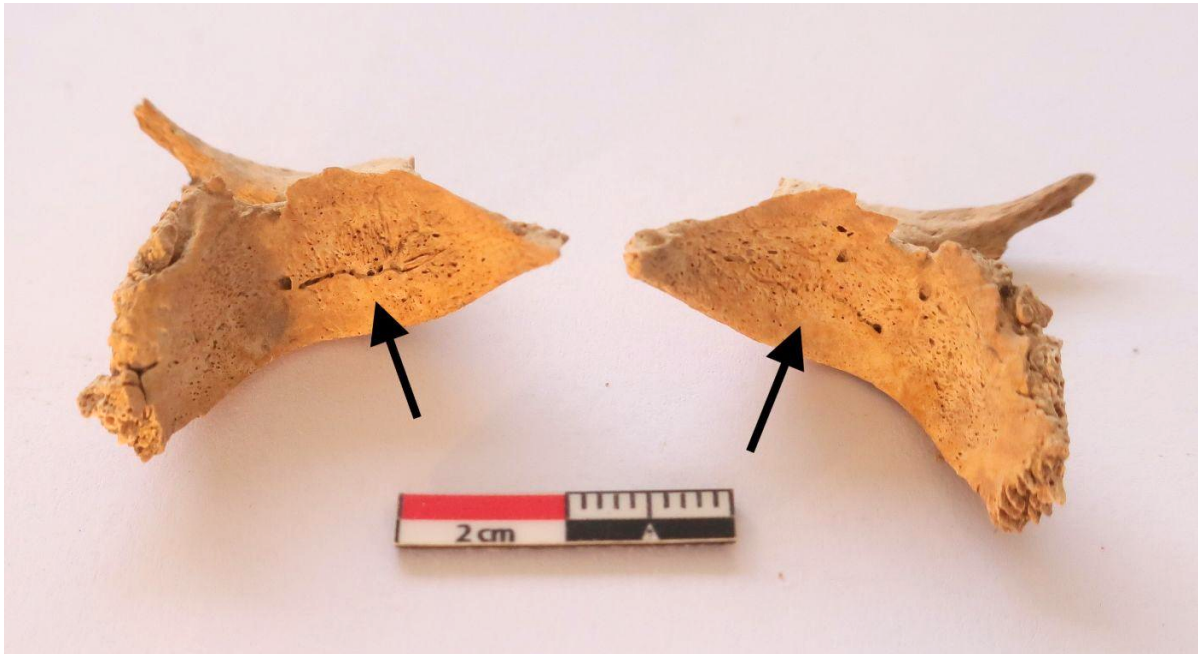

Figure 60: *2022-1 — Abnormal porosity of the internal zygomatics (photo: M. Liston)*

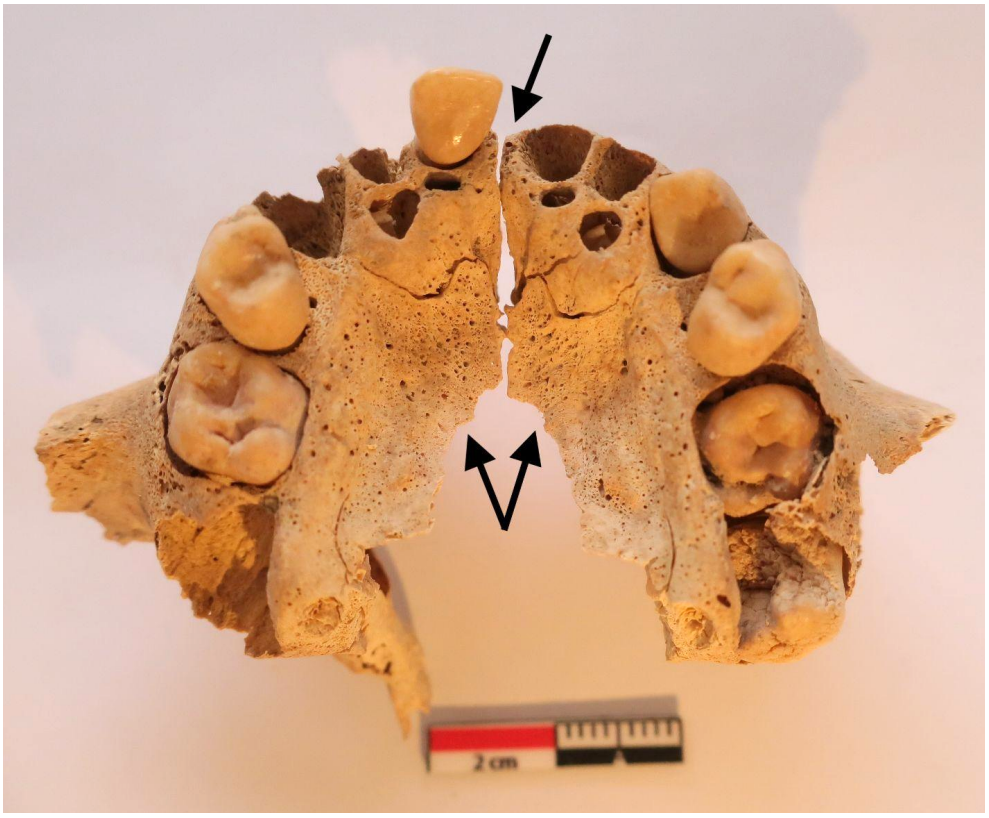

Figure 61: *2022-1 — Abnormal porosity of the inferior maxilla and alveolar bone (photo: M. Liston)*

Figure 62: *2022-1 — Abnormal porosity and reactive bone formation of the sinus (photo: M. Liston)*

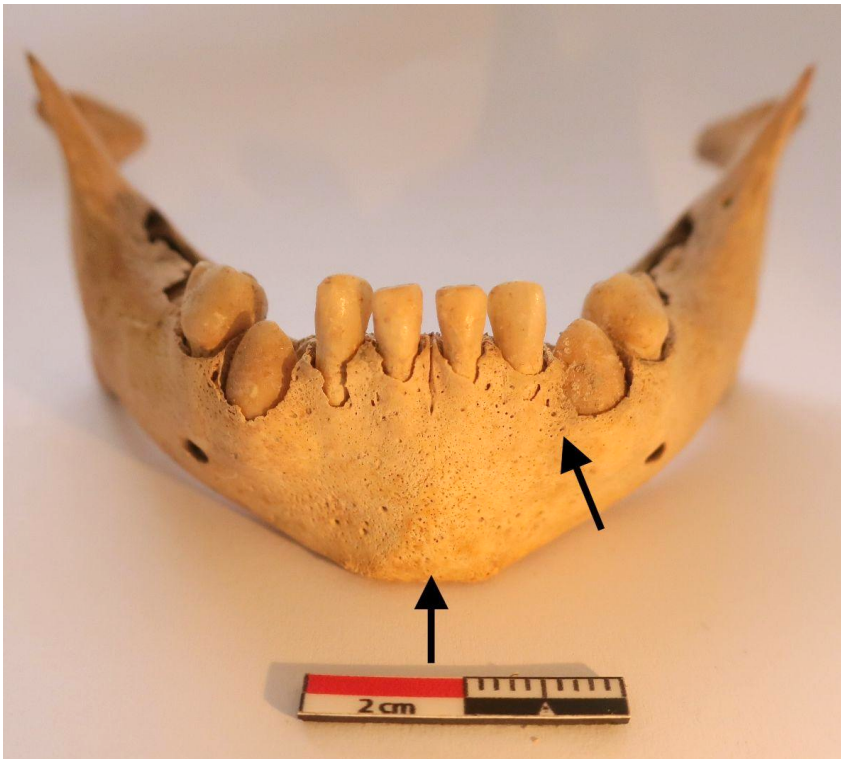

Figure 63: *2022-1 — Abnormal porosity of the medial surface of the mandible (photo: M. Liston)*

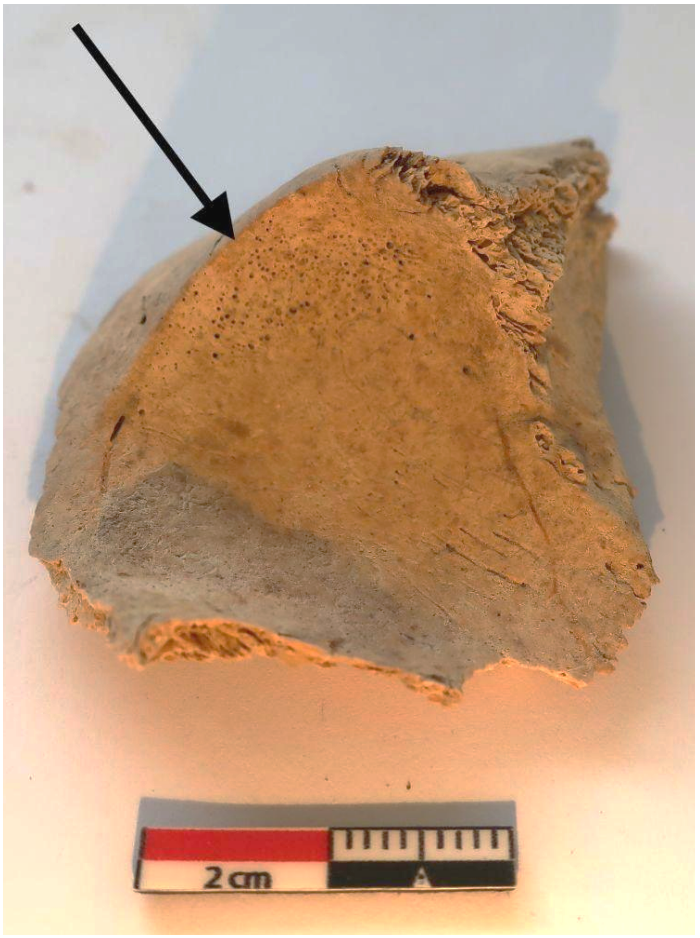

Figure 64: *2022-1 — Cribra orbitalia of the eye orbit (photo: M. Liston)*

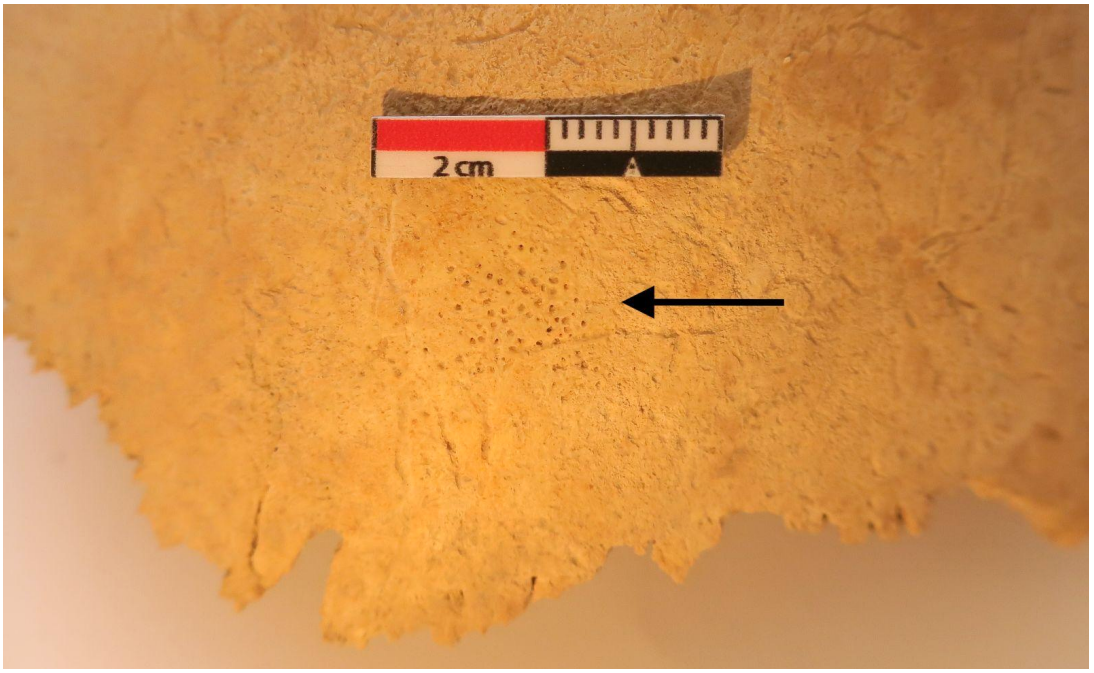

Figure 65: *2022-1 — Abnormal cranial porosity (porotic hyperostosis) of the right posterior parietal (photo: M. Liston)*

Skeleton Number: 17
Sex: Unknown
Age-at-death: 1.8-3.0 years (+/- 0.17-0.22)

Description: Evidence for abnormal porosity was noted on the external surface of the greater wings of the sphenoid (*Figure 66*) and the inferior maxilla (*Figure 67*). Cribra orbitalia was also noted (*Figure 68*). There is an accessory suture between the right parietal and frontal bone (*Figure 69*). Possible endocranial pathology was noted in a posterior parietal fragment along the suture line (*Figure 70*).

The abnormal porosity seen in multiple cranial bones of these two infants were examined and diagnosis with reference to Ortner and Ericksen (1997), Ortner et al. (1999; 2001), Brickley and Ives (2008) Snoddy et al. (2018) and Brickley and Mays (2019). Refer to *Table 5* for a differential diagnosis.

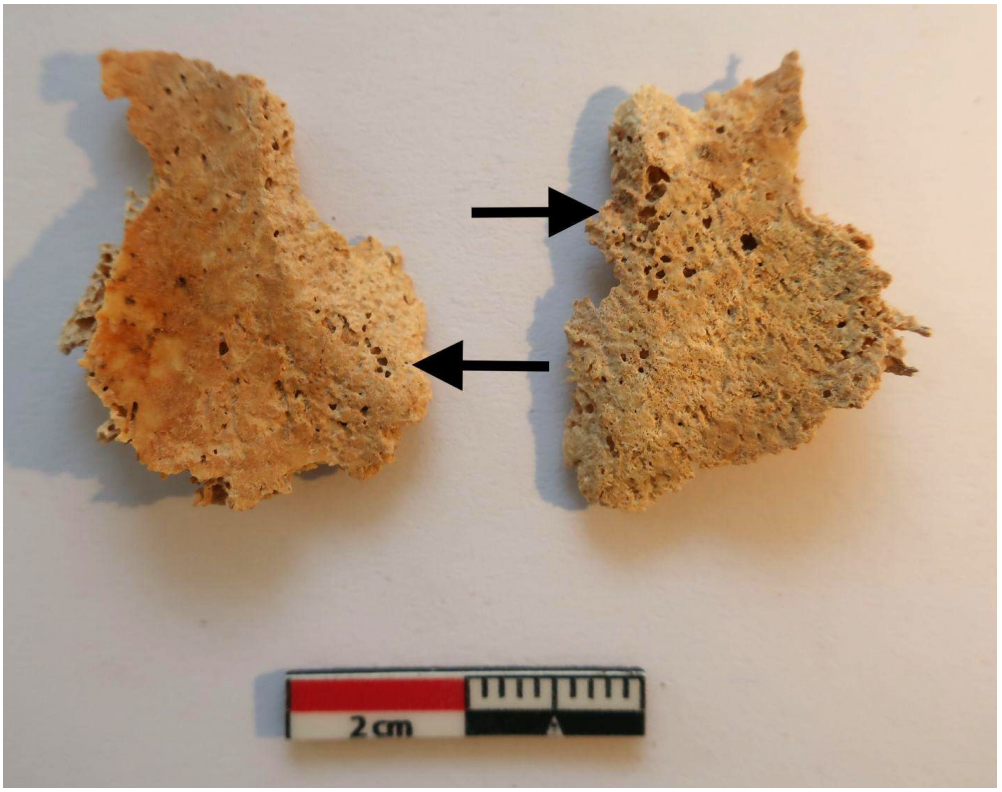

Figure 66: *Skeleton 17 — Bilateral abnormal porosity of the external surface of the greater wings of the sphenoid (photo: M. Liston)*

Figure 67: *Skeleton 17 — Abnormal porosity of the inferior maxilla (photo: M. Liston)*

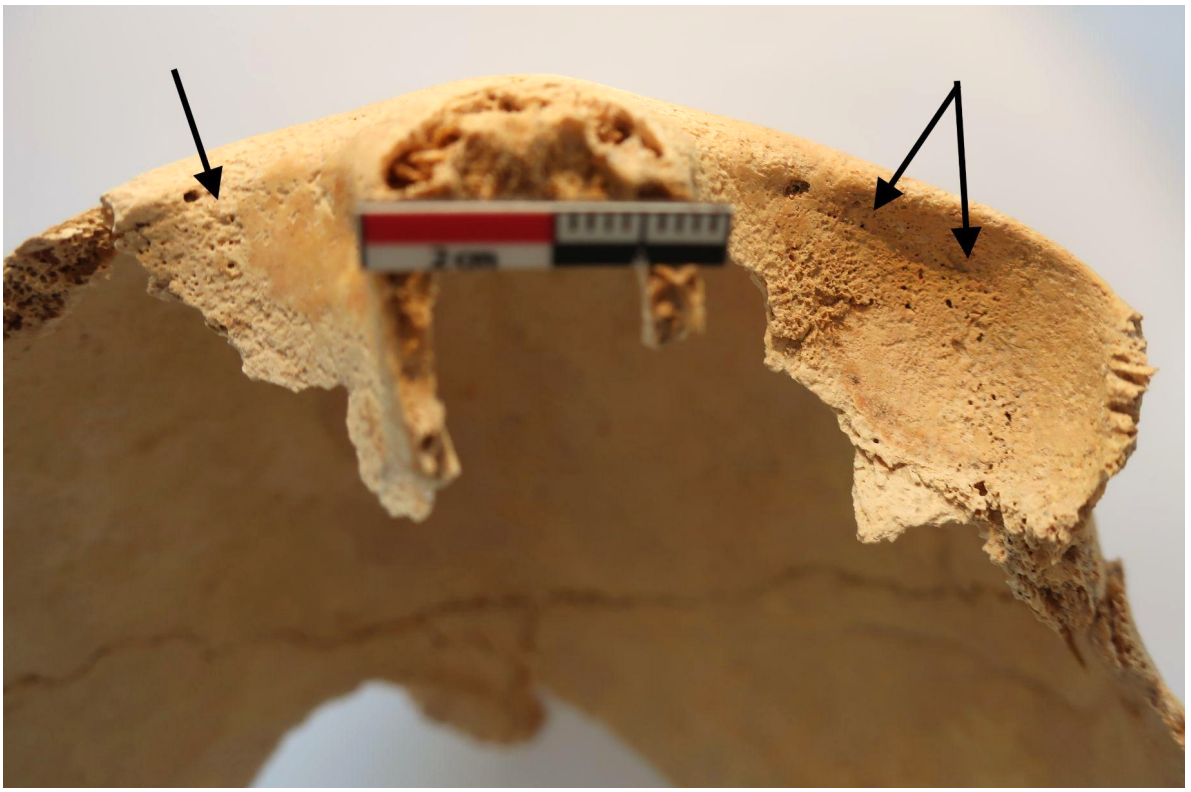

Figure 68: *Skeleton 17 — Cribra orbitalia of the eye orbits (photo: M. Liston)*

Figure 69: *Skeleton 17 — Accessory suture (photo: M. Liston)*

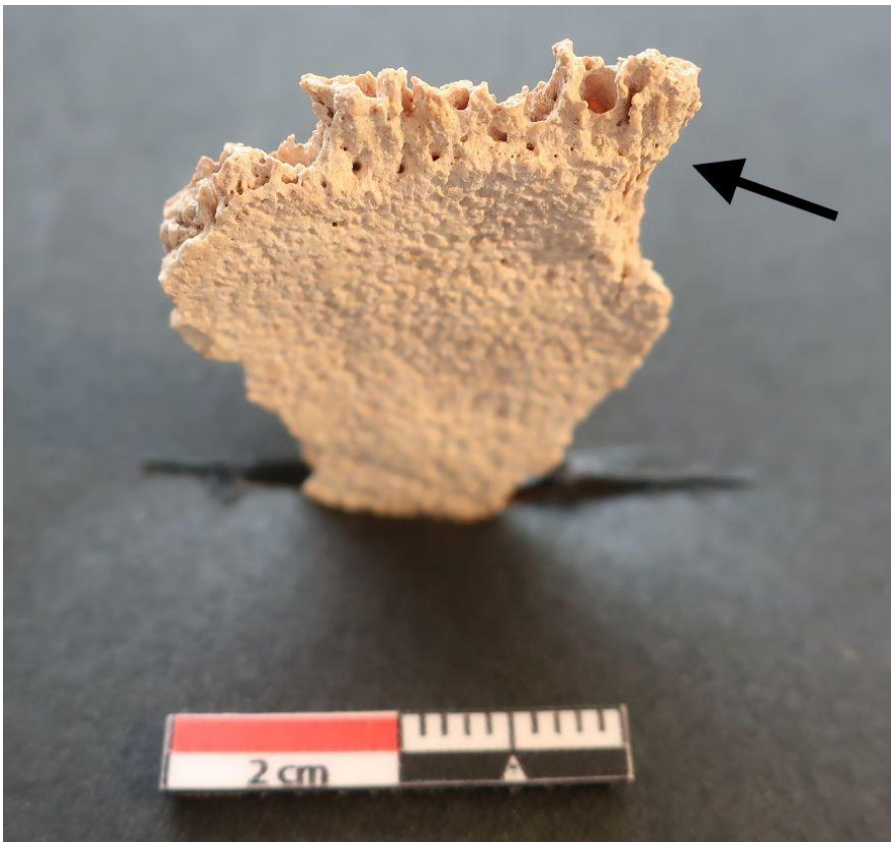

Figure 70: *Skeleton 17 — Possible endocranial pathology (photo: M. Liston)*

In juvenile skeletons, scurvy — or vitamin C deficiency — is a likely diagnostic option when there is abnormal bilateral porosity on the greater wings of the sphenoid (Ortner & Ericksen, 1997). The sphenoid is attached to the temporalis muscle, which is responsible for chewing. These infants have bilateral porosity on the greater wings of their sphenoid, which is likely the result of an inflammatory response to chronic hemorrhage in the deep vasculature associated with temporalis muscle function (Ortner & Ericksen, 1997). When a child is deficient in vitamin C, the formation of connective tissues including collagen and cement material in blood vessels is impacted (Ortner & Ericksen, 1997). This defect in cement material causes increased susceptibility to hemorrhage that results from muscle activity such as chewing (Ortner & Ericksen, 1997: 213). Ortner and Ericksen (1997: 218) argue that "this muscle activity is, at least in some cases of infantile and childhood scurvy, adequate to cause chronic hemorrhage and the associated inflammatory response in the areas of the skull anatomy related to chewing". This specific anatomical location and inflammatory response should differentiate it from other conditions such as anemia, where abnormal porosity develops in areas with red or mixed bone marrow (Brickley, 2018).

Table 5: Differential Diagnosis for 2022-1 and Skeleton 17 Cranial Porosity

Disease Characteristics	Scurvy	Leukemia	Thalassemia (anemia)	2022-1	Skeleton 17
Bilateral porosity on the external surface of the greater wings of the sphenoid	**x**			**x**	**x**
Porosity on the medial surface of the zygomatic	**x**			**x**	
Porosity on the inferior surface of the maxilla	**x**			**x**	**x**
Porosity on the medial surface of the mandible	**x**			**x**	**x**

Porosity on the maxillary and/or mandibular alveolar bone	**x**			**x**	
Porosity on the orbital walls (cribra orbitalia)	**x**	**x**	**x**	**x**	**x**
Ectocranial porosity on the cranial vault (porotic hyperostosis)	**x**	**x**	**x**	**x**	
Thickened diploë of cranial vault			**x**		
Hypertrophic bone formation (skull)	**x**			**x**	**x**
Periosteal bone formation (skull, long bones, ribs)		**x**			
Subperiosteal bone formation			**x**		
Porous cortical surface of the metaphyses		**x**			

The porosity seen in the eye orbits of these two infants (cribra orbitalia) differs from the porosity noted in the other juvenile, 2019-10. The porosity seen in the two infants has reactive, hypertrophic bone formation that is associated with scurvy (Ortner & Ericksen, 1997). This is unlike cases of anemia where bone changes are not hypertrophic, but a response to marrow expansion (Brickley, 2018). The porosity seen in the two infants is likely the result of chronic inflammation that penetrated the compact bone, and in the case of hypertrophy, the porosity is "superficial to existing compact bone" (Ortner et al., 2001: 345-346) This particular case of cribra orbitalia is likely related to inadequate vitamin C intake, and resulting hemorrhage from muscle activity controlling eye movement (Ortner & Ericksen, 1997).

Archaeological cases of infant scurvy in Greece are relatively limited (Bourbou, 2014). In a region of the world like the Mediterranean, where there is a temperate climate and rich cultivation of vitamin C-rich foods, scurvy was long believed to be rare (Bourbou, 2014). Humans do not produce their own vitamin C like other mammals (Brickley & Ives, 2008). Vitamin C is water soluble and is not stored in the body, thus frequent consumption of vitamin C rich foods is vital to prevent scurvy at all ages (Brickley & Ives, 2008). Human breast milk is a rich source of vitamin C, and unless the mother is deficient herself, breastfeeding is an adequate way for infants to receive this vitamin (Brickley & Ives, 2008).

Early weaning practices and nutritional disturbances can contribute to an infant developing scurvy (Brickley & Ives, 2008). This gradual transitional period from breastmilk to solid foods can raise the risk of scurvy if there is an introduction of food with low qualities of vitamin C (Brickley & Ives, 2008). Bourbou (2014: 92) notes that in ancient Greece, Byzantine physicians of the 4th-7th centuries C.E. recommended children be “brought up on milk until the age of 2 years". Afterwards, their diet should be changed to cereal foods. This would have significantly put infants at risk of developing scurvy, as cereals lack vitamin C (Brickley & Ives, 2008: 42). Written sources also document introducing goat’s milk and honey to infants during weaning, which could have had serious complications (Bourbou et al., 2013). Goat’s milk is low in cobalamine and folic acid, which has resulted in infants developing megaloblastic anemia due to folic acid deficiency (Bourbou et al., 2013). Moreover, honey is sometimes contaminated with *Clostridium botulinum* spores, a bacterium responsible for producing a severe form of food poisoning (Bourbou et al., 2013).

A stable isotope analysis of bone samples taken from juvenile skeletons from eight Byzantine (6th-15th centuries C.E.) sites in Greece suggests that weaning is typically completed by the fourth year of life (Bourbou et al., 2013). Since there was minor tooth wear noted in 2022-1 and Skeleton 17, it can be inferred that they had been introduced to

supplementary foods, and were eating solids. This gradual transition from breastmilk to adult foods may have been a factor in the development of scurvy in these two infants, as their age-at-death coincides with written sources for weaning ages in ancient Greece.

Natural disasters also play a role in malnourishment and dietary deficiencies such as scurvy (Brickley & Ives, 2008). Crop disease, famine, pests, storms, drought, earthquakes, epidemics, and warfare are all possible situations that factor into the development of metabolic bone disease, due to their potential impact on food supplies (Brickley & Ives, 2008). Corinth is no stranger to such events. Earthquakes were considered as a possible reason for cases of scurvy from a proto-Byzantine (6th - 7th century C.E.) site at Eleutherna, Greece (Bourbou, 2003a, 2003b; Brickley & Ives, 2008). Earthquakes have been reported in Ancient Corinth in 521/522 C.E. and again in 1858 C.E. (Sanders et al., 2018: 9). While this is an interesting thing to note, it is uncertain if the 1858 C.E. earthquake occurred when these two infants were alive. Until radiocarbon dating reveals a time estimate for the NET skeletons, the specific etiology for scurvy seen in these two juveniles remains multifactorial and speculative.

2.8 Discussion & Conclusions

Ancient Corinth has an extensive history, and part of that history involves disease, earthquakes, and many hardships (Williams et al., 1998). The various joint diseases and skeletal changes identified in the adult skeletons from the NET Cemetery indicate that these individuals lived physically demanding lives, likely associated with strenuous activities needed to sustain life in post-12th century C.E. Corinth. The dentitions were relatively healthy, however the presence of LEH in three adults (2019-1, 2019-5, 2022-2) and one juvenile (2019-10) indicate that they went through non-specific periods of stress in their childhood. The adults survived whatever stress events they experienced, and reached skeletal maturity. The juvenile (2019-10) died between the ages of 12-15 years, and the infants

succumbed very early in life, likely the result of nutritional deficiencies associated with scurvy and possibly weaning.

The identification of spinal TB in the 27-40 year old male (2019-6) indicates that there was infectious disease in the community. Due to the fact that TB rarely affects the skeleton in those who are infected with the disease, "absence of evidence is not evidence of absence" (Roberts & Buikstra, 2003: 87). Were the other individuals buried in the NET Cemetery infected with TB at the time of death? Moreover, since LEH results from either metabolic stress, nutritional deficiency, or childhood illness (Roberts & Manchester, 2007), this may indicate that these individuals had a compromised immune system. Poor nutrition leading to under or malnutrition can impact one's immunity, which can influence the severity and duration of diseases such as TB (Roberts & Buikstra, 2003). "Infection and nutritional stress are inextricably linked", therefore Roberts and Buikstra (2003: 54) suggest that poverty and TB have a strong connection — today and in the past.

The earliest identified case of TB in Greece is from 900 B.C.E. (Angel, 1984; Roberts & Buikstra, 2003), and continues to persist today. To date, no skeletal cases of TB, or scurvy, have been identified in Ancient Corinth. Modern cases of TB are highly factored by poverty, poor nutrition, compromised immune systems, urban environments, high population density, poor access to health care and resistance to drugs (Roberts, 2011). In England, TB began to flourish in the post-medieval period, particularly during the 12th-16th century C.E. (Roberts, 2011). Although not specific to Greece, or Ancient Corinth, these post-medieval dates associated with a rise in TB in Europe coincide with the tentative date for the NET Cemetery. Michaleas et al. (2022) note that from 1918-1939 C.E. TB was characterized as a social disease in Greece. This is because the disease spread to the lower social classes, including people living in refugee camps (Michaleas et al., 2022). Again, we do not know the precise

date of the NET Cemetery, therefore, making further interpretations into the specific social and biological entanglements of TB in this context is not possible at this time.

The pathological conditions presented in this study have complex and multifactorial etiologies. These must be considered with respect to the highly variable and ever "complex social interactions between humans, humans and their environments, and varying physiological needs throughout the life course" (Grauer & Buikstra, 2019: 30). It is vital to consider the small sample size of this study, and the fact that this is the first analysis of these individuals. The interpretations and narratives formed throughout this thesis represent only a small portion of potential research avenues to be explored. The Corinth Excavations plan to extend the excavation, which may reveal more graves associated with this cemetery.

2.9 Future Directions

One of the first steps necessary to proceed further with this research is to radiocarbon date the skeletons. The biggest limitation is not knowing the specific time period that these people are from, which makes contextualizing the paleopathological data within a cultural context challenging. It would also be useful to radiocarbon date the two infants excavated to the south of the NET Cemetery. Since the specific cause of scurvy is unknown, perhaps situating them temporally will give further clues to the etiology of the metabolic disease.

Moreover, evidence for disease and pathological conditions in skeletal remains are investigated directly or indirectly. This study used indirect methods for recording and interpreting the data — through observation. In the future, direct methods such as chemical bone analysis could be considered for the NET skeletons. For example, stable isotope analysis of carbon and nitrogen values in the protein of teeth, and stable isotope analysis of carbon, oxygen, and strontium from bones and teeth may reveal more in-depth interpretations regarding diet and migration (Kinaston et al., 2019). Stable isotope analysis may be of particular interest in the case of the two infants with scurvy; perhaps the specific weaning

time can be estimated, as well as which supplementary foods were introduced during this time (Kinaston et al., 2019).

Since there is a case of TB in the NET Cemetery, and skeletal changes are so rare, it is possible that other individuals buried in the NET Cemetery were infected with TB at the time of death, but did not develop skeletal lesions (Wood et al., 1992). If skeletal preservation is suitable, an area of future research is to evaluate potential pathogen DNA of *Mycobacterium tuberculosis* and/or *Mycobacterium bovis,* which both cause TB in humans and may produce skeletal changes (Roberts & Buikstra, 2003). This may contribute to our understanding of past human health in Ancient Corinth, and reveal whether or not more people from the cemetery were infected with TB.

More in-depth dental studies is also an area of future research. Four NET skeletons have LEH, however estimating the individual's age and LEH formation was not presented in this research. Finally, future directions for research are heavily influenced by continuing the NET excavations to explore the limits of the NET Cemetery. Perhaps there are many more graves, and more questions can be answered about the individual's buried northeast of the ancient theatre.

References

AlQahtani, S. J., Liversidge, H. M., & Hector, M. P. (2010). Brief communication: The London atlas of human tooth development and eruption. *American Journal of Physical Anthropology, 142*(3), 481-490. DOI: 10.1002/ajpa.21258.

American School of Classical Studies at Athens. (2022). *Ancient Corinth.* Retrieved March 13, 2022, from https://www.ascsa.edu.gr/excavations/ancient-corinth.

American School of Classical Studies at Athens. (2022). *About the Excavations.* Retrieved March 13, 2022, from https://www.ascsa.edu.gr/excavations/ancient-corinth/about-the-excavations-1.

American School of Classical Studies at Athens. (2022). *Education and Outreach.* Retrieved December 20, 2022, from https://www.ascsa.edu.gr/excavations/ancient-corinth/outreach-and-education.

Angel, J. L. (1944). A racial analysis of the ancient Greeks: An essay on use of morphological types. *American Journal of Physical Anthropology*, *2*(4), 329-376.

Angel, J. L. (1945). Skeletal material from Attica. *Hesperia: The Journal of the American School of Classical Studies at Athens*, *14*(4), 279-363.

Angel, J. L. (1947). The length of life in Ancient Greece. *Journal of Gerontology, 2*(1), 18-24. DOI: 10.1093/geronj/2.1.18.

Angel, J. L. (1964). Osteoporosis: Thalassemia? *American Journal of Physical Anthropology*, *22*(3), 369-373.

Angel, J. L. (1966). Porotic hyperostosis, anemias, malarias, and marshes in the prehistoric eastern Mediterranean. *Science*, *153*(3737), 760-763.

Angel, J. L. (1969). The bases of paleodemography. *American Journal of Physical Anthropology, 30,* 427-438. DOI:10.1002/ajpa.1330300314.

Angel, J. L. (1972). Ecology and population in the eastern Mediterranean. *World Archaeology*, *4*(1), 88-105.

Angel, J. L. (1984). Health as a crucial factor in the changes from hunting to developed farming in the Eastern Mediterranean. In M. N. Cohen & G. J Armelagos (Eds.), *Paleopathology at the origins of agriculture* (pp. 51-74). London: Academic Press.

Barnes, E. (2003). The dead do tell tales. *Corinth: Results of Excavations Conducted by the American School of Classical Studies at Athens*, 435-443.

Barnes, E. (2012). *Atlas of developmental field anomalies of the human skeleton: A paleopathology perspective.* Wiley-Blackwell.

Barnes, E., & Ortner, D. J. (1997). Multifocal eosinophilic granuloma with a possible trepanation in a fourteenth century Greek young skeleton. *International Journal of Osteoarchaeology*, *7*(5), 542-547.

Bass, W. M. (1987). *Human osteology: A laboratory and field manual* (3rd ed.). Missouri: Missouri Archaeology Society.

Boldsen, J. L., Milner, G. R., Konigsberg, L. W., & Wood, J. W. (2002). Transition analysis: A new method for estimating age from skeletons. In R. D. Hoppa & J. W. Vaupel (Eds.), *Paleodemography: Age distributions from skeletal samples* (pp. 73-106). Cambridge University Press. DOI: 10.1017/CBO9780511542428.005.

Bourbou, C. (2003a). Health patterns of proto-byzantine populations (6th-7th centuries AD) in South Greece: The cases of Eleutherna (Crete) and Messene (Peloponnese). *International Journal of Osteoarchaeology, 13*, 303-313. DOI: 10.1002/oa.702.

Bourbou, C. (2003b). The interaction between a population and its environment: Probable case of subadult scurvy from proto-byzantine Greece. *Eres Arqueología/Bioantropología, 11,* 105-114.

Bourbou, C., Fuller, B. T., Garvie-Lok, S. J., & Richards, M. P. (2013). Nursing mothers and feeding bottles: Reconstructing breastfeeding and weaning patterns in Greek Byzantine populations (6th–15th centuries AD) using carbon and nitrogen stable isotope ratios. *Journal of Archaeological Science*, *40*(11), 3903-3913. DOI: 10.1016/j.jas.2013.04.020.

Bourbou, C. (2014). Evidence of childhood scurvy in a Middle Byzantine Greek population from Crete, Greece (11th-12th centuries A.D.). *International Journal of Paleopathology, 5,* 86-94. DOI: 10.1016/j.ijpp.2013.12.002.

Brickley, M. (2002). An investigation of historical and archaeological evidence for age-related bone loss and osteoporosis. *International Journal of Osteoarchaeology, 12,* 364-371. DOI: 10.1002/oa.635.

Brickley, M., & Ives, R. (2008). *The bioarchaeology of metabolic bone disease.* Elsevier Academic Press.

Brickley, M. B. (2018). *Cribra orbitalia* and porotic hyperostosis: A biological approach to diagnosis. *American Journal of Physical Anthropology, 167,* 896-902. DOI: 10.1002/ajpa.23701.

Brickley, M. B., & Mays, S. (2019). Metabolic disease. In J. E. Buikstra (Ed.), *Ortner's identification of pathological conditions in human skeletal remains* (pp. 531-566). Elsevier Academic Press. DOI: 10.1016/B978-0-12-809738-0.00015-6.

Brooks, S. T., & Suchey, J. M. (1990). Skeletal age determination based on the os pubis: A

comparison of the Acsádi-Nemeskéri and Suchey-Brooks methods. *Human Evolution, 5,* 227-238.

Brothwell, D. R. (1981). *Digging up bones: The excavation, treatment and study of human skeletal remains* (3rd edition). Ithaca, New York: Cornell University Press.

Buikstra, J. E. (2019). *Ortner's identification of pathological conditions in human skeletal remains* (3rd ed.). (J. E. Buikstra, Ed.). Elsevier Academic Press.

Buikstra, J. E., & Ubelaker, D. H. (Eds.). (1994). *Standards for data collection from human skeletal remains.* Fayetteville, Arkansas: Arkansas Archaeological Survey Report Number 44.

Buikstra, J. E., & DeWitte, S. (2019). A brief history and 21st century challenges. In J. E. Buikstra (Ed.), *Ortner's identification of pathological conditions in human skeletal remains* (pp. 11- 19). Elsevier Academic Press. DOI: 10.1016/B978-0-12-809738-0.00002-8.

Churchill, R. W., Munoz, J., & Ahmad, C. S. (2016). Osteochondritis dissecans of the elbow. *Current Reviews in Musculoskeletal Medicine, 9,* 232-239. DOI: 10.1007/s12178-016-9342-y.

Clark, M. A., Cheverko, C. M., Simon, A., Lagan, E. M., & Hubbe, M. (2022). The decade under review: Recent trends and challenges in the use of macroscopic age-at-death estimation methods in bioarchaeology. *International Journal of Osteoarchaeology,* 1-14. DOI: 10.1002/oa.3142.

Danforth, L. M., & Tsiaras, A. (1982). *The death rituals of rural Greece.* Princeton University Press.

DeWitte, S. N., & Bekvalac, J. (2010). Oral health and frailty in the medieval English cemetery of St Mary Graces. *American Journal of Physical Anthropology*, *142*(3), 341-354. DOI: 10.1002/ajpa.21228.

Dubisch, J. (1989). Death and social change in Greece. *Anthropology Quarterly, 62*(4). 189-200. DOI: 10.2307/3317615.

Duday, H. (2009). *The archaeology of the dead: Lectures in archaeothanatology* (A. M. Cipriani & J. Pearce, Trans.). Oxbow Books, Oxford, UK.

Faccia, K. J., & Williams, R. C. (2008). Schmorl's nodes: Clinical significance and implications for the bioarchaeological record. *International Journal of Osteoarchaeology, 18,* 28-44. DOI: 10.1002/oa.924.

Fox Leonard, S. C. (1997). *Comparative health from paleopathological analysis of the human skeletal remains dating to the Hellenistic and Roman periods, from Paphos, Cyprus and Corinth, Greece.* [Unpublished doctoral dissertation]. The University of Arizona.

Garvie-Lok, S. J. (2001). *Loaves and fishes: a stable isotope reconstruction of diet in medieval Greece.* [Unpublished doctoral dissertation]. The University of Calgary.

Gellhorn, A. C., Katz, J. N., & Suri, P. (2013). Osteoarthritis of the spine: The facet joints. *Nature Reviews Rheumatology, 9*(4), 216-224. DOI: 10.1038/nrrheum.2012.199.

Grauer, A. L., & Buikstra, J. E. (2019). Themes in paleopathology. In J. E. Buikstra (Ed.), *Ortner's identification of pathological conditions in human skeletal remains* (pp. 21-33). Elsevier Academic Press. DOI: 10.1016/B978-0-12-809738-0.00003-X.

Grauer, A. L. (2019). Circulatory, reticuloendothelial, and hematopoietic disorders. In J. E. Buikstra (Ed.), *Ortner's identification of pathological conditions in human skeletal remains* (pp. 491-529). Elsevier Academic Press. DOI: 10.1016/B978-0-12-809738-0.00014-4.

Hillson, S. (1996). *Dental anthropology*. Cambridge University Press.

International Journal of Paleopathology. (2022). *Guide for Authors.* Accessed February 27, 2022, from https://www.elsevier.com/journals/international-journal-of-paleopathology/1879-9817/guide-for-authors.

Kinaston, R., Willis, A., Miszkiewicz, J. J., Tromp, M., & Oxenham, M. F. (2019). The dentition: Development, disturbances, disease, diet and chemistry. In J. E. Buikstra (Ed.), *Ortner's identification of pathological conditions in human skeletal remains* (pp.749-797). Elsevier Academic Press. DOI: 10.1016/B978-0-12-809738-0.00021-1.

Klaus, H. D., & Lynnerup, N. (2019). Abnormal bone: Considerations for documentation, disease process identification, and differential diagnosis. In J. E. Buikstra (Ed.), *Ortner's identification of pathological conditions in human skeletal remains* (pp. 59-89). Elsevier Academic Press. DOI: 10.1016/B978-0-12-809738-0.00005-3.

Knutsen, E. J., & Goldfarb, C. A. (2014). Madelung's deformity. *Hand, 9,* 289-291. DOI: 10.1007/s11552-014-9633-y.

Koudela, K. Jr., Koudelová, J., Koudela, K. Sr., & Zeman, P. (2015). Concave impressio ligamenti costoclavicularis ("rhomboid fossa") and its prevalence and relevance to clinical practice. *Surgical and Radiologic Anatomy, 37*(3), 239-245. DOI: 10.1007/s00276-014-1342-2.

Kurtz, D. C., & Boardman, J. (1971). *Greek burial customs*. Ithaca, New York: Cornell University Press.

Kyle, B., Reitsema, L. J., Tyler, J., Fabbri, P. F., & Vassallo, S. (2018). Examining the

osteological paradox: Skeletal stress in mass graves versus civilians at the Greek colony of Himera (Sicily). *American Journal of Physical anthropology*, *167*(1), 161-172. DOI: 10.1002/ajpa.23624.

Lewis, M. (2019). Skeletal dysplasias and related conditions. In J. E. Buikstra (Ed.), *Ortner's identification of pathological conditions in human skeletal remains* (pp. 615-637). Elsevier Academic Press. DOI: 10.1016/B978-0-12-809738-0.00018-1.

Lovejoy, C. O., Meindl, R. S., Pryzbeck, T. R., & Mensforth, R. P. (1985). Chronological metamorphosis of the auricular surface of the ilium: A new method for the determination of age at death. *American Journal of Physical Anthropology, 68,* 15-28.

Ludwisiak, K., Podgórski, M., Biernacka, K., Stefańczyk, L., Olewnik, Ł., Majos, A., Polguj, M. (2019). Variation in the morphology of spinous processes in the cervical spine - An objective and parametric assessment based on CT study. *PLoS One, 14*(6), e0218885. DOI: 10.1371/journal.pone.0218885.

Luna, L. H., Aranda, C. M., & Santos, A. L. (2017). New method for sex prediction using the human non-adult auricular surface of the ilium in the collection of identified skeletons of the University of Coimbra. *International Journal of Osteoarchaeology, 27*, 898–911. DOI: 10.1002/oa.2604.

Mariotti, V., Facchini, F., & Belcastro, M. G. (2004). Enthesopathies — Proposal of a standardized scoring method. *Collegium Antropologicum, 28*(1), 145-159.

Martin, D. L., & Harrod, R. P. (2016). The bioarchaeology of pain and suffering: Human adaptation and survival during troubled times. *Archeological Papers of the American Anthropological Association, 27,* 161-174. DOI: 10.1111/apaa.12080.

Mays, S. (2006). Age-related cortical bone loss in women from a 3rd–4th century AD population from England. *American Journal of Physical Anthropology, 129*, 518-528. DOI: 10.1002/ajpa.20365.

Meindl, R.S., & Lovejoy, C. O. (1985). Ectocranial suture closure: A revised method for the determination of skeletal age at death based on the lateral-anterior sutures. *American Journal of Physical Anthropology, 68,* 57-66.

Meindl, R. S., & Lovejoy, C. O. (1989). Age changes in the pelvis: Implications for paleodemography. In M. Y. Iscan (Ed.), *Age Markers in the Human Skeleton* (pp. 137-168). Springfield, Illinois: Charles C. Thomas.

Merriam-Webster. (n.d.). Public. In *Merriam-Webster.com dictionary*. Retrieved November 10, 2022, from https://www.merriam-webster.com/dictionary/public.

Michaleas, S. N., Protogerou, A. D., Sipsas, N. V., Panayiotakopoulos, G., Angelakis, A.C., Michailidou, C., & Karamanou, M. (2022). The anti-tuberculosis battle in Greece in the 1800s and 1900s. *Cureus, 14*(6):e26023. DOI: 10.7759/cureus.26023.

Milella, M., Giovanna Belcastro, M., Zollikofer, C. P., & Mariotti, V. (2012). The effect of age, sex, and physical activity on entheseal morphology in a contemporary Italian skeletal collection. *American Journal of Physical Anthropology, 148*(3). 379-388. DOI: 10.1002/ajpa.22060.

Milner, G. R., Ousley, S. D., Boldsen, J. L., Getz, S. M., Weise, S., & Tarp, P. (2019). Transition Analysis 3 (TA3) Trait Manual–Public Distribution Manual Ver 1.0. *Public Distribution Version*, *1*.

Ortner, D. J., & Ericksen, M. F. (1997). Bone changes in the human skull probably resulting from scurvy in infancy and childhood. *International Journal of Osteoarchaeology, 7,* 212–220.

Ortner, D. J., Kimmerle, E. H., & Diez, M. (1999). Probable evidence of scurvy in subadults from archaeological sites in Peru. *American Journal of Physical Anthropology, 108*(3)*,* 321-331.

Ortner, D. J., Butler, W., Cafarella, J., & Milligan, L. (2001). Evidence of probable scurvy in subadults from archaeological sites in North America. *American Journal of Physical Anthropology, 114,* 343-351.

Parker Pearson, M. (1999). *The archaeology of death and burial.* Texas A&M University Press.

Pfaff, C. A. (2020). Corinth, 2018: Northeast of the theatre. *Hesperia: The Journal of the American School of Classical Studies at Athens, 89*, 125-190.

Pfaff, C. A. (2021). Corinth, 2019: Northeast of the theatre. *Hesperia: The Journal of the American School of Classical Studies at Athens, 90*(4), 773-818.

Poulou-Papadimitriou, N., Tzavella, E., & Ott, J. (2012). Burial practices in Byzantine Greece: Archaeological evidence and methodological problems for its interpretation. In M. Salamon, M. Wołoszyn, A. Musin, & P. Špehar (Eds.), *Rome, Constantinople and Newly-Converted Europe: Archaeological and Historical Evidence* (pp. 377-428). Leipzig — Rzeszów — Warszawa.

Phenice, T. W. (1969). A newly developed visual method of sexing the os pubis. *American Journal of Physical Anthropology*, *30*(2), 297–301. DOI: 10.1002/ajpa.1330300214.

Redfern, R., & Roberts, C. A. (2019). Trauma. In J. E. Buikstra (Ed.), *Ortner's identification of pathological conditions in human skeletal remains* (pp. 211-284). Elsevier Academic Press. DOI: 10.1016/B978-0-12-809738-0.00009-0.

Renshaw, L., & Powers, N. (2016). The archaeology of post-medieval death and burial.

Post-Medieval Archaeology, 50(1), 159-177. DOI: 10.1080/00794236.2016.1169491.

Resnick, D., Goergen, T., & Niwayama, G. (1995). Physical injury: Concepts and terminology. In D. Resnick (Ed.), *Diagnosis of Bone and Joint Disorders* (3rd edition). (pp. 2561-2695). Philadelphia, PA.

Roberts, C. (2011). The bioarchaeology of leprosy and tuberculosis: A comparative study of perceptions, stigma, diagnosis, and treatment. In S. C. Agarwal & B. A. Glencross (Eds.), *Social bioarchaeology* (pp. 252-281). Wiley-Blackwell Publishing Ltd.

Roberts, C. A., & Buikstra, J. E. (2003). *The bioarchaeology of tuberculosis: A global view on a reemerging disease.* University Press of Florida.

Roberts, C. A., & Buikstra, J. E. (2019). Bacterial infections. In J. E. Buikstra (Ed.), *Ortner's identification of pathological conditions in human skeletal remains* (pp. 321-439). Elsevier Academic Press. DOI: 10.1016/B978-0-12-809738-0.00011-9.

Roberts, C., & Manchester, K. (2007). *The archaeology of disease* (3rd edition). Cornell University Press: New York.

Rogers, N. L., Flournoy, L. E., & McCormick, W. F. (2000). The rhomboid fossa of the clavicle as a sex and age indicator. *Journal of Forensic Sciences, 45*(1), 61-67.

Sanders, G. D. R., James, S. A., & Johnson, A.C. (2017). *Corinth Excavations Archaeological Manual.* The Digital Press at the University of North Dakota.

Sanders, G. D. R., Palinkas, J., Tzonou-Herbst, I., & Herbst, J. (2018). *Ancient Corinth: Site guide* (7th ed.). American School of Classical Studies at Athens. Princeton, New Jersey.

Schaefer, M., Black, S., & Scheuer, L. (2009). *Juvenile osteology: A laboratory and field manual*. London: Elsevier.

Scheuer, L., & Black, S. (2004). *The juvenile skeleton.* Elsevier Academic Press.

Schultz, M. (2001). Paleohistopathology of bone: A new approach to the study of ancient disease. *Yearbook of Physical Anthropology, 44,* 106-147. DOI: 10.1002/ajpa.10024.

Siek, T. (2014). *A study in paleo-oncology: On the identification of neoplastic disease in archaeological bone.* [Unpublished master's thesis]. The University of Waterloo.

Snoddy, A. M. E., Buckley, H. R., Elliott, G. E., Standen, V. G., Arriaza, B. T., & Halcrow, S. E. (2018). Macroscopic features of scurvy in human skeletal remains: A literature synthesis and diagnostic guide. *American Journal of Physical Anthropology, 167,* 876-895. DOI: 10.1002/ajpa.23699.

Stuart-Macadam, P., Glencross, B., & Kricun, M. (1998). Traumatic bowing deformities in tubular bones. *International Journal of Osteoarchaeology, 8,* 252-262.

Suchey, J., & Katz, D. (1986). Skeletal age standards derived from an extensive multiracial sample of modern Americans. Abstract. *American Journal of Physical Anthropology, 69*, 269.

Todd, T. W. (1921a). Age changes in the pubic bone. I: The male white pubis. *American Journal of Physical Anthropology, 3*, 285-334.

Todd, T. W. (1921b). Age changes in the pubic bone. III: The pubis of the white female. IV: The pubis of the female white-negro hybrid. *American Journal of Physical Anthropology, 4,* 1-70.

Ubelaker, D. H. (1989). *Human skeletal remains: Excavation, analysis, interpretation* (2nd ed.). Taraxacum, Washington.

Walker, P. L., Bathurst, R. R., Richman, R., Gjerdrum, T., & Andrushko, V. A. (2009). The causes of porotic hyperostosis and cribra orbitalia: A reappraisal of the iron-deficiency-anemia hypothesis. *American Journal of Physical Anthropology*, *139*(2), 109-125. DOI: 10.1002/ajpa.21031.

Weiss-Krejci, E. (2011). The formation of mortuary deposits: Implications for understanding mortuary behaviour of past populations. In S. C. Agarwal & B. A. Glencross (Eds.), *Social bioarchaeology* (pp. 68-106). Wiley-Blackwell Publishing Ltd.

Wells, C. (1974). Osteochondritis dissecans in ancient British skeletal material. *Medical History, 18,* 365–369. DOI: 10.1017/s0025727300019815.

White, T. D., & Folkens, P. A. (2005). *The human bone manual.* Elsevier Academic Press.

Williams, C. K., Synder, L. M., Barnes, E., & Zervos, O. H. (1998). Frankish Corinth: 1997. *Hesperia: The Journal of the American School of Classical Studies at Athens, 67*(3), 223-281. https://doi.org/10.2307/2668470.

Wood, J. W., Milner, G. R., Harpending, H. C., & Weiss, K. M. (1992). The osteological paradox. *Current Anthropology, 33*(4), 343-370.

Yusof, M. I., Hassan, E., Rahmat, N., & Yunus, R. (2009). Spinal tuberculosis: The association between pedicle involvement and anterior column damage and kyphotic deformity. *Spine*, *34*(7), 713-717. DOI: 10.1097/BRS.0b013e31819b2159.

Zervos, O. H., Rohn, A. H., Barnes, E., & Sanders, G. D. R. (2009). An Early Ottoman Cemetery at Ancient Corinth. *Hesperia: The Journal of the American School of Classical Studies at Athens, 78*(4), 501-615. http://www.jstor.org/stable/25622710.

Zúñiga Thayer, R., Suby, J., Luna, L., & Flensborg, G. (2020). *Osteochondritis dissecans* and physical activity in skeletal remains of ancient hunter-gatherers from Southern Patagonia. *International Journal of Osteoarchaeology, 31,* 77-87. DOI: 10.1002/oa.2926.

Appendix A: Tables 6-8

Table 6: Methods Used for Biological Sex and Age-at-death Estimations

Grave Number	Biological Sex	Age-at-death	Methods Used
2022-2	Female	30-39 years	***Biological Sex:*** **Os Coxae morphology** (Buikstra & Ubelaker, 1994: 16-19; Phenice, 1969) **Cranial morphology** — nuchal crest, mastoid process, and mental eminence only (Buikstra & Ubelaker, 1994: 19-20) ***Age-at-death:*** **Auricular surface** — L/R Phase 3-4 (Lovejoy et al., 1985; Meindl & Lovejoy, 1989; Buikstra & Ubelaker, 1994: 24-32) **Transition Analysis 2.0** (Boldsen et al., 2002)
2019-1	Male	30-40 years	***Biological Sex:*** **Cranial morphology** (Buikstra & Ubelaker, 1994: 19-20) **Femur head diameter: 46.8 mm** (Bass, 1987: 219) ***Age-at-death:*** **Auricular surface** — R Phase 3 (Lovejoy et al., 1985; Meindl & Lovejoy, 1989; Buikstra & Ubelaker, 1994: 24-32) **Transition Analysis 2.0** (Boldsen et al., 2002)
2019-2	Male	20-29 years	***Biological Sex:*** **Os Coxae morphology** — greater sciatic notch only (Buikstra & Ubelaker, 1994: 16-19; Phenice, 1969) **Cranial morphology** (Buikstra & Ubelaker, 1994: 19-20) **Femur head diameter: 44 mm (ambiguous)** (Bass, 1987: 219) ***Age-at-death:***

			Standards of Occlusal Wear of Molar Teeth for Age Classification (Brothwell, 1981) **Transition Analysis 2.0** (Boldsen et al., 2002) **Fused epiphyses of the right proximal and left distal radius, and right distal humerus** (Buikstra & Ubelaker 1994: 43)
2019-3	Male?	Late 20's - early 30's?	***Biological Sex:*** Estimated based on in-situ appearances: narrow subpubic angle ***Age-at-death:*** Estimated based on in-situ appearances: fused epiphyses and lack of arthritis
2019-4	Female?	18-25 years	***Biological Sex:*** **Cranial morphology** — nuchal crest and mental eminence only (Buikstra & Ubelaker, 1994: 19-20) ***Age-at-death:*** **Standards of Occlusal Wear of Molar Teeth for Age Classification** (Brothwell, 1981) **Unfused medial epiphysis of left clavicle** (Buikstra & Ubelaker 1994: 43)
2019-5	Male?	40-44 years	***Biological Sex:*** **Cranial morphology** — nuchal crest, right mastoid process, and mental eminence only (Buikstra & Ubelaker, 1994: 19-20) **Femur head diameter: 43 mm (ambiguous)** (Bass, 1987: 219) ***Age-at-death:*** **Auricular surface** — L R Phase 5 (Lovejoy et al., 1985; Meindl & Lovejoy, 1989; Buikstra & Ubelaker, 1994: 24-32) **Standards of Occlusal Wear of Molar Teeth for Age Classification** (Brothwell, 1981) **Transition Analysis 2.0** (Boldsen et al., 2002)

2019-6	Male	27-40 years	***Biological Sex:*** **Os Coxae morphology** — greater sciatic notch only (Buikstra & Ubelaker, 1994: 16-19; Phenice, 1969) **Cranial morphology** (Buikstra & Ubelaker, 1994: 19-20) ***Age-at-death:*** **Public symphysis** — L Phase 5 (Todd, 1921a, 1921b) — L Phase 2-3 (Brooks & Suchey, 1990; Suchey & Katz, 1986; Buikstra & Ubelaker, 1994: 22-24) **Auricular surface** — L Phase 3 (Lovejoy et al., 1985; Meindl & Lovejoy, 1989; Buikstra & Ubelaker, 1994: 24-32) **Transition Analysis 2.0** (Boldsen et al., 2002)
2019-7	Female	35-45 years	***Biological Sex:*** **Cranial morphology** (Buikstra & Ubelaker, 1994: 19-20) ***Age-at-death:*** **Auricular surface** — R Phase 4-5 (Lovejoy et al., 1985; Meindl & Lovejoy, 1989; Buikstra & Ubelaker, 1994: 24-32) **Standards of Occlusal Wear of Molar Teeth for Age Classification** (Brothwell, 1981) **Transition Analysis 2.0** (Boldsen et al., 2002)
2019-8	Male	18-25 years	***Biological Sex:*** **Os Coxae morphology** — preauricular sulcus only (Buikstra & Ubelaker, 1994: 16-19; Phenice, 1969) **Cranial morphology** — mental eminence, flared gonial angle (Buikstra & Ubelaker, 1994: 19-20) **Femur head diameter: 51 mm** (Bass, 1987: 219) ***Age-at-death:***

			Auricular surface — R Phase 1 (Lovejoy et al., 1985; Meindl & Lovejoy, 1989; Buikstra & Ubelaker, 1994: 24-32) **Transition Analysis 2.0** (Boldsen et al., 2002) **Unfused medial epiphysis of left clavicle** (Buikstra & Ubelaker 1994: 43)
2019-9	Male?	35-45 years	***Biological Sex:*** **Os Coxae morphology** — greater sciatic notch and preauricular sulcus only (Buikstra & Ubelaker, 1994: 16-19; Phenice, 1969) ***Age-at-death:*** **Public symphysis** — R Phase 7-8 (Todd, 1921a, 1921b) — R Phase 4-5 (Brooks & Suchey, 1990; Suchey & Katz, 1986; Buikstra & Ubelaker, 1994: 22-24) **Auricular surface** — L/R Phase 5 (Lovejoy et al., 1985; Meindl & Lovejoy, 1989; Buikstra & Ubelaker, 1994: 24-32) **Transition Analysis 2.0** (Boldsen et al., 2002)
2019-10	Unknown	12-15 years	***Biological Sex:*** **Cranial morphology attempted** — nuchal crest, mastoid process, supraorbital margin, mental eminence (Buikstra & Ubelaker, 1994: 19-20) Note: Scores were attempted, and all within the female-range. This is typical of a prepubescent skeleton. Biological sex for this individual remains inconclusive. ***Age-at-death:*** **Dental Development** (Ubelaker, 1989) **Atlas of Human Tooth Development and Eruption** (AlQahtani et al., 2010)
2022-1	Unknown	1.1-1.6 years (+/- 0.17-0.25)	***Age-at-death:*** **Regression equation for estimating age (yrs) in detention** (Schaefer et al., 2009)

			Postcranial measurements (Schaefer et al., 2009) **Dental Development** (Ubelaker, 1989)
Skeleton 17	Unknown	1.8-3.0 years (+/- 0.17-0.22)	***Age-at-death:*** **Regression equation for estimating age (yrs) in detention** (Schaefer et al., 2009) **Dental Development** (Ubelaker, 1989)

Table 7: Tooth Measurements Used for Age-at-death Estimations of the Juveniles
(With reference to Schaefer et al., 2009: 79)

Grave Number	Tooth	Measurement	Age-at-death Estimation
2022-1	Mandibular right first deciduous incisor (Rdi1)	12.02 mm	1.1 years +/- 0.19
	Mandibular left first deciduous incisor (Ldi1)	12.16 mm	1.1 years +/- 0.19
	Mandibular right second deciduous incisor (Rdi2)	12.82 mm	1.4 years +/- 0.17
	Mandibular left second deciduous incisor (Ldi2)	12.74 mm	1.4 years +/- 0.17
	Maxillary right first deciduous incisor (Rdi1)	13.12 mm	1.2 years +/- 0.19
	Maxillary right first deciduous molar (Rdm1)	8.68 mm	1.11 years +/- 0.25
	Maxillary left deciduous canine (Ldc1)	9.75 mm	1.4 years +/- 0.22
	Maxillary left first permanent molar (LM1)	5.07 mm	1.55 +/- 0.25
Skeleton 17	Mandibular left deciduous canine (Ldc1)	15.16 mm	2.5 years +/- 0.22
	Maxillary left first permanent incisor (LI1)	8.33 mm	3.0 years +/- 0.21

	Maxillary left second deciduous incisor (Ldi2)	15.4 mm	1.78 years +/- 0.17
	Maxillary left deciduous canine (Ldc1)	16.6 mm	2.8 years +/- 0.22

Table 8: Postcranial Measurements Used for Age-at-death Estimation of 2022-1
(With reference to Schaefer et al., 2009)

Element	**Measurement** (approximations made when distal/proximal ends were damaged)	**Age-at-death Estimation**
R/L Humerus	90.94 mm	~ 6 months
L Ulna	~77-80 mm	~ 6 months
R/L Radii	~66-68 mm	~ 6 months
R Femur	113 mm	~ 6 months
R/L Tibiae	~90-95 mm	~ 6 months
R/L Fibulae	~83-85 mm	~ 6 months
R/L Clavicle	53.21-53.34 mm	~ 7-12 months
R Scapula Length R Scapula Width	52.74 mm 36.72 mm	6 months - 1 year 6 months - 1 year
R Ilium Length L Ilium Length R/L Ilium Width	47.84 mm 47.47 mm ~ 44 mm	10-12 months 10-12 months 7-9 months

Appendix B: Transition Analysis 2.0 Scores

TA2 is not widely applied in bioarchaeological studies (Clark et al., 2022). There were some inconsistencies between the age-at-death estimated using standardized methods (Buikstra & Ubelaker, 1994) vs. applying Transition Analysis 2.0 (Boldsen et al., 2002). 2019-5, 2019-7, and 2019-9 have tenuous results.

2019-5, when male, has a point estimate of 71.3 years old at the time of death. When changed to female, and with the same scores, the point estimate changed to 40.1 years, which was in-line with the standardized methods used with reference to *Standards for Data Collection from Human Skeletal Remains* (Buikstra & Ubelaker, 1994). The reason why there would be a 30 year age-at-death difference between the sexes, with the same scores, is unknown. 2019-7 has a point estimate of 69.0 years, which is not in-line with estimations made with reference to *Standards for Data Collection from Human Skeletal Remains* (Buikstra & Ubelaker, 1994). 2019-9 has a point estimate of 28.2 years, which again, is not in-line with estimations made with reference to *Standards for Data Collection from Human Skeletal Remains* (Buikstra & Ubelaker, 1994).

The use of TA2 in this study reveals that this is a promising, but imperfect method for estimating age-at-death in adult skeletons. The estimations were in-line with the estimations made with reference to *Standards for Data Collection from Human Skeletal Remains* (Buikstra & Ubelaker, 1994) for five out of the eight skeletons from this sample. However, since three skeletons had questionable TA2 results, this method remains imperfect, and standardized methods (Buikstra & Ubelaker, 1994) may continue to be preferred.

Transition Analysis Scoring and Analysis

Observations

Skeleton: Corinth 2022-2

Cranial Sutures	min/max
Coronal Pterica	☐ ☐
Sagittal Obelica (midline)	☐ ☐
Lambdoidal Asterica	☐ ☐
Interpalatine (midline)	☐ ☐
Zygomaticomaxillary	2 2

Pubic Symphysis	Left (min/max	Right (min/max
Symphyseal Relief	☐ ☐	☐ ☐
Symphyseal Texture	☐ ☐	☐ ☐
Superior Apex / Protuberance	☐ ☐	☐ ☐
Ventral Symphyseal Margin	☐ ☐	☐ ☐
Dorsal Symphyseal Margin	☐ ☐	☐ ☐

Auricular Surface	Left (min/max	Right (min/max
Superior Demiface Topography	2 2	2 2
Inferior Demiface Topography	2 2	2 2
Superior Surface Morphology	3 3	3 3
Middle/Apical Surface Morphology	3 4	3 4
Inferior Surface Morphology	3 3	3 3
Inferior Surface Texture	2 2	1 2
Superior Posterior Iliac Exostoses	2 2	2 2
Inferior Posterior Iliac Exostoses	3 3	☐ ☐
Posterior Exostoses	2 3	☐ ☐

Age Estimation

Hazard Model: Archeological White Female

	L_95%	Point_	U_95%	DF	Chi-sq	p
Corrected	15.8	29.1	50.0	-	-	-
Uncorrected	16.2	29.6	50.1	1	0.1	0.82
Cranial Sutures	15.0	23.1	109.7	0	-	1
Auricular Area	16.2	30.2	52.4	9	10	0.35

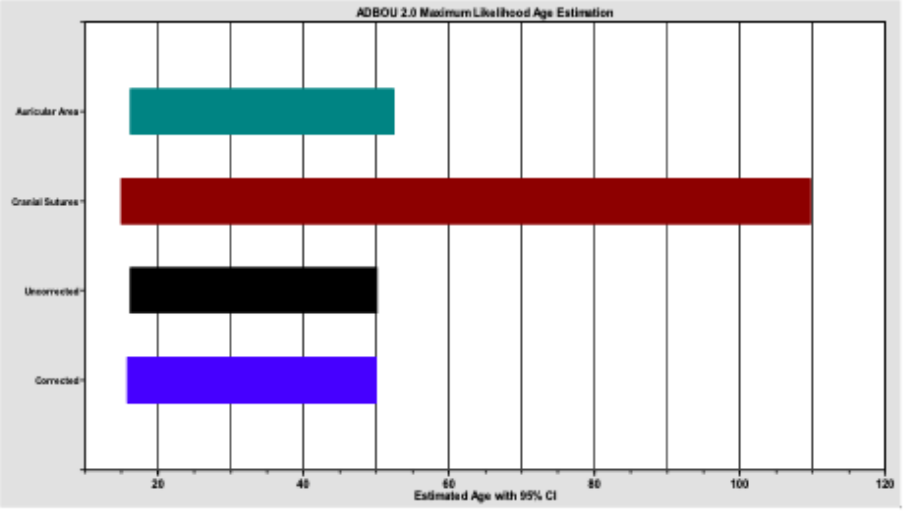

Transition Analysis Scoring and Analysis

Observations

Skeleton: Corinth 2019-1

Cranial Sutures	min	max
Coronal Pterica	4	4
Sagittal Obelica (midline)	3	4
Lambdoidal Asterica	2	2
Interpalatine (midline)		
Zygomaticomaxillary		

Pubic Symphysis	Left (min/max		Right (min/max	
Symphyseal Relief				
Symphyseal Texture				
Superior Apex / Protuberance				
Ventral Symphyseal Margin				
Dorsal Symphyseal Margin				

Auricular Surface	Left (min/max		Right (min/max	
Superior Demiface Topography			2	2
Inferior Demiface Topography				
Superior Surface Morphology			3	3
Middle/Apical Surface Morphology			3	3
Inferior Surface Morphology			3	3
Inferior Surface Texture				
Superior Posterior Iliac Exostoses				
Inferior Posterior Iliac Exostoses				
Posterior Exostoses				

Age Estimation

Hazard Model: Archeological White Male

	L_95%	Point	U_95%	DF	Chi-sq	*p*
Corrected	19.9	32.6	57.4	-	-	-
Uncorrected	20.3	33.0	56.2	1	0.8	0.38
Cranial Sutures	21.2	42.8	110.0	2	0.3	0.85
Auricular Area	15.0	25.5	53.6	2	2.5	0.28

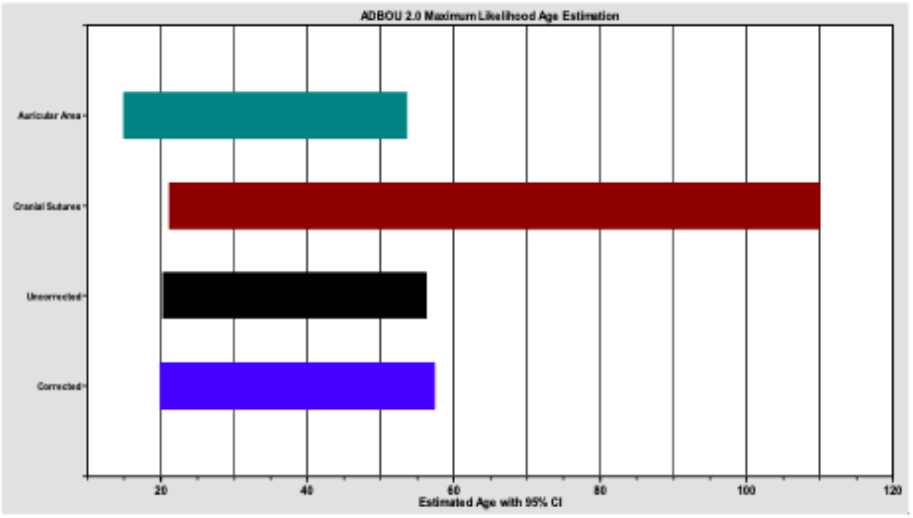

Transition Analysis Scoring and Analysis

Observations

Skeleton: Corinth 2019-2

Cranial Sutures	min	max
Coronal Pterica	2	2
Sagittal Obelica (midline)	2	2
Lambdoidal Asterica	2	2
Interpalatine (midline)		
Zygomaticomaxillary	2	3

Pubic Symphysis	Left (min/max		Right (min/max	
Symphyseal Relief				
Symphyseal Texture				
Superior Apex / Protuberance				
Ventral Symphyseal Margin				
Dorsal Symphyseal Margin				

Auricular Surface	Left (min/max		Right (min/max	
Superior Demiface Topography			1	1
Inferior Demiface Topography				
Superior Surface Morphology			1	2
Middle/Apical Surface Morphology				
Inferior Surface Morphology			1	2
Inferior Surface Texture				
Superior Posterior Iliac Exostoses			1	1
Inferior Posterior Iliac Exostoses				
Posterior Exostoses			1	1

Age Estimation

Hazard Model: Archeological White Male

	L_95%	Point_	U_95%	DF	Chi-sq	*p*
Corrected	**16.2**	16.2	**29.5**	-	-	-
Uncorrected	16.8	16.8	30.0	1	0.7	0.41
Cranial Sutures	15.0	21.8	36.6	3	0.5	0.91
Auricular Area	15.0	15.0	31.7	3	0	1

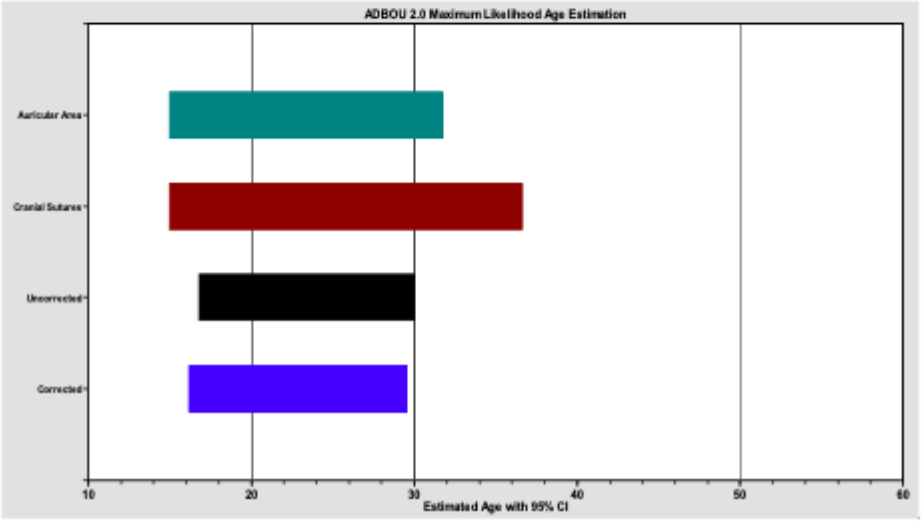

Transition Analysis Scoring and Analysis

Observations

Skeleton: Corinth 2019-5

Cranial Sutures	min/max
Coronal Pterica	☐ ☐
Sagittal Obelica (midline)	☐ ☐
Lambdoidal Asterica	☐ ☐
Interpalatine (midline)	☐ ☐
Zygomaticomaxillary	☐ ☐

Pubic Symphysis	Left (min/max		Right (min/max	
Symphyseal Relief	☐	☐	☐	☐
Symphyseal Texture	☐	☐	☐	☐
Superior Apex / Protuberance	☐	☐	☐	☐
Ventral Symphyseal Margin	☐	☐	☐	☐
Dorsal Symphyseal Margin	☐	☐	☐	☐

Auricular Surface	Left (min/max		Right (min/max	
Superior Demiface Topography	☐	☐	1	2
Inferior Demiface Topography	☐	☐	☐	☐
Superior Surface Morphology	☐	☐	4	4
Middle/Apical Surface Morphology	☐	☐	4	4
Inferior Surface Morphology	☐	☐	4	4
Inferior Surface Texture	☐	☐	☐	☐
Superior Posterior Iliac Exostoses	☐	☐	2	2
Inferior Posterior Iliac Exostoses	☐	☐	☐	☐
Posterior Exostoses	☐	☐	☐	☐

Age Estimation

Hazard Model: Archeological White Male

	L_95%	Point_	U_95%	DF	Chi-sq	p
Corrected	**20.5**	71.3	**89.5**	-	-	-
Uncorrected	18.3	57.2	102.8	0		-
Auricular Area	18.3	57.2	102.8	3	0.9	0.82

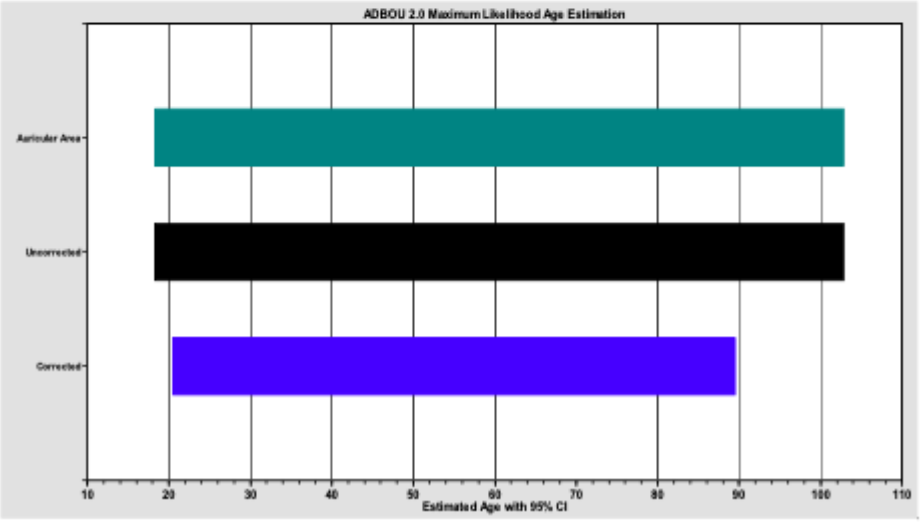

Transition Analysis Scoring and Analysis

Observations

Skeleton: Corinth 2019-5

Cranial Sutures	min/max
Coronal Pterica	☐ ☐
Sagittal Obelica (midline)	☐ ☐
Lambdoidal Asterica	☐ ☐
Interpalatine (midline)	☐ ☐
Zygomaticomaxillary	☐ ☐

Pubic Symphysis	Left (min/max	Right (min/max
Symphyseal Relief	☐ ☐	☐ ☐
Symphyseal Texture	☐ ☐	☐ ☐
Superior Apex / Protuberance	☐ ☐	☐ ☐
Ventral Symphyseal Margin	☐ ☐	☐ ☐
Dorsal Symphyseal Margin	☐ ☐	☐ ☐

Auricular Surface	Left (min/max	Right (min/max
Superior Demiface Topography	☐ ☐	1 2
Inferior Demiface Topography	☐ ☐	☐ ☐
Superior Surface Morphology	☐ ☐	4 4
Middle/Apical Surface Morphology	☐ ☐	4 4
Inferior Surface Morphology	☐ ☐	4 4
Inferior Surface Texture	☐ ☐	☐ ☐
Superior Posterior Iliac Exostoses	☐ ☐	2 2
Inferior Posterior Iliac Exostoses	☐ ☐	☐ ☐
Posterior Exostoses	☐ ☐	☐ ☐

Age Estimation

Hazard Model: Archeological White Female

	L_95%	Point_	U_95%	DF	Chi-sq	*p*
Corrected	**40.1**	40.1	**85.4**	-	-	-
Uncorrected	40.8	40.8	83.5	0		-
Auricular Area	15.0	40.8	83.5	3	1.8	0.61

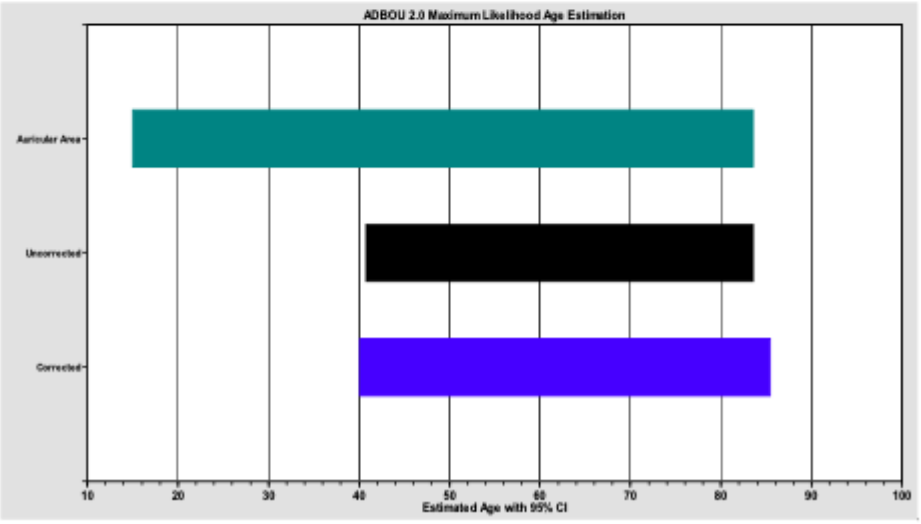

Transition Analysis Scoring and Analysis

Observations

Skeleton: Corinth 2019-6

Cranial Sutures	min/max	
Coronal Pterica		
Sagittal Obelica (midline)	4	5
Lambdoidal Asterica	2	3
Interpalatine (midline)	3	3
Zygomaticomaxillary		

Pubic Symphysis	Left (min/max		Right (min/max	
Symphyseal Relief	3	4		
Symphyseal Texture	2	3		
Superior Apex / Protuberance				
Ventral Symphyseal Margin	4	5		
Dorsal Symphyseal Margin	3	4		

Auricular Surface	Left (min/max		Right (min/max	
Superior Demiface Topography	1	2		
Inferior Demiface Topography				
Superior Surface Morphology	2	3	2	3
Middle/Apical Surface Morphology				
Inferior Surface Morphology	2	3	2	3
Inferior Surface Texture				
Superior Posterior Iliac Exostoses	2	3	3	4
Inferior Posterior Iliac Exostoses				
Posterior Exostoses				

Age Estimation

Hazard Model: Archeological White Male

	L_95%	Point_	U_95%	DF	Chi-sq	*p*
Corrected	**22.3**	31.5	**47.6**	-	-	-
Uncorrected	22.5	31.8	47.7	2	0.8	0.67
Cranial Sutures	15.0	55.9	110.0	2	0.1	0.95
Pubic	22.4	32.5	52.6	3	1	0.80
Auricular Area	15.0	20.7	60.4	3	0.5	0.92

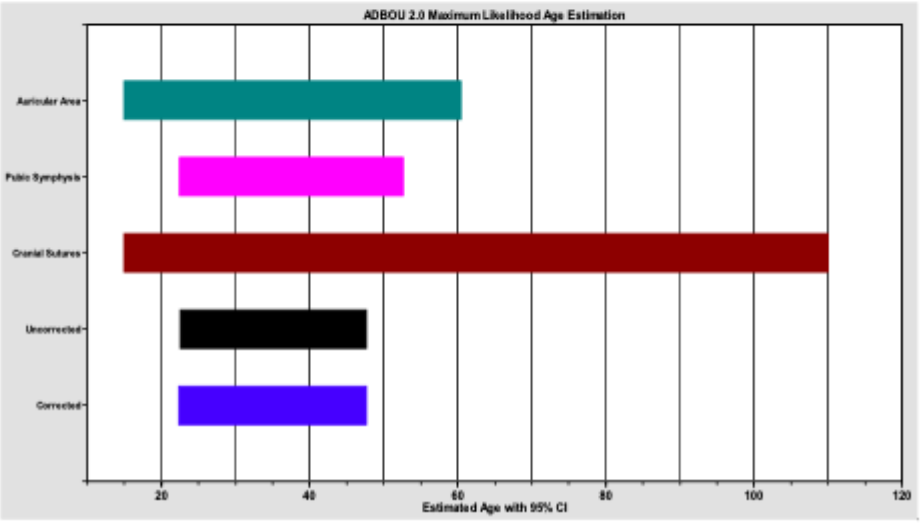

Transition Analysis Scoring and Analysis

Observations

Skeleton: CORINTH 2019-7

Cranial Sutures	min	max
Coronal Pterica		
Sagittal Obelica (midline)	4	5
Lambdoidal Asterica	2	3
Interpalatine (midline)		
Zygomaticomaxillary	3	4

Pubic Symphysis	Left (min/max		Right (min/max	
Symphyseal Relief				
Symphyseal Texture				
Superior Apex / Protuberance				
Ventral Symphyseal Margin				
Dorsal Symphyseal Margin				

Auricular Surface	Left (min/max		Right (min/max	
Superior Demiface Topography				
Inferior Demiface Topography			2	3
Superior Surface Morphology				
Middle/Apical Surface Morphology	3	4	3	3
Inferior Surface Morphology				
Inferior Surface Texture			1	1
Superior Posterior Iliac Exostoses				
Inferior Posterior Iliac Exostoses				
Posterior Exostoses				

Age Estimation

Hazard Model: Archeological White Female

	L_95%	Point_	U_95%	DF	Chi-sq	*p*
Corrected	**69.0**	69.0	**89.7**	-	-	-
Uncorrected	40.9	40.9	103.0	0		-
Auricular Area	15.0	40.9	103.0	3	0.4	0.94

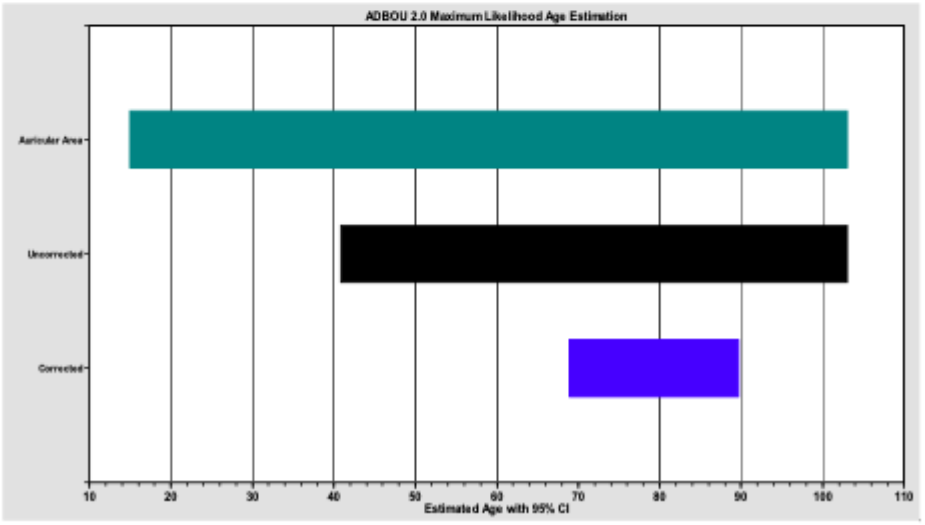

Transition Analysis Scoring and Analysis

Observations

Skeleton: Corinth 2019-8

Cranial Sutures	min/max
Coronal Pterica	☐ ☐
Sagittal Obelica (midline)	☐ ☐
Lambdoidal Asterica	☐ ☐
Interpalatine (midline)	☐ ☐
Zygomaticomaxillary	☐ ☐

Pubic Symphysis	Left (min/max	Right (min/max
Symphyseal Relief	☐ ☐	☐ ☐
Symphyseal Texture	☐ ☐	☐ ☐
Superior Apex / Protuberance	☐ ☐	☐ ☐
Ventral Symphyseal Margin	☐ ☐	☐ ☐
Dorsal Symphyseal Margin	☐ ☐	☐ ☐

Auricular Surface	Left (min/max	Right (min/max
Superior Demiface Topography	☐ ☐	1 1
Inferior Demiface Topography	☐ ☐	1 2
Superior Surface Morphology	☐ ☐	1 2
Middle/Apical Surface Morphology	☐ ☐	1 2
Inferior Surface Morphology	☐ ☐	1 2
Inferior Surface Texture	☐ ☐	1 1
Superior Posterior Iliac Exostoses	☐ ☐	1 2
Inferior Posterior Iliac Exostoses	☐ ☐	☐ ☐
Posterior Exostoses	☐ ☐	1 1

Age Estimation

Hazard Model: Archeological White Male

	L_95%	Point_	U_95%	DF	Chi-sq	p
Corrected	**15.0**	15.0	**29.2**	-	-	-
Uncorrected	15.0	15.0	30.1	0		-
Auricular Area	15.0	15.0	30.1	7	0	1

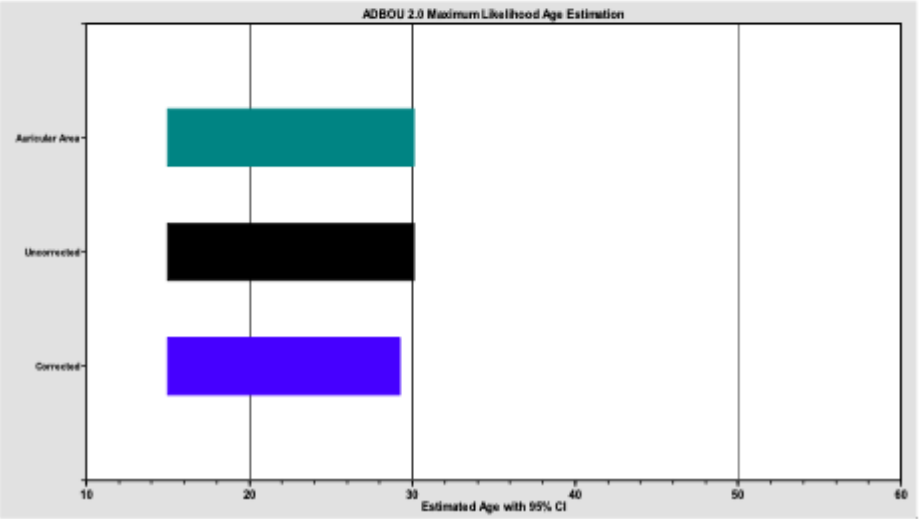

Transition Analysis Scoring and Analysis

Observations

Skeleton: Corinth 2019-9

Cranial Sutures	min/max
Coronal Pterica	
Sagittal Obelica (midline)	
Lambdoidal Asterica	
Interpalatine (midline)	
Zygomaticomaxillary	

Pubic Symphysis	Left (min/max		Right (min/max	
Symphyseal Relief			3	3
Symphyseal Texture			2	2
Superior Apex / Protuberance			2	3
Ventral Symphyseal Margin			3	4
Dorsal Symphyseal Margin			3	4

Auricular Surface	Left (min/max		Right (min/max	
Superior Demiface Topography	2	2	1	2
Inferior Demiface Topography	2	2	2	2
Superior Surface Morphology	3	4	3	3
Middle/Apical Surface Morphology	4	4	3	4
Inferior Surface Morphology	3	4	3	3
Inferior Surface Texture	1	1	1	1
Superior Posterior Iliac Exostoses	2	2	1	1
Inferior Posterior Iliac Exostoses	2	2	1	2
Posterior Exostoses	1	1	2	3

Age Estimation

Hazard Model: Archeological White Male

	L_95%	Point_	U_95%	DF	Chi-sq	*p*
Corrected	**21.7**	28.2	**38.3**	-	-	-
Uncorrected	21.7	28.4	38.5	1	0.2	0.64
Pubic	20.7	27.4	38.9	4	2.8	0.59
Auricular Area	16.2	32.0	54.3	9	13.8	0.13